Development of a Numerical Modeling Approach for Large-Scale Fluid Mud Flow in Estuarine Environments

Von der Fakultät für Bauingenieurwesen und Geodäsie
der Gottfried Wilhelm Leibniz Universität Hannover

zur Erlangung des Grades

DOKTOR-INGENIEUR
Dr.-Ing.

genehmigte Dissertation

von

M.Sc. Dennis Oberrecht

geboren am 28. Dezember 1984

in Neuenkirchen

Hannover, 2021

Referent:	Prof. Dr.-Ing. habil. Torsten Schlurmann
Korreferenten:	Prof. Dr. rer nat. habil. Christian Winter
	Prof. Dr.-Ing. habil. Martin Achmus
Gutachter:	Dr.-Ing. Andreas Wurpts
Tag der mündlichen Prüfung:	18. September 2020

Kurzfassung

Ästuare gehören zu den empfindlichsten und zugleich produktivsten Ökosystemen der Welt. Aufgrund ihrer küstennahen Lage mit ihrer verknüpfenden Funktion zum Meer, haben Ästuare auch eine wichtige Bedeutung für die Ökonomie. Durch die Industrialisierung und Urbansierung haben sich im Laufe der Zeit große Hafenanlagen als Endpunkte wichtiger Transportrouten angesiedelt. Infolge immer weiter steigender Güterfrachten und daraus resultierendem Anstieg des Tiefganges, von See- und Binnenschiffen, wurden die Wasserstraßen zunehmend vertieft, um die Wirtschaftlichkeit aufrechtzuerhalten. Die daraus hervorgehenden anthropogenen Eingriffe zur Erhaltung der nautischen Tiefe, hatten gravierende Auswirkungen auf den Sedimenthaushalt und die Ökologie der Ästuare.

Der Sedimenthaushalt eines Ästuars beschreibt den Sedimenttransport und dessen Bilanz durch Umlagerungen von Sohlsedimenten, Bildung von Trübungszonen, sowie den Import von Land- und Seeseite. Anthropogene Eingriffe (Vertiefungen, Begradigungen) haben partiell große Auswirkungen auf die Morphologie und den Sedimenttransport und somit auf den Sedimenthaushalt. Im Prinzip wird in Folge der Vertiefungen, die natürliche Rückstellkraft zur Erhaltung eines natürlichen dynamischen Gleichgewichtes aus Hydrodynamik und Morphologie, verstärkt. Durch den morphologischen Rückstellungsmechanismus kann es zu einem erhöhten Eintrag, Verlagerung der Trübungzone und Transport von Sedimenten kommen. Als Folge kann sich bei sehr hohen Suspensionskonzentrationen *Flüssigschlick* bilden, was eine Suspension mit den Hauptbestandteilen aus Klei, Ton und organische Verbindungen ist. *Flüssigschlick* weist nicht-Newtonsches Fließverhalten auf, dessen Wechselwirkung mit der freifließenden Wassersäule ausgesprochen komplex ist und dessen großflächige Dynamik Gegenstand aktueller Forschung ist. Insbesondere die zeitabhängige Entstehung der sediment-geschichteten Verhältnisse in der Wassersäule durch *Flüssigschlick* ist bisher nicht ausreichend verstanden. Aufgrund hoher Depositionsraten kommt es durch die Entstehung von *Flüssigschlick* zu einem deutlich höheren Unterhaltungsaufwand der Schifffahrtswege. Außerdem findet in der Flüssigschlickschicht ein verstärkter Sauerstoffabbau statt, wodurch die Ausbildung von hypoxischen Bereichen innerhalb des Flusslaufes die Flora und Fauna gefährden.

Für wissenschaftliche Untersuchungen der Ästuardynamik und dem daraus resultierenden Sedimenttransport werden heutzutage numerische Modelle auf Basis der Reynolds- gemittelten Navier-Stokes Gleichung (RANS) eingesetzt. Mit diesen Modellen ist es möglich die großräumigen Strömungs- und Transportprozesse bei hinreichender Interaktion miteinander zu untersuchen. In diesen Modellen kann Sedimenttransport sowohl von nicht-kohäsiven als auch von kohäsiven Sedimenten hinreichend abgebildet werden um z.B. die Ausbildung der Trübungszone zu evaluieren. Allerdings konnte die Bildung und großräumige Dynamik von *Flüssigschlick* bisher nicht dargestellt werden, da eine praxistaugliche und die wesentlichen Charakteristika der Interaktion von Flüssigschlick und freier Wassersäule

berücksichtigende Implementierung rheologischer Modelle bislang ausstand. Aufgrund des Fließverhaltens, das sich erheblich von der des ungeschichteten, frei fließenden Newtonschen Fluids in der übrigen Wassersäule unterscheidet, kommen die bisher eingesetzten Modellansätze zur dreidimensionalen Modellierung von Ästuaren an ihre Grenzen. Aus diesem Grund sind die bisherigen Kenntnisse zur großräumigen Bildung und Dynamik von *Flüssigschlick* unzureichend erforscht. Die physikalischen Eigenschaften von *Flüssigschlick* (nicht-Newtonsches Fließverhalten, komplexes Sinkverhalten, laminare Strömung, Rheologie, sowie der Einfluss auf die Turbulenzausbreitung) mit der Interaktion des Wasser- und anstehenden Bodenkörpers, ist essenziell zur Beschreibung der Dynamik, werden aber bisher kaum berücksichtigt. Einige der vorgenannten Eigenschaften (Rheologie, Sinkverhalten) wurden bereits separat in Modellen untersucht, allerdings existierte bislang kein Modell, das die genannten Eigenschaften berücksichtigt, so dass state-of-the-art Modellierungen von Ästuaren mit hinreichender Berücksichtigung des Flüssig-schlicks bislang nicht möglich waren.

Die vorliegende Arbeit erweitert die Ästuarmodellierung um die Möglichkeit der großräumigen numerischen Modellierungen von *Flüssigschlick* in RANS-Modellen und entsprechend großer räumlicher und zeitlicher Skalen. Ein besonderer Fokus liegt auf dem bisher nicht ausreichend bekannten Einfluss des nicht-Newtonschen Fluids auf die vertikale Turbulenzausbreitung, sowie der Fähigkeit zum zeitabhängigen laminaren Fließen (Thixotropie). Der hier entwickelte Ansatz erlaubt die gleichzeitige Modellierung newtonscher, turbulenter und nicht-newtonscher, laminarer Fließvorgänge innerhalb eines Rechengitters mit stetigem Übergängen zwischen beiden Zuständen. Anhand umfangreicher, teils zielgerichtet für die Validierung des Modellansatzes erhobener Feldmessdaten aus dem Ems-Ästuar konnte dieser belastbar validiert werden. Die Verifizierung zeigt, dass der hier erweiterte Modellansatz in der Lage ist, sowohl die Dynamik des Wasserkörpers, als auch der hochkonzentrierten Suspension hinreichend genau abzubilden. Des Weiteren wird auf Basis der Modellergebnisse der Einfluss von *Flüssigschlick* auf die Hydrodynamik und Ästuarzirkulation am Beispiel des Ems-Ästuars verdeutlicht. Die Ergebnisse zeigen deutlich, dass eine Berücksichtigung der Eigenschaften des *Flüssigschlick* in numerischen Modellen erforderlich ist um eine realistische Abbildung der Hydrodynamik und Ästuarzirkulation, sowie des großräumigen Sedimenttransportes erreichen zu können. Mit dem nun vorliegenden Modell steht ein Werkzeug bereit, das unmittelbar für die Klärung weitergehender Fragen zum Systemverständnis Flüssigschlick-geschichteter Ästuare oder auch zur Prüfung und Umsetzung konkreter behördlicher Maßnahmen eingesetzt werden kann.

Schlüsselwörter: Ästuardynamik, Flüssigschlick, Rheologie, laminare Strömung, laminar-turbulenter Übergang, Ems Ästuar

Abstract

Tidal estuaries are belong the most sensitive and at the same time most productive ecosystems in the world. Due to their coastal location with their linking function to the sea, estuaries are also important for the economy. Through industrialization and urbanization, large port facilities with important transport routes have been established. As a result of ever increasing cargo loads and the resulting increase in draft of the vessels, the waterways were increasingly deepened in order to maintain navigability. The anthropogenic interventions carried out to maintain the nautical depth have been shown to have serious effects on the sediment balance and the ecology of the estuaries.

The overall sediment balance of an estuary describes the sediment transport and its balance by rearrangement of bed sediments, formation of turbidity zones, as well as the sediment import from land and sea side. Anthropogenic interventions (deepening, straightening) sometimes have a major impact on morphology and sediment transport and thus on the sediment balance. In principle, as a result of deepening, the natural restoring mechanism for maintaining a natural dynamic equilibrium of hydrodynamics and morphology is increased. The increased morphological restoration mechanism can lead to increased sediment import, shifting of the turbidity zone and increased sediment transport. As a result, *fluid mud* can form at very high suspension concentrations. *Fluid mud* is a suspension of silt, clay and organic matter. It tends to form stratified layers in the water column, which exhibit non-Newtonian, laminar flow properties, the higher the sediment concentration is. The interaction with the free-flowing upper water column is physically complex and the large-scale dynamics are subject of current research. In particular, the time-dependent formation of the sediment-stratified conditions in the water column induced by *fluid mud* has not yet been sufficiently understood. Due to the increasing deposition rates, the formation of *fluid mud* leads to a significantly higher maintenance effort for shipping routes. In addition, an increased oxygen depletion in the *fluid mud* layer arises, which supports the formation of hypoxic areas and endangers the flora and fauna.

Nowadays, numerical models based on the Reynolds-averaged Navier-Stokes (RANS) equations are used for the scientific analysis of estuarine dynamics and the resulting sediment transport. With these models it is possible to examine large-scale flow and transport processes with sufficient interaction between both. The sediment transport of non-cohesive and cohesive sediments can be sufficiently represented, e.g. evaluation of the formation of a turbidity zone. However, the formation and large-scale dynamics of *fluid mud* have not yet been sufficiently considered, since a practical implementation of the physical characteristics of the interaction of *fluid mud* with upper free water column is not available. Due to the flow behavior of *fluid mud*, which differs from unsaturated, free-flowing Newtonian fluid in the upper water column, the previously used model approaches for three-dimensional modeling of estuaries were not applicable. Therefore, the hitherto existing knowledge of

the large-scale formation and dynamics of *fluid mud* suffer from the lack in system understanding. The physical properties and dynamics of *fluid mud* (non-Newtonian flow behavior, complex settling, laminar flow, rheology, and the influence on turbulent mixing) with the interaction of the water body and sediment bed are essential for a consideration, but have so far hardly been considered. Some of the aforementioned physical properties (rheology, settling behavior) have already been investigated separately, but so far no model exists, that takes the mentioned physical properties of *fluid mud* into account. Therefore, a state-of-the-art modeling approach for estuaries with sufficient consideration of *fluid mud* dynamics has not yet been proposed.

The present work extends the estuarine modeling practice by the implementation of *fluid mud* dynamics and large scale application within a single-phase RANS-model. It focus on the hitherto insufficiently known impact of the non-Newtonian fluid on the vertical turbulent mixing, as well as the ability for time-dependent laminar flow (thixotropy). The approach developed here allows the simultaneous modeling of Newtonian, turbulent and non-Newtonian, laminar flow processes within one numerical grid with continuous transitions between the two states. Based on extensive available data and data from own measurement campaign, the developed model approach could be reliably validated. The verification shows that the extended model approach is able to map the dynamics of the Newtonian water body as well as the highly concentrated suspensions with sufficient accuracy. Furthermore, based on model results of the Ems estuary, the influence of *fluid mud* on hydrodynamics, estuarine circulation and sediment transport is illustrated and discussed. The results clearly show, that consideration of the physical properties of *fluid mud* in numerical models is required in order to achieve a realistic representation of the large-scale estuarine dynamics. With the extended model approach, a tool is available that can be used directly to clarify further questions about the system understanding of *fluid mud*-stratified estuaries or to proof concrete administrative measures.

Keywords: Estuarine Dynamics, Fluid Mud, Rheology, Laminar Flow, Laminar-Turbulent Transition, Ems Estuary

Contents

Nomenclature

Nomenclature

List of Symbols

a	empirical aggregate recovery parameter	[-]
b	empirical aggregate break-up parameter	[-]
B_k	buoyancy term turbulence closure	$[m^2\ s^{-4}]$
C	sediment concentration	$[kg\ m^{-3}]$
C_b	near bed sediment concentration	$[kg\ m^{-3}]$
C_d	empirical parameter turbulence closure	[-]
C_D	bed roughness parameter	[-]
C_{gel}	reference concentration for hindered settling	$[kg\ m^{-3}]$
D	deposition rate	[kg $m^{-2}\ s^{-1}$)]
d_{50}	equivalent sediment diameter	[m]
E	erosion rate	[kg $m^{-2}\ s^{-1}$)]
E_0	Erosion rate	$[kg\ m^{-2}\ s^{-1}]$
$f_{u,v}$	Coriolis force in u, v direction	$[m\ s^{-2}]$
g	gravitational acceleration	[m s^{-2}]
H	water depth	[m]
k_s	equivalent sediment roughness	[m]
l_m	Prandtl mixing length scale	[-]
m	empirical exponential coefficients	[-]
n	empirical exponential coefficients	[-]
P	hydrostatic pressure	[kg $m^{-1}\ s^{-1}$]
P_k	production of turbulent kinetic energy	$[m^2\ s^{-3}]$
Re	Reynolds number	[-]
Ri_g	Richardson Gradient Number	[-]
TKE	turbulent kinetic energy	$[m^2\ s^{-2}]$
$\overline{u}$	mean velocity components in x,direction	[m s^{-1}]
u'	fluctuating velocity component in x direction	[m s^{-1}]
u^+	dimensionless velocity component	[-]
u_*	bed shear velocity	[m s^{-1}]
$\overline{v}$	mean velocity components in y direction	[m s^{-1}]
v'	fluctuating velocity component in x direction	[m s^{-1}]

$\overline{w}$	mean velocity components in z direction	[m s^{-1}]
w'	fluctuating velocity component in x direction	[m s^{-1}]
w_s	settling velocity	[m s^{-1}]
$w_{s,0}$	single particle settling velocity	[m s^{-1}]
z^+	dimensionless distance to the wall	[-]
z_0	effective roughness length	[m]
η	Kolmogorov length scale	[m]
ϵ	energy dissipation	[m^2 s^{-3}]
$\epsilon_{x,y,z}$	horizontal and vertical turbulent diffusivity	[m^2 s^{-2}]
$\dot{\gamma}$	shear rate	[1 s^{-1}]
κ	von Karman constant	[-]
λ	structure parameter	[-]
λ_0	previous aggregation state	[-]
μ	dynamic viscosity	[kg $m^{-1}s^{-1}$]
μ_0	initial dynamic viscosity	[kg $m^{-1}s^{-1}$]
μ_∞	infinity dynamic viscosity	[kg $m^{-1}s^{-1}$]
μ_m	dynamic molecular viscosity	[Pas]
μ_r	dynamic rheological viscosity	[Pas]
ν_t	turbulent viscosity	[m^2 s^{-2}]
ν_m	molecular viscosity	[m^2 s^{-2}]
ν_h	horizontal turbulent viscosity	[m^2 s^{-1}]
ν_v	vertical turbulent viscosity	[m^2 s^{-1}]
ν_v	rheological turbulent viscosity	[m^2 s^{-1}]
τ	shear stress	[Pa]
τ_b	bed shear stress	[Pa]
τ_B	Bingham yield stress	[N m^{-2}]
τ_e	critical erosion shear stress	[N m^{-2}]
τ_f	Reynolds shear stress	[N m^{-2}]
τ_{mol}	molecular shear stress	[N m^{-2}]
τ_r	rheological shear stress	[Pa]
τ_t	turbulent shear stress	[N m^{-2}]
ρ	fluid density	[kg m^{-3}]
ρ_0	initial density	[kg m^{-3}]
$\rho_{T,S}$	temperature and salinity induced density	[kg m^{-3}]

List of Acronyms

ADCP	Acoustic Doppler Current Profiler
CTD	Conductivity-Temperature and Pressure meter
DO	dissolved oxygen concentration
ECM	Electro-Current-Meter
EFC	equilibrium flow curve
ETM	estuarine turbidity maximum
MHW	Mean High Water
MSL	Mean Sea Level
NHN	Normalhöhen Null
RANS	Reynolds-Averaged Naiver-Stokes
SSC	suspended sediment concentration

List of Figures

List of Tables

1 Introduction

1.1 Introduction and Motivation

Estuaries are partially enclosed basins which build the connection of one or more river system to the open sea (Cameron and Pritchard, 1963). Estuarine dynamics are dominated by tidal forcing, river discharge and the mixing of marine salt water and fluvial fresh water in a process termed *baroclinic circulation* (e.g. Dyer, 1973; Geyer and MacCready, 2014). Additionally, mentioned hydrodynamic force also leads to sediment transport and trapping of sandy and muddy sediments mainly in the so called estuarine turbidity maximum (ETM) (Allen et al., 1980; Dyer, 1986; Burchard et al., 2018). These characteristics offer a number of habitats for flora and fauna and make estuaries a diverse and unique ecosystem. Due to the coastal location of estuaries, they often serve as important waterways connecting large economic areas and harbors to sea shipping routes. To maintain access of ships with ever-increasing draft to the ports, navigational channels are frequently deepened and subject to constant maintenance dredging. Therefore, navigational channels in estuaries are subject to extensive anthropogenic interventions.

The estuarine sediment balance is a measure of sediment import from land and seaside such as local sediment redistributions within an estuary. Therefore the sediment balance is a result of the equilibrium between hydrodynamics and morphodynamics. The massive deepening and ongoing maintenance activities have a major impact on the morphology of an estuary and its corresponding transport processes (e.g. Kerner, 2007; Maren et al., 2015). The naturally acting restoring force, acting towards a dynamic morphological and hydrodynamic equilibrium, is amplified by greater anthropogenic interference, and can result in higher suspended sediment loads (e.g. Bolle et al., 2010; Jonge et al., 2014). If the suspended sediment load in the water column exceeds a certain order of magnitude, a fluid mud layer can be formed, which has different physical characteristics compared to clear water (e.g. Faas, 1984; Granboulan et al., 1989; McAnally et al., 2007). Fluid mud itself is a mixture of clay, silt and organic matter, which is formed not only in deep channels of estuaries, but also in harbors as well as calm side areas of coastal zones. Familiar estuaries with fluid mud formation are the Seine (Dupont et al., 1994), and the Gironde estuary in France (Abril et al., 1999), as well as the Weser (Schrottke et al., 2006) and Ems (Van Leussen, 1988) estuaries in Germany. Furthermore, in the freshwater region of the Elbe estuary (Germany) with its large port facility in Hamburg, fluid mud layers were found. Additionally, at the Amazon shelf (Kineke et al., 1996) or Jiangiong estuary in China (Guan et al., 1998) a fluid mud layer formation was observed at specific boundary conditions (tidal force and discharge). Increased sediment transport rates associated with increased suspended sediment concentration (SSC), and the specific flow and settling behavior of fluid mud in the water column results in high deposition rates of predominantly fine sediment during slack water periods. As a result, even more dredging is required to maintain the navigational depth.

Field measurements from estuaries with frequently fluid mud formation have shown, that fluid mud has a significant negative influence on the ecological state of an estuary (Abril et al., 2000). This essentially results from higher oxygen strain consumption of bacteria adhering on the surface of sediment particles (Edwards and Rolley, 1965). This means, the larger the sediment concentration, the stronger the sediment induced oxygen consumption. The Ems estuary in Germany exhibits a high oxygen consumption during summer (low discharge) and reaches anoxic conditions (dissolved oxygen concentration (DO) < 2 mg l^{-1}) for almost six months per year (Talke et al., 2009), while during winter conditions with higher discharge and lower temperature the situation is uncritical. Previous studies describe the physical behavior of fluid mud (e.g. Coussot and Piau, 1994; Faas, 1984), but the large-scale formation, resulting dynamics and corresponding mechanisms are not yet well understood (e.g. Burchard et al., 2018). Therefore, this understanding is essential to assess the environmental impacts of anthropogenic interventions in estuaries.

Large-scale estuarine dynamics are best investigated by means of complex numerical models, because temporally and spatially dependent field measurements doesn't allow derivations to detailed large-scale dynamics. The reason is the complex three-dimensional, at least partially stratified flow structure which can not be covered by synoptic field measurements in sufficient detail. For these kind of numerical studies, common models used (e.g. Delft3D, Telemac or SCHISM), which are based on the Reynolds-averaged Navier-Stokes equations. Sediment transport of cohesive and/or non-cohesive sediments is solved based on the advection-diffusion equation. In contrast to non-cohesive sediments, the settling behavior of cohesive fines is much more complex and can not be defined as a constant value. Many previous studies dealing with cohesive sediment transport simplify the settling behavior as a constant value (e.g. Maren et al., 2015; Hesse et al., 2019). This simplified implementation of settling excludes the formation of fluid mud in the models. Furthermore, specific cohesive properties such as the complex settling formulation of flocculation, hindered settling and consolidation is missing, as well as the non-Newtonian flow behavior.

Modeling studies, which include the fluid mud specific behavior mainly include only one vertical dimension (1DV-Model) focusing on the complex settling behavior and therefore neglecting the estuarine specific three-dimensional flow behavior (e.g. LeHir et al., 2000; Hsu et al., 2007; Kämpf et al., 2018). These models follow an approach which calls *the continuous modeling approach* (LeHir et al., 2000). It allows mixing and interaction of the non-Newtonian fluid mud and Newtonian flow of the water body. Wehr (2012) developed a three-dimensional fluid mud layer flow model, which is based on the isopycnical modeling concept. The isopycnical model concept is limited to only stable stratified flow conditions. In highly turbulent flows, this concept cannot adequately reproduce mixing and associated upward flux of cohesive fines into the upper water column due to its vertical discretization. Guan et al. (2005) and Roland et al. (2012) applied Le Hir's continuous modeling approach to estuarine environments, using a three dimensional model. They have shown that the model is case sensitive to empirical parameters of the turbulence and rheological model formulation and requires process-based studies to improve the parametrization.

The reduction of horizontal flow velocities in the high concentrated fluid mud layer and the transition to the upper, free flowing layer could not be adequately reproduced in previous mentioned studies. However, the horizontal transport reduction has a great impact on the total sediment transport rate within a tidal cycle (Becker et al., 2018). This effect should be a large impact to determine residual transport pathways in an estuary as well as spatial extension of the ETM. Additionally, the effect of fluid mud on the turbulence production could not be verified in previous model studies, but it appears as one of the main physical drivers to estimate the fluid mud-water exchange (LeHir et al., 2000).

Literature review shows a lack of numerical models, which are capable to reproduce the three-dimensional behavior of fluid mud-water mixtures exists. There is, so far, no model implementation available which allows sufficent large scale and long term model investigations of fluid mud carrying estuaries. Such model technology is a major step towards a better understanding of such estuaries and also their management. The main motivation of this work is therefore to contribute to the understanding of large-scale fluid mud formation and corresponding dynamics in estuarine environments by developing a general modeling concept, which improves the physical understanding of fluid mud influenced dynamic behavior.

1.2 Objective & Methods

The objective of this study focuses on the large-scale dynamics of cohesive sediments forming fluid mud in an estuarine environment. For estuarine circulation modeling, three dimensional model concepts with large-scale density driven buoyancy and stratification effects by salinity (e.g. Pritchard, 1952) are state of the art. Within this study a state-of-the-art hydro-morphodynamical estuarine model (Delft3D) was extended with focus on fluid mud dynamics. The implemented formulation include:

- Complex settling velocity with a continuous transition between flocculation, hindered settling and consolidation
- Non-Newtonian rheological behavior: kinematic viscosity, shear thinning with a yield stress, thixotropy
- Buoyancy-driven turbulence damping
- Rheology (non-Newtonian)-induced turbulence damping, including laminar flow regime

The consideration of mentioned fluid mud behavior requires a steady transition between Newtonian and non-Newtonian flow behavior within the same numerical grid. This in turn requires a three-dimensional modeling approach including sediment transport and salinity.

With those extensions, the model is enabled to reproduce complex stratified situations of Newtonian and non-Newtonian flow dynamics caused by density-stratifications (salinity and/or sediment) and/or rheology. The extended model approach is not only limited to the verification test case (Ems estuary) or areas with fluid mud. It can also be applied to any

other estuary or coastal zone, because extended model processes allows only a formation of fluid mud in regions where required conditions present (existing amount of sediment, hydrodynamic).

Based on this fluid mud like high suspended sediment concentrations and resulting density stratification, it may have a major impact on the estuarine circulation. However, when large-scale fluid mud layers form, these can dominate the entire estuarine circulation because of the high impact on density. The second objective is related to investigations of the large-scale formation of fluid mud, in order to discuss essential effects on hydrodynamics and residual sediment transport and get basic understanding of this special case of estuarine dynamics.

1.3 Structure of the Thesis

Fig. 1.1 gives an overview of the thesis structure, which can be grouped into three main parts. The first part describes the-state-of-the-art as theoretical background and currently used modeling approach for the simulation of cohesive sediment transport in estuaries. The second part describes relevant processes, the model approach developed here and its verification. The third part extends the basic knowledge of the estuarine dynamics by a discussion of the formation and mixing of large-scale fluid mud layers in the Ems estuary, based on model results.

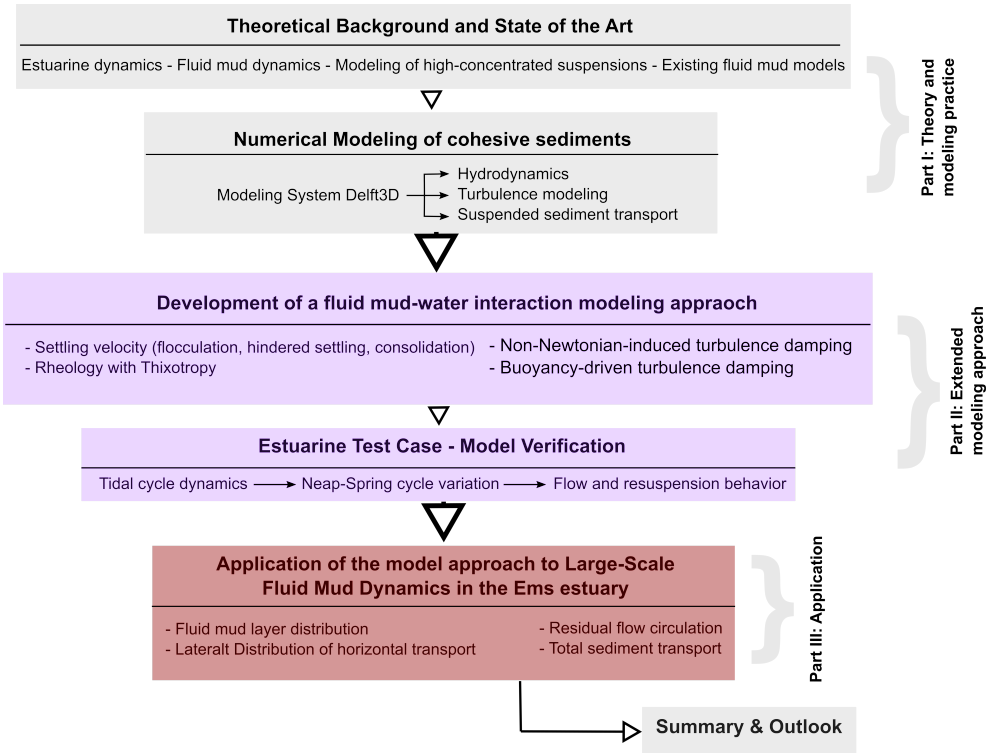

Figure 1.1: Overview of the structure of the thesis.

2 Theoretical Background and State of the Art

2.1 Estuarine Dynamics

2.1.1 General Characteristics

Estuaries transfer water, sediments, nutrients and pollutants collected from a river catchment to coastal seas. Thus, estuaries form a transition zone between the open sea and adjacent river systems (Cameron and Pritchard, 1963; Pritchard, 1967). Estuarine dynamics are driven by marine forcing, such as tides, wind-induced swell and salt water intrusion on the one hand, and fluvial forcing, such as freshwater discharge and transport of terrestrial sediments on the other hand (Fig. 2.1). Mixing of saline seawater and fresh water takes place in the process of baroclinic circulation, which is also referred to as estuarine circulation or gravitational circulation (Dyer, 1973; Geyer and MacCready, 2014). Mixing of the two water masses naturally provides a high level of nutrients in estuarine environments, both in the water column and in the sediment. This makes estuaries to one of the most productive natural habitats in the world (McLusky and Elliot, 2004).

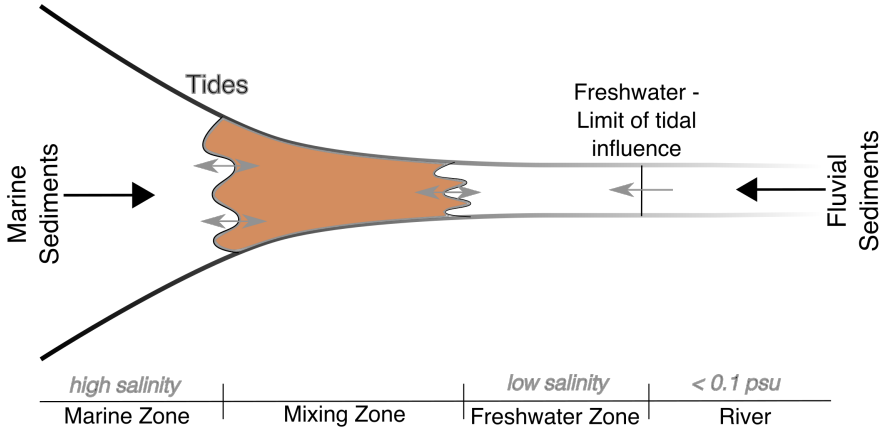

Figure 2.1: Sketch of classic estuarine zonation depicted from the head region, where fluvial processes dominate, to the mid and mouth regions where tides are the dominant controlling physical forces, respectively (adopted from Bianchi, 2013)

The coastal location and the high value of their natural habitat have made estuaries an attractive region for humans. Estuaries are often a part of global trading routes, where large port facilities along their course are often found. Due to increasing consumption in industrialized countries and the associated increase in cargo, which needs to be transported, ever larger ships with increasing draft are necessary. Most estuaries do not naturally offer the required depth and width for the safe navigation of the larger ships, and thus need

to be deepened and/or straightened. Changes in the course of a river always have an influence on the hydrodynamics and consequently on sediment transport mechanisms. The tidal pumping effect, which describes the continuation of marine sediment import into the estuary, has been shown to increase due to deepening induced by significant increase of estuarine circulation (Winterwerp and Wang, 2013). As a result, an increase in sediment transport rates and corresponding accumulation are observed (Ems estuary: Jonge et al., 2014; Weser: Schrottke et al., 2016; Loire: Walther et al., 2012). This makes maintenance dredging necessary to guarantee the nautical depth and consequently affect the entire ecosystem and natural circulation of the particular estuary (Winterwerp and Wang, 2013).

2.1.2 Estuarine Circulation

Stratification induced classification A geomorphological classification includes the hydrodynamic properties only indirectly, because it is focused exclusively on its origin. The hydrodynamic situation depends on tributary river discharge and seasonal variations of the weather such as wind or rain fall (Fischer, 2013). In another categorization, Hansen and Rattray (1966) proposed a method based on the vertical variation of salinity and the strength of internal density-driven circulation. Pritchard (1967) and Bowden and Gilligan (1971) distinguished three major categories (salt wedge, well-mixed and partially stratified). This classification is based on the relation of seawater inflow to freshwater discharge, which affects mainly the mixing of both water bodies (Fig. 2.2):

- **Salt wedge** estuaries form where a large fresh water discharge is combined with low or moderate tidal range (e.g. Mississippi, USA; Vellar, India). The existing fresh water holds back a wedge of intruding seawater. Because fresh water is less dense than salt water, it flows in the upper part of the water column seawards. This mechanism results in a strong bottom front (salt wedge), which is advected by tidal currents back and forth. Due to strong stratification in the water column, buoyancy effects exceed the turbulent mixing.

- **Well-mixed** estuaries form where river discharge is small and tidal range becomes moderate to high. Well-mixed conditions tend to occur in shallow estuaries, where tidal currents can thoroughly mix fresh and saltwater. Isohalines are straight from surface to bottom along the estuary. The mass balance will be achieved through landward mixing of salt and mixing (destratifying) processes tend to dominate over stratifying tendencies from river discharge.

- **Partially stratified** estuaries are transitions between salt-wedge and well-mixed types and occur in deeper estuaries with moderately strong tidal currents and larger river discharge. Vertical stratification is apparent throughout the water column and inflow/outflow volumes are similar. Furthermore, mixing competes equally with buoyancy tendencies.

Although the hydrodynamic quantification of many estuaries can be described by this

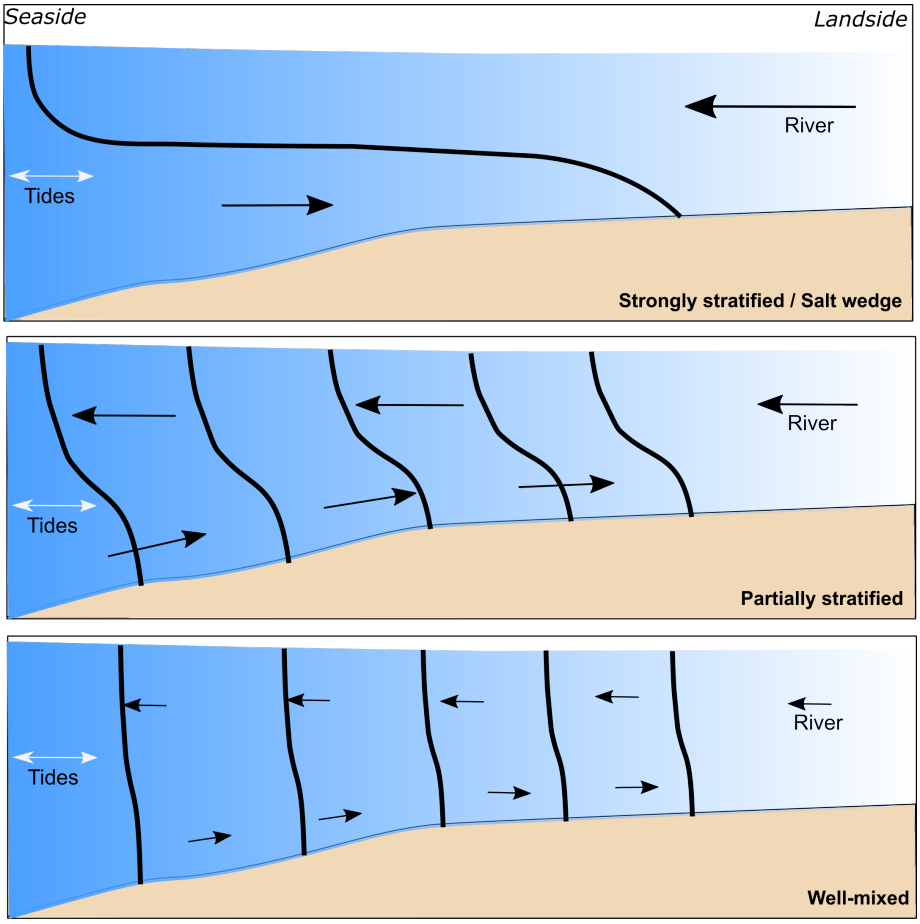

Figure 2.2: Classification of estuaries based on the vertical density-driven structure of salinity. The three different types of vertical stratification (solid black lines) are based on relation of river discharge to tidal strength. Latters are illustrated by the length of the arrows (adopted form Valle-Levinson, 2010).

classification, it also has disadvantages because many estuaries may change from one type to another in matter of days, months or seasons. For example, the Connecticut estuary changes from a partially stratified to salt-wedge circulation pattern depending on the discharge (Ralston et al., 2010).

2.1.3 Sediment trapping

Knowledge of sediment transport and sedimentation in estuaries is important for assessing the ecologic situation as well as for the planning of maintenance activities. Generally, sediment is transported into an estuary through the landward and seaward boundaries. Trapping and transport of sediment in estuarine environments depend on the hydrodynamic conditions (Fig. 2.3). Difference between ebb and flood transport capacity describes a net sediment transport and it is known as tidal-pumping (e.g. Geyer and Signell, 1992).

Latter leads to a permanent trapping of marine sediments in an estuarine environment. The spatial extent in which sediments are trapped is referred to as the turbidity zone or ETM.

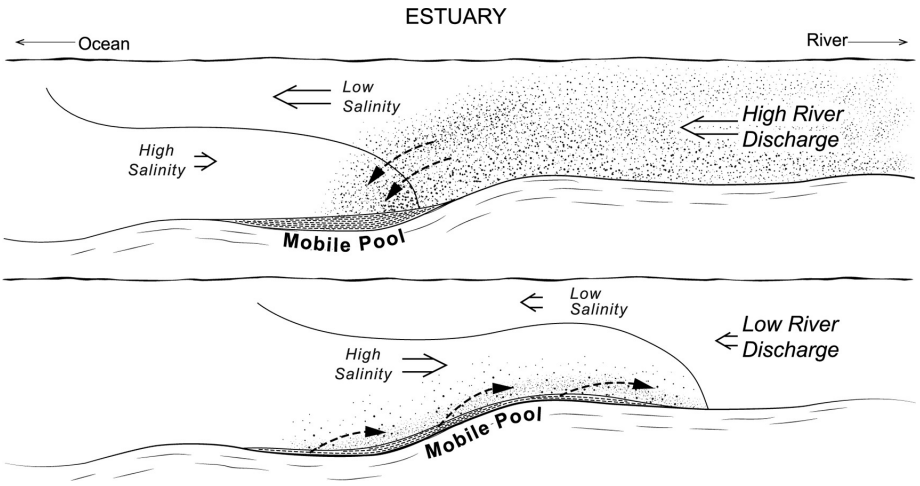

Figure 2.3: Example of sediment trapping and transport of cohesive fines in a strongly stratified estuary (Geyer and Ralston, 2018)

In general, sediment transport is divided into bed load and suspension transport. Bed load transport takes place purely on the sediment bed and is characterized by rolling, sliding, saltation of sediment particles over the river bed. On a mobile bed, bedforms such as ripples or dunes are created, which has an effect on the bed roughness and hydrodynamic quantities e.g. tidal wave propagation. Bed load transport is only assumed for sandy sediments.

The suspension transport takes place exclusively in the water column and has been observed for both sandy and silty sediments. If the flow over the bed exceeds a critical bed shear stress for erosion of sediments, bed materials are eroded and entrained into the upper water column. For sandy sediments, the critical bed shear stress depends on the grain size and is generally derived from the Shields diagram (Hjulstrom, 1935; Shields, 1936). For silty sediments, the critical bed shear stress depends also on the degree of consolidation (Dade et al., 1992), expressed by the dry bulk density, which increases with time through self-weight compaction of the sediment matrix. In this case, water is released from the pore volume into the water column. Consequently, the higher the degree of consolidation, the bigger the shear stress must be for erosion of silty sediment.

Silty sediments are characterized by a grain size smaller than 63 μm and are only transported in suspension. In contrast to sandy sediments, silty and cohesive sediments tend to form aggregates or flocs, which can reach diameters of several hundred μm. Due to the cohesive effect, the settling is not as trivial as for sandy sediments, but depends primarily on sediment concentration. In high concentrations, an aggregate of flocs may form due

to its complex sinking behavior. Flocs hinder each other by frictional forces when they settle. As flow and turbulence decelerate, the material remains in the water column and does not directly accumulate. In this case, the suspension is referred to fluid mud that has another flow behavior compared to clear water (Coussot, 1997). By keeping fine sediment in suspension, the fluid mud exerts a major impact on the ecology. Due to high concentration and associated large surface area of flocs, bacteria adhere to them and may e.g. decompose organic matter and consume oxygen (e.g. Ems estuary (Talke et al., 2009); Scheldt estuary (Cox et al., 2003)). Due to trapping of sediments in suspension, a strong density stratification (lutocline) builds, which can exceed the stratification intensities of salinity-driven stratification by order of magnitude (e.g. Uncles et al., 2006).

Development of estuarine turbidity zones Temporal and spatial formation of a turbidity zone depends on several boundary conditions. Basically, locally residual sediment transport leading to ETM formation, can occur in estuaries based on different mechanisms. Following previous studies, four main mechanisms could be identified, where sediment trapping in estuaries arises. Turbidity zones may arise due to barotropic, baroclinic, topographic, and lateral effects (summarized by Burchard et al., 2018). The mechanisms are illustrated in Fig. 2.4 and described in the following.

Postma and Kalle (1955) have shown that baroclinic circulation drives an up-estuary transport and leads to a sediment entrapment. A turbidity zone forms near the landward limit of the salt intrusion. Mixing of marine and fluvial water ensures that suspended sediment accumulates upstream of the mixing zone. Festa and Hansen (1978) supports this hypothesis by means of a steady-state model study. They found, that in addition to the baroclinic circulation, the sedimentation rate and the sediment transport rate over the seaward and landward boundary are of crucial importance for the size and location of the ETM. The strength of baroclinic circulation depends thereby on external forces, such as gravitational force and freshwater discharge. These also cause a change in eddy viscosity (Jay and Musiak, 1994) and density stratification (Geyer, 1993), which is accompanied by a change in the expression and location of the ETM. Summarized, the landward bottom flux combined with surface seaward transport acts as driver for a residual sediment transport at the landward limit of the salt intrusion.

A barotropic circulation alone can also lead to sediment trapping in estuaries. This kind of circulation is characterized by tidal asymmetries in e.g. maximum current velocities, bed shear stress or tidal phase duration. In most cases, the turbidity zone forms in the fresh water zone. This mechanism was reported by Allen et al. (1980) based on flow patterns in various French estuaries (e.g. Seine, Gironde). Further studies have shown that this pattern mainly occurs in well-mixed estuaries, where no or only weak density-driven circulation at certain times exists (e.g. spring tides) and gravitational-induced circulation dominates (e.g. Uncles and Stephens, 1993; Brenon and Le Hir, 1999). The spatial extension and location of the turbidity zone is dependent on the freshwater inflow, which forms a residual transport in the fresh water zone together with the landward directed up-estuary transport.

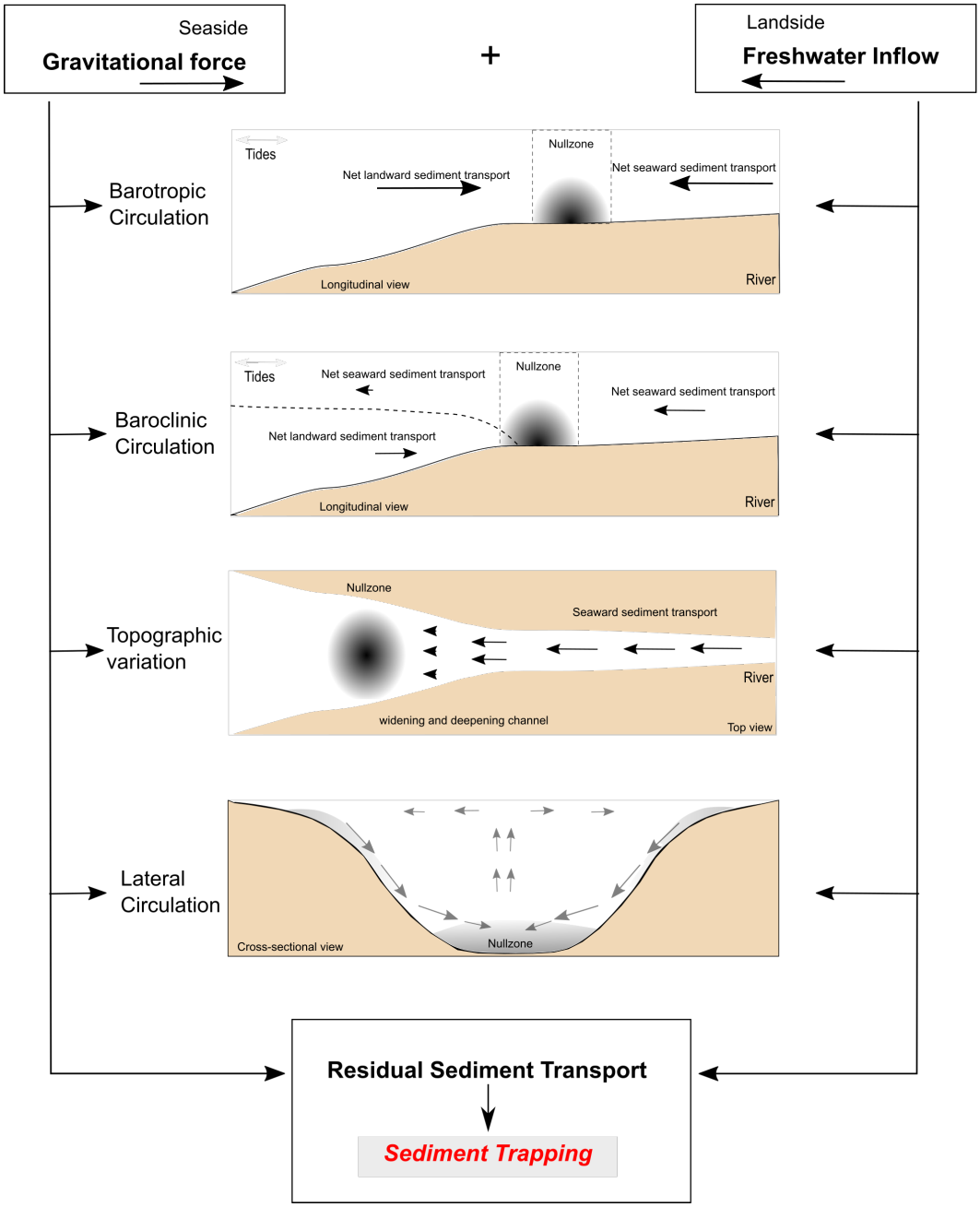

Figure 2.4: Sketch of possible circulations and flow dynamics caused sediment trapping and ETM formation (Null-zone) in estuarine environments

Strong topographical changes can also lead to sediment accumulation and deposition. This happens due to a strong decrease of flow velocities in a widening system or narrow but deep depressions. This behavior is observed in e.g. Columbia River (Jay and Musiak ,1994), Chesapeake Bay (North and Houde, 2001), Elbe estuary (Kappenberg and Grabemann, 2001), York River (Lin and Kuo, 2003), Hudson River (Geyer et al., 2001) and Delaware

estuary (Sommerfield and Wong, 2011). Furthermore, lateral changes in the topography can form lateral density gradients and thus lateral stratification effects. Here, transport from shallower regions into the deep channel leads to accumulation of sediments in deeper regions.

As a special phenomenon, high sediment transport rates of fine sediment can lead to formation of fluid mud layers, especially in sediment trapping zones such as ETM's. This behavior has already been observed in many estuaries and coastal zones worldwide. The fluid mud layer can have a thickness from a few centimeters to several meters. On the Amazon Shelf, Kineke et al. (1996) found a fluid mud layer near the salt front of several meters thickness. Talke and De Swart (2006) also observed a thick layer in the ETM of the Ems estuary (1-2 meters). The formation of fluid mud in estuaries has been demonstrated in other studies (e.g. Kineke et al., 1996; Lesourd et al., 2003; Guan et al., 2005; Uncles et al., 2006) and observed in calmed lateral areas (e.g. harbors or banks).

Timescales of estuarine turbidity zones The natural formation and dynamic evolution of turbidity zones takes place on different time scales. The response to changes in extent and location can be related to neap-spring, and to seasonal variations in hydrodynamics and freshwater inflow (e.g. Marchand, 1993). Furthermore, anthropogenic interventions and climate change can also lead to significant long-term changes (e.g. Jiang, Li, and Swart, 2012; Mittal et al., 2014; Mittal et al., 2016). Changes in the neap-spring cycle result from varying tidal amplitudes and associated effects on barotropic and baroclinic circulation. At neap tides, weaker flow velocities as well as amplified density-induced stratification results in weakening of turbulent mixing. With spring tides the turbulent mixing increases due to higher flow velocities and reduced stratification effects. This can lead to weakening of the density-induced stratification or its complete revocation. As a result, seaward or landward shift of an ETM can move over an extended area of several kilometers. At seasonal variations, with rising discharge a seaward shift and with decreasing discharge a landward shift of the turbidity zone occurs (e.g. Martin et al., 2008). The duration of the shifting process varies greatly with the type of sediment. Accumulation of fine material and sediment trapping may remove the response to increasing discharge (Winterwerp et al., 2017).

Other mechanisms which lead to a permanent shift of an ETM are associated to anthropogenic interventions. Massive extraction of water (e.g. dam building) in the upstream reaches of an estuary usually creates a landward shift (e.g. Jinghui et al., 2005). Anthropogenic interventions in the form of deepening or straightening may also lead to a landward shift of the turbidity zone (e.g. Talke and De Swart, 2006).

2.2 Fluid Mud Dynamics

Fluid mud layers with thickness of several meters can have a significant impact on the estuarine dynamics and local hydrodynamics as they occupy most of the water column (Abril et al., 1999; Talke and De Swart, 2006). According to Uncles (2002), the formation of fluid mud in estuaries is strongly dependent on the hydrodynamic boundary conditions. In a tidal cycle, the fluid mud body creates its own cycle of deposition, partial consolidation and resuspension (Fig. 2.5). Due to the accumulation and dynamics of fluid mud in turbidity zones, a reduction of the local bed shear stress is also achieved. This can lead to an acceleration of the tidal wave propagation causing an increase in tidal amplitude (e.g. Maren et al., 2015). The change in latter mechanism also have an effect in enhancement and increase of sediment transport rates (Gabioux et al., 2005).

As shown in Figure 2.5, a fluid mud layer can be classified in a mobile and a stationary layer (Schrottke et al., 2006; Becker et al., 2018). The mobile layer is classified by sediment concentration higher than 8-10 gl^{-1}. It consists of a non-Newtonian flow behavior with weak apparent viscosities and is acting on a tidal timescale (entrainment and formation). The settling behavior is described as hindered settling (McAnally et al., 2007). The stationary layer consists of concentrations greater than around 50 gl^{-1} and is acting on a neap-spring cycle (Abril et al., 1999). This layer only has a non-Newtonian flow behavior (high apparent viscosities) and is separated with a strong lutocline from above mobile layer (Papenmeier et al., 2013).

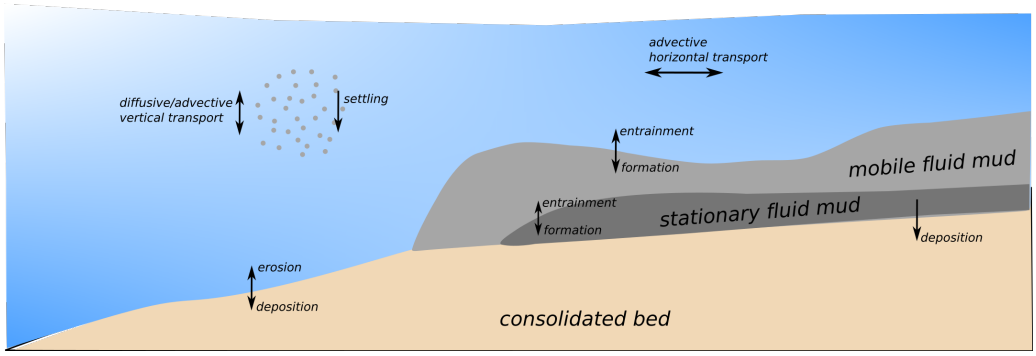

Figure 2.5: Sketch of significant cohesive sediment transport processes including formation of fluid mud layer.

Ecological effects caused by accumulation of fluid mud layers in estuarine environments have been observed by many authors (e.g. Abril et al., 1999) and are of great importance. It was observed that a rapid decrease in dissolved oxygen (DO) concentrations eventually leads to anoxic conditions in the transition from the free water body to the fluid mud body. The strain of dissolved oxygen is mainly evident in macro and mesotidal estuaries, where a turbidity zone is developed (Allen et al., 1980; Sottolichio and Castaing 1999). In

ETM, light is limited to the water column, whereby the production of dissolved oxygen is inhibited by the photosynthesis of phytoplankton (Garnier et al., 2001). In addition, primary production is reduced as a result of light attenuation, resulting in a limitation of phytoplankton (Goosen et al., 1999). Furthermore, turbidity also limits gas exchange with the atmosphere and thus an important parameter of oxygen supply. This simplified behavior clearly increases with the formation of fluid mud layers, since the formation also has a greatly increased sediment transport and thus increases the turbidity by a multiple. Therefore, understanding of fluid mud dynamics are of great importance to overall estuarine flow dynamics and ecology state.

2.2.1 Formation and composition

Fluid mud is a clay-silt mixture with portion of organic matter and is generally referred as a high concentrated aqueous cohesive sediment suspension. The concentration range varies from 10 gl^{-1} to a few hundred gl^{-1}, depending on mud sources and composition (Ross and Metha, 1989; Winterwerp and Van Kesteren, 2004). Fluid mud is additionally defined in which settling is substantially hindered by the proximity of sediment grains and flocs (McAnally et al., 2007). For the formation of fluid mud, sufficient amount of fine sediment must be available in the water column. The high amount of fine sediments then forms a fluid mud layer in combination with its settling processes and effect on turbulence.

The cohesive sediment particles agglomerate into flocs and deposit due to collisions between the sediment grains. The latter are caused by electrochemical forces (cohesion), sinking speed, turbulence and Brownian motion (Van Leussen, 1988). Furthermore, the formation of fluid mud is also influenced by biological processes (Widdows and Brinsley, 2002). Bacteria and microphytobenthos tend to stabilize sediments as they secrete sticky Extracellular Polymeric Substances (EPS; Wotton, 2004). The flexible EPS coat connects particles of the sediment and is known to enhance cohesion and adhesion of cohesive sediments (Black et al., 2002). Formation and flow behavior of fluid mud layers results from local hydrodynamic constituents caused by external forces like waves, currents or gravitational flow. The presence and formation of fluid mud layers can result in very high transport rates of cohesive sediments, even though the flow velocity is relatively small (Kranenburg, 1998). This behavior is caused due to the much higher kinematic viscosity of high-concentrated fluid mud compared to e.g. clear water. The viscosity of fluid mud can be several magnitudes higher than that of water. The increase in viscosity is caused by sediment-particle interaction. Following Kranenburg (1994) this particle-interaction starts at very low volumetric concentrations of around 8 % depending on of fractal dimension of particle aggregates. This volumetric concentration can also be considered as the beginning of hindered settling state. In the hindered settling range, non-Newtonian flow behavior becomes important or even dominant.

Fluid mud describes a certain state of cohesive sediments, which is assigned to specific physical or biological processes (e.g. Kirby, 1988; Winterwerp, 1999; Bruens, 2003). Mainly,

fine cohesive sediment dynamics can be classified by its sediment concentration as summarized in Fig. 2.6. This relatively simple classification incorporates local suspension concentration, vertical stratification intensity, settling rate, and flow behavior. It includes all relevant physical properties that are imperative for a large-scale numerical modeling without consideration of detailed biological activities.

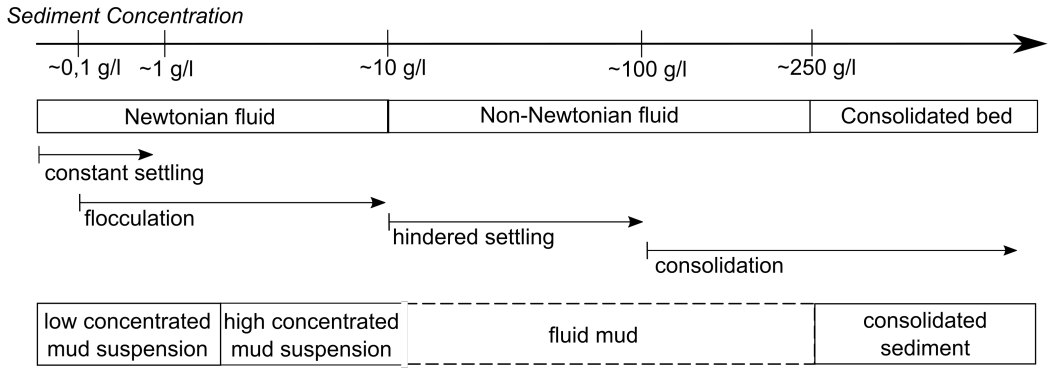

Figure 2.6: Classification of silty sediment states depending on sediment concentration (adopted from Nakagawa et al., 2012).

2.2.2 Rheology

Fluid mud properties, particularly its rheological ones, are important for the prediction of its flow behavior (e.g. whether mud deposited on a slope can flow under gravity), for the estimation of sensitivity to erodibility, and damping of turbulence (Kranenburg and Winterwerp, 1997). Following Coussot (1997), fluid mud is classified as a non-Newtonian fluid with a high viscosity and generally allows laminar flow conditions. In contrast to a Newtonian fluid, fluid-mud serves as non-Newtonian fluid, where the rheological shear stress and viscosity is a function of the shear rate (Fig. 2.7). The rheological flow behavior of fluid mud is classified as a shear-thinning and thixotropic behavior with changes in viscosity by an order of magnitude and more.

The rheological properties become important, when suspended sediments reach a volumetric sediment concentration of approximately $\sim 8\%$, where a network of aggregates may be present (Kranenburg, 1994). The exact threshold depends on the fractal dimensions of the aggregate particles. Properties of fluid mud are strongly influenced by hydrodynamics and mud composition (sediment concentration, salinity, mineralogical composition, organic matter and pH) (Berlamont et al., 1993). Therefore, a process-based analysis of rheological induced parameters is essential to understand the affected flow behavior. Extensive research has been already carried out to take into account rheological properties in lab

investigations based on estuarine water samples. Studies and investigations were carried out for example in the Caland Channel (Van Kessel and Blom, 1998), Haihe estuary (Bai et al., 2002), Eckernförde Bay and Kieler Förde (Faas and Wartel, 2006), Hangzhou Bay (Huang and Aode, 2009), Weser and Ems estuary (Papenmeier et al., 2013), Yangtze River (Yang et al., 2014), Lianyungang (Xu and Huhe, 2016).

The rheology deals with the flow behavior of suspensions and the deformation behavior of solids. A dependence between the flow behavior and the deformation consists in the fact that deformations caused by shearing forces reduces the resistance of substances to flow. Every natural substance has a viscous and an elastic part. This behavior is called viscoelastic behavior and describes the flow behavior below a given yield point (τ_y). The viscous part behaves according to the Newtonian law and the elastic part, which describes the deformation, according to Hooke's law. Viscous behavior is called when a relative movement of the particles is enforced and thereby usually an internal friction process takes place which leads to a viscous shear heating. Due to the shearing process, portions of the substance consume deformation energy which, due to the relative movements, leads to a lasting change and creates a permanent deformation. Above the yield point, a plastic behavior of the substance is observed, which describes the ability to irreversibly deform under the action of force and begins to flow, and to maintain deformation. The viscoelastic flow behavior is described for Newtonian fluids by the Newton law:

$$\tau = \mu\dot{\gamma} \tag{2.1}$$

The dynamic viscosity μ describes the flow resistance due to relative motion. For Newtonian fluids, the shear stress is linearly related to the shear rate and the viscosity is independent of the magnitude and duration of the shear stress (Fig. 2.7).

Non-Newtonian fluids are characterized by a varying viscosity as a function of shear stress or applied shear rate. Thereby, most of common non-Newtonian fluids are showing shear thinning flow, where the viscosity decreases with increasing shear rate. Typical rheological flow curves in double logarithmic scale are mostly used to illustrate this flow behavior. At low shear rates, non-Newtonian fluids are characterized by an initial viscosity, also termed zero shear viscosity. This initial viscosity results from particle interactions and regenerative effects of Brownian motion. Highly shear-thinning fluids (fluid mud) consists of a yield stress, where the initial viscosity becomes infinite and the material characteristic behaves like a solid. Below the yield stress the material is able to build an interparticle network of the biogenic content by means of extracellular polymeric substances (binding force). This network must be broken for the material to flow. After yielding this threshold, a decrease of particle interaction combined with an increase of space between particles leads to the decrease of the viscosity. The drop of viscosity is limited up to the infinite shear viscosity, which is associated with the maximum degree of orientation of the network. This minimum viscosity is largely dependent on the suspended particle concentration and related hydrodynamic force. When the shear thinning behavior is reversible by decreasing

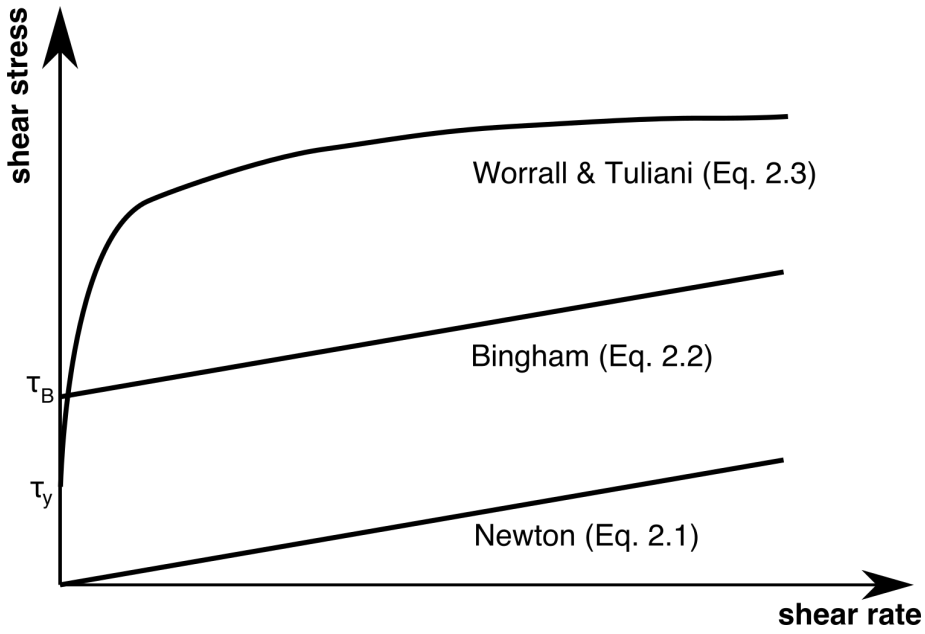

Figure 2.7: Rheological constitutive laws describes behavior of shear rate to shear stress.

shear rate but time dependent the fluid is considered additionally to be thixotrope.

The flow behavior of the non-Newtonian fluid viscosity or shear stress related to applied shear rate can be mathematically described by rheological models. Dependent on data availability and range to be considered in analysis, different models are developed in previous studies. For example take into account only the decrease in viscosity the *power law* model is one of the most common models. There are other models available considering additionally a yield stress (Bingham, 1922; Herschel and Bulkley, 1926) or thixotropic behavior (Worrall and Tuliani, 1964; Toorman, 1997). These models were developed in the last decades to describe the flow behavior of non-Newtonian fluids. Differences in mentioned models are mainly based on the number of parameters and respectively accuracy to describe shear deformation of the fluid. It can be assumed, using rheological models with three or more parameter, a better description of shear stress at low shear deformation rates could be achieved (Bartosik, 2010).

The simplest rheological model consisting of a yield stress is the Bingham plastic model, where the flow behavior above the yield stress is described as a Newtonian fluid:

$$\tau = \tau_B + \mu\dot{\gamma} \tag{2.2}$$

Here, the relation between shear rate and stress is linear, with the yield stress defined as intercept. The Bingham Model neglects shear thinning behavior where viscosity decreases with increasing shear rate.

The often used Bingham plastic rheological model is only suitable describing flow behavior at shear rates above 20 s^{-1}, as it fails to describe the structural changes at lower shear rates (Van Kessel and Blom, 1998). The Bingham model should therefore not be used for typical situations, where the shear rates become small and the fluid is characterized as a shear thinning fluid. Shear rates typically encountered in the field of estuaries are quite low and often not exceed a few s^{-1}. Toorman (1997) has described the Bingham yield stress were only derived due to errors in rheological analysis and the true yield stress must be currently much lower. Regarding this lower shear rate range, shear thinning must be incorporated in the model approach, which requires a multi parameter model. Such a model was presented by Worrall and Tuliani (1964), incorporating thixotropy and structural changes within particles aggregation due to shearing and is also used by previous modeling studies of fluid mud flow (e.g. Wehr, 2012). The mathematical formulation of the viscosity to shear rate following the approach of Worrall & Tuliani is written as:

$$\tau = \tau_y + \mu_\infty \dot{\gamma} + (\mu_0 - \mu_\infty)\dot{\gamma}\lambda \tag{2.3}$$

The rheological model derives a constitutive approach with a structure parameter (λ) to consider the aggregation state. The structure parameter describes the recovery and break-up of floc aggregates. This parameter is usually parameterized by a rate-equation. Moore (1959) firstly derived such a differential rate-equation based on the structural kinematic theory for the recovery and break-up of floc structure and its thixotropic behavior:

$$\frac{\partial \lambda}{\partial t} = a(\lambda_0 - \lambda)^\alpha - b\dot{\gamma}\lambda^\delta \tag{2.4}$$

The model proposed by Worrall and Tuliani (1964) is based on the model of Moore (1959) and it is extended with a yield stress. Here, the break-up of the floc structure depends on the shear rate as well as historical deformation state of the floc structure itself. The empirical coefficients (α, δ) are generally set to one which corresponds to the original first-order rate equation proposed by Moore (1959). For a mathematical description of the rheological fluid, empirical parameters must be analyzed by means of lab investigations. Experiments are performed using a rheometer with couette, parallel plate, or cone and plate geometry. Thereby, shear stress and viscosity is measured dynamically as a function of shear rate. Afterwards, an empirical fit of measured data determines required model constants (μ_∞, μ_0, τ_y, a, b).

2.2.3 Laminar to turbulent flow transition

From previous literature it is known that fluid mud has a significant damping effect on turbulence production and can provide laminar flow behavior (e.g. Coussot, 1994; Kessel and Kranenburg, 1996; Parsons et al., 2001). The potential damping of turbulence due to vertical density gradients (buoyancy driven) can be described by the well-known Richardson

Gradient Number (Richardson, 1922):

$$Ri_g = \frac{-g\frac{\partial \rho}{\partial z}}{\rho\left[\left(\frac{\partial u}{\partial z}\right)^2 + \left(\frac{\partial v}{\partial z}\right)^2\right]} \tag{2.5}$$

The Richardson Gradient Number describes the ratio of buoyancy force to shear rate induced turbulence production. For $Ri_g \geq 0$ the flow is stable stratified, whereby for $Ri_g < 0$ the flow is unstable stratified. However, the scope of the application of the Richardson Gradient Number is only limited to turbulent flow conditions, where turbulent production is generated from velocity shear or the boundary shear layer. Laminar flows can also show a vertical velocity gradient, which cannot be associated to turbulence production. Therefore, turbulence cannot only be damped according to mentioned density-induced gradient criteria in potentially laminar flow conditions.

Another parameter which is often used in laminar to turbulent flow transition is the Reynolds Number (Re). This number describes the transition from laminar to turbulent flow behavior in e.g. pipe flows (Reynolds, 1883a; Reynolds, 1883b):

$$Re = \frac{uL}{\nu_m} \tag{2.6}$$

Here, the ratio of a velocity length scale (distance from the wall and local mean flow velocity) to the kinetic viscosity of the fluid describes the current flow conditions. From literature a critical value of Re > 2300 is known, where laminar flow switches suddenly to a turbulent flow. Below the critical Reynolds number, the flow is still laminar and might show vertical velocity shear. Based on required velocity length scale for calculating the Reynolds number, the transient flow from laminar to turbulent flow regime is dependent on the distance to the wall. In laminar flow regime, the viscous sub-layer increases with decreasing Reynolds number. Therefore, describing the flow regime by the Reynolds number requires a flow transition based on only bottom generated viscous flow. For a non-Newtonian fluid, such as fluid mud, the flow condition is not only directly dependent on the development of the viscous sub-layer, but also on the specific properties of material. This shows that the Reynolds number is not a suitable parameter describing the transition from laminar to turbulent flow regime of fluid mud, or the turbulence damping effect of rheology-induced flow effects in open channel flows.

Previous modeling investigations by Hsu and Traykovski (2007) used a turbulence damping approach as a function of volumetric suspended concentration to the gel concentration. Turbulent mixing is totally suppressed above a concentration, which corresponds to the gel concentration. This has the disadvantage that no entrainment from the stationary fluid mud layer (concentrations above the gel concentration) or bed sediments will occur. This contrasts with the neap-spring variability of observed stationary fluid mud layer behavior (e.g. Abril et al., 1999). It is suggested, that during the change from neap to spring tide

material is entrained from the stationary layer, mixed and transported into the upper water column. When switching from spring to neap tide, settling from mobile into stationary layer arises and leads to an increase of this high-concentrated layer. Becker et al. (2018) have confirmed the entrainment behavior from the stationary layer by high resolution stationary measurements within a tidal cycle. Therefore, a dependence of the turbulence damping on the volumetric concentration in long-term morphological investigations, especially of natural estuaries would entail a restriction to local sediment transport rates. Moreover, this approach would lead to an underestimation of the long-term development of the morphology. In summary, proposed approach by Hsu and Traykovski (2007) for damping of vertical momentum and mass transfer cannot be applied to the numerical modeling of large-scale fluid mud layer and sediment transport dynamics in estuarine environments.

However, a physical description of the transitional flow effect is necessary to include the influence of highly concentrated suspensions on hydrodynamics. This influence was already suggested in many previous studies, but could not be verified so far and is further unclear (e.g. Revil-Baudard et al., 2015). Nevertheless, accounting the required effect of fluid mud layer dynamics on turbulent momentum exchange is a key physical mechanism.

2.2.4 Settling of cohesive sediment

Settling of sediment particles are important determining deposition, erosion and transport of sediment in suspension (e.g. Chesher and Ockenden, 1997; Van Ledden, 2002; Baugh and Manning, 2007; Waeles, Le Hir, and Lesueur, 2008; Soulsby et al., 2013). In dilute suspensions, particles have no tendency to flocculate and settle as individual, because non existing significant interaction with neighboring particles occur. At higher suspension concentrations ($\sim$0.1 g l^{-1} < C < $\sim$10 g l^{-1}) floc size increases and consequently the settling velocity increases with suspension concentration (flocculation). Chemical precipitates formed in coagulation and other destabilization processes tend to agglomerate, while settling as a result of inter-particle collisions. This process is also strongly dependent on the local turbulence and various formulations, which can be found in the literature (e.g. Piirto and Saarenrinne, 1999).

Fluid mud itself owns two different types of settling (Fig. 2.6 & Fig. 2.8). The first is known as hindered settling, which reduces the effective settling rate by means of particle interaction (Dankers and Winterwerp, 2007). It is expressed by an empirical correlation as a function of the effective volumetric concentration. The concentration range at hindered settling begins at SSC = 8-12 g l^{-1} (Mehta et al., 1989), which also describes the beginning of fluid mud like behavior. Secondly, if the suspension concentration becomes greater than the gel concentration, settling behavior will shift into a weak consolidation (Kirby and Parker, 1983). Both rates of settling are differentiated by strong lutoclines in the vertical SSC profile (e.g. Abril et al., 1999).

Fluid mud in hindered settling state is described as mobile fluid mud and during weak consolidation as stationary fluid mud (e.g. Papenmeier et al., 2012). Additionally, stationary

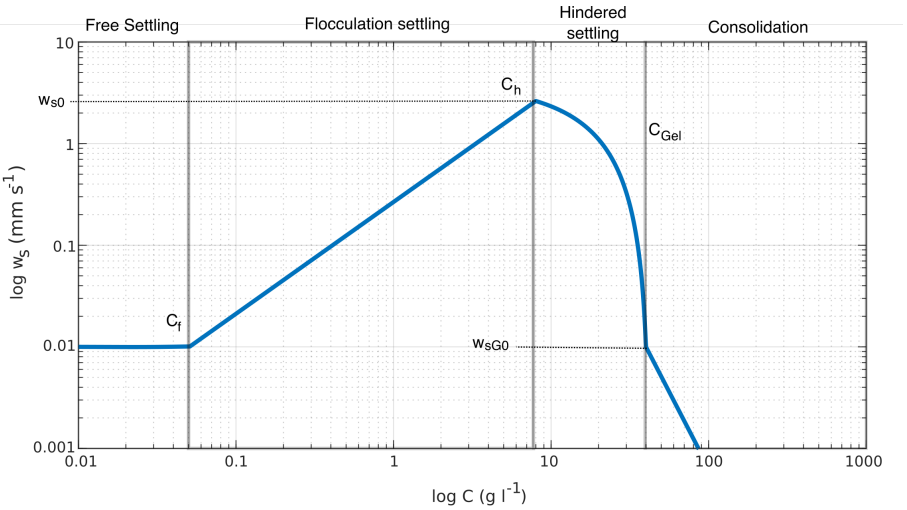

Figure 2.8: Double logarithmic sketch of the settling velocity approximation against suspended sediment concentration. Settling of cohesive fines is divided in four regimes with free settling, flocculation, hindered settling and consolidation regime

fluid mud is characterized by a prevailing measurable effective stress (difference between the total stress and pore water pressure) (Fig. 2.9).

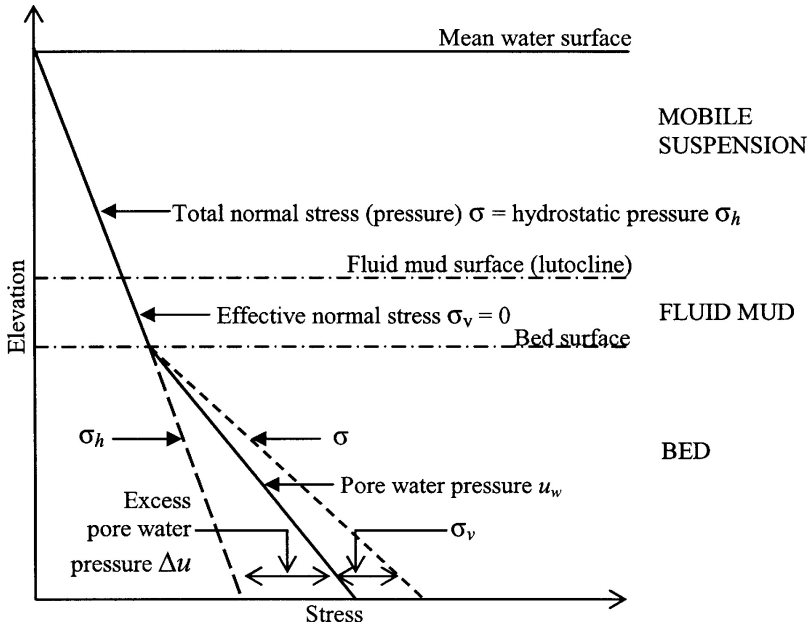

Figure 2.9: Schematic of instantaneous stress profiles in a water-mud system (Mehta et al. 1994)

The difference between aforementioned two layers by forming an effective strain has been

described firstly by Terzaghi and Peck (1948). Based on the presence of the effective pressure, a threshold between mobile and stationary fluid mud may be defined. This threshold e.g. is measured in the Combwich estuary between 80 and 220 g l^{-1} (Sills and Elder, 1986) and in the Ems estuary between 90 to 120 g l^{-1} (Seifert, 2011). However, the threshold depends on various criteria, such as sedimentation rate, initial concentration and time or stress history (Sills and Elder, 1986), which is also described as the gel concentration. The mathematical description of the degree of consolidation becomes an important parameter in modeling of long-term morphological changes. The further consolidation has progressed, the higher the resistance of sediment material against erosion caused by progressing increase of the dry bed density (e.g. Toorman, 1996; Winterwerp, 1999; Merckelbach, 2000).

2.3 Modeling of high-concentrated suspensions

2.3.1 Introduction to Numerical Models

Estuaries are dynamic ecosystems, which show complex physical relations to the sea-side tidal force and landside river discharge variation. The mixing of different dense water masses combined with fluctuating water level elevations and corresponding fluctuating flow conditions lead to a complex physical behavior. Numerical models are often used to investigate these complex phenomena. Depending on the type of an estuary, different numerical models have been used to investigate these specific hydro- and morphodynamic current and/or transport characteristics:

- *1D* are one dimensional models and often used for modeling river systems or floodplains (e.g. Dimitriadis et al., 2016). The flow direction is assumed to be only in longitudinal direction, because this models represents the bathymetry and landscape as a sequence of cross-sections. It computes the flow behavior as time-averaged velocity over the local depth at each computational grid point (Cook and Merwade, 2009).

- *2D* models used for stationary or instationary flow conditions, where the fluid can flow in both directions, longitudinal and lateral. It is often used in ocean, river, coastal areas or in well-mixed estuaries, where density-driven flows can be neglected (e.g. HongbinZhou and Lianxiang, 1988; Guo et al., 2011). Turbulence production by horizontal velocity shear is neglected in such models. Only bottom boundary induced turbulence is applied by the assumption on an algebraic logarithmic distributed velocity profile.

- *3D* models are used in coastal zone or partially and strong stratified estuarine environments, where a more complex geometry is present (e.g. Maren et al., 2015; Hesse et al., 2019). Turbulence production is resolved in horizontal and vertical direction. It allows not only bed boundary driven turbulence production, but also induced by vertical velocity shear.

Partially mixed and fully stratified estuaries must always be modeled using a three dimensional model approach. Latter is required caused by temporally and/or spatially occurrence of strong vertical and/or horizontal density gradients (Kent and Pritchard, 1959). These mainly salinity-induced stratifications are the main driver of the estuarine (baroclinic) circulation and corresponding development of an ETM. In past decades, a whole series of numerical models have been developed taking into account this complex baroclinic mode (e.g. Mike3, Telemac, Delft3D, SMOR3, SCHISM). Some models are available as open-source, which significantly increases the number of users and thus gives the opportunity for further developments as well as community discussions.

One of the key mechanism in numerical modeling is related to the reproduction of natural physics, which requires a detailed calibration based on specific data-sets. Measured data can only represent a limited part of the real estuarine physics, therefore models are involved to analyze the large-scale dynamics. This is reasonable, because measurements are temporally and spatially restricted to solve such dynamics. Data sets alone describing a clear understanding of an estuary are usually too time-consuming and expensive. Therefore, using models studying large-scale dynamics requires a detailed validation of the estuarine circulation and hydrodynamic force (e.g. tidal wave propagation). The mixing of salt and fresh water as well as corresponding horizontal and vertical stratification effects induced by density gradients are coupled with complex mechanisms (Geyer and MacCready, 2014). These processes also have a strong influence on the sediment transport and extend the understanding of a complete system. Especially for partially and strong stratified estuaries with higher sediment transport rates, this remains usually a challenge (Kärnä et al., 2015).

However, modeling of density driven dynamics associated with its complex flow conditions have to be reproduced by the model and its individual configuration. Salinity as well as sediment dynamics are mainly controlled by the turbulence interaction with its buoyancy driven turbulence damping functions. A further important aspect of high concentrated sediments is related to the settling velocity, where in contrast to sandy sediments, the settling velocity of silty sediments is more dependent on the sediment concentration, rather than on the grain size. These physical mechanisms, as well as turbulence interaction in shallow water conditions will be further discussed in this section.

2.3.2 Reynolds-Averaged Navier-Stokes equations

The Reynolds-Averaged Naiver-Stokes (RANS) equations describe the flow of a viscous Newtonian fluid and are derived from the Navier-Stokes equation through temporal averaging of instantenous velocities. This simplification results in a shift of correlated fluctuating velocities from the momentum equation to Reynolds stress terms (τ_{ij}). The three-dimensional RANS equations including two kinds of equations, the continuity equation (2.7) for the conservation of mass (here for a non-compressible fluid) and the momentum

equations (2.8 - 2.10) for each flow direction (x, y, z):

$$\frac{\partial u}{\partial x} + \frac{\partial v}{\partial y} + \frac{\partial w}{\partial z} = 0 \tag{2.7}$$

$$\frac{\partial u}{\partial t} + u\frac{\partial u}{\partial x} + v\frac{\partial u}{\partial y} + w\frac{\partial u}{\partial z} - f_v = -\frac{1}{\rho_0}\frac{\partial p}{\partial x} + \frac{1}{\rho_0}(\frac{\partial \tau_{xx}}{\partial x} + \frac{\partial \tau_{xy}}{\partial y} + \frac{\partial \tau_{xz}}{\partial z}) \tag{2.8}$$

$$\frac{\partial v}{\partial t} + u\frac{\partial v}{\partial x} + v\frac{\partial v}{\partial y} + w\frac{\partial v}{\partial z} - f_u = -\frac{1}{\rho_0}\frac{\partial p}{\partial y} + \frac{1}{\rho_0}(\frac{\partial \tau_{xy}}{\partial x} + \frac{\partial \tau_{yy}}{\partial y} + \frac{\partial \tau_{yz}}{\partial z}) \tag{2.9}$$

$$\frac{\partial w}{\partial t} + u\frac{\partial w}{\partial x} + v\frac{\partial w}{\partial y} + w\frac{\partial w}{\partial z} = -\frac{1}{\rho_0}\frac{\partial p}{\partial z} + \frac{1}{\rho_0}(\frac{\partial \tau_{xz}}{\partial x} + \frac{\partial \tau_{yz}}{\partial y} + \frac{\partial \tau_{zz}}{\partial z}) + \frac{1}{\rho_0}\rho g \tag{2.10}$$

As mentioned, the continuity equation represents the conservation of mass within a control volume by the balance of mass fluxes into and out of the volume. The momentum equations consisting of six different types of forces, which are balancing the sum of applied forces acting on a fluid element:

- The time-dependent change of a moving fluid element (first term on the left side)
- The advection force (second term on the left side)
- The Coriolis force acting on the x and y direction (third term). This parameter is important when modeling large water bodies.
- The pressure force (first term on the right side)
- The viscous force (second term on the right side)
- The gravity force acting in the z-plane

The Reynolds stress terms (τ_{ij}) are representing the shear tensor, which consists of the molecular and turbulent (Reynolds) stresses. Generally, the molecular stress is much smaller than the turbulent ones and are mainly neglected in large-scale numerical modeling approaches. However, the turbulent stresses cannot be neglected and have to be computed to achieve closure of the RANS equations. The Reynolds (turbulent) stress terms have to be solved by a so-called turbulence closure model.

2.3.3 Turbulence

Free surface natural flows are turbulent and have to be considered in numerical modeling of natural environments. Turbulent flow is not generally defined, but determined as chaotic, deterministic and could mathematically be described by the Navier-Stokes equations. Turbulence generally increases vertical and/or horizontal exchange of momentum and suspended or dissolved material. The turbulent transport itself can be quantified based on the Reynolds-Averaging method. At a specific location, as instantaneous variable (e.g.

velocity) can be divided into a mean and a fluctuating time-dependent part:

$$\overrightarrow{u} = \overline{u} + u' \tag{2.11}$$

Flow velocities in RANS equations are averaged in time over a certain period and they are creating a new term called Reynolds shear stress tensor, which is assumed to be symmetric. This term includes the correlations of fluctuating velocities and is unknown (*closure problem*). The closure problem is solved by so-called empirical turbulence models.

Turbulent motion consists of a kinetic energy spectrum with different scales, which are described by its eddy size. Application of the *Fourier analysis* on a specific time series of the fluctuating velocity component gives a representative way to calculate the turbulent kinetic energy spectrum. The turbulent kinetic energy is generally the sum of all three fluctuating velocity components:

$$TKE = \frac{1}{2}\left(\overline{u'^2} + \overline{v'^2} + \overline{w'^2}\right) \tag{2.12}$$

In Figure 2.10 a typical turbulent energy spectrum of the turbulent structures (eddies) compared to the wave length is shown. It illustrates the production, the transfer and the dissipation of turbulent eddies at corresponding frequencies (scales).

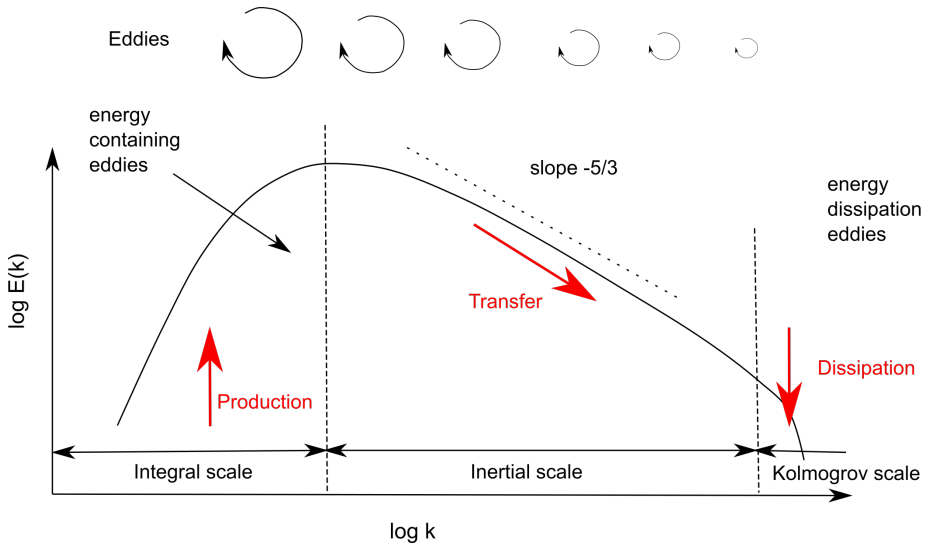

Figure 2.10: Turbulent kinetic energy spectrum illustrating integral, inertial and Kolmogorov eddy scales during cascade process (modified from Chorin, 1994).

The energy spectrum can be classified in three zones of different scales:

- Integral scale: Production of turbulent kinetic energy
- Inertial subrange: Transfer of energy from larger eddies to smaller eddies

- Kolmogorov scale: Dissipation, where kinetic energy is transformed into thermal energy

Largest eddies are of the order of the flow geometry and receive their energy from the mean flow, while kinetic energy from smallest eddies are dissipated into thermal energy by viscous forces (stresses). The smallest eddies correspond to the value of the molecular viscosity and have no dependencies on larger eddies or mean flow. Their size is defined as the Kolmogorov micro-scale:

$$\eta = \left(\frac{\nu_m^3}{\epsilon}\right)^{1/4} \tag{2.13}$$

The dissipation (ϵ) is proportional to the kinetic molecular viscosity and the larger the viscosity, the larger scales are dissipated. The transfer of kinetic energy from larger to smaller eddies is referred to as cascade process. The existence of this process requires highly turbulent fluid flow (high Reynolds Number). During cascade process (transfer), large scale macro eddies are stretched by local velocity gradients into smaller micro-scale eddies and kinetic energy is destroyed by viscous (frictional) forces. This exists at all scales, but they are larger the smaller the eddies. The strength of the velocity gradients depends on the content of energy being transformed. It makes clear that the higher the energy to be transformed, the higher the velocity gradients have to be. More information about the energy cascade and responsible as well as involved conditions/dynamics can be found in e.g. Chorin (1994).

Turbulent Boundary Layer Knowledge of the velocity and turbulence distribution near the wall is of particular interest in shallow water regions such as estuaries. This is because, the rough bed induced turbulence production is important for the tidal wave propagation and corresponding vertical and horizontal velocity distribution as well as stratification behavior. Turbulence production caused by the bed roughness is advected upward and affects the upper velocity profile. Close to the wall, the turbulent structure is dissipated to zero caused by acting no-slip condition. Immediately on the wall, the flow is strongly disturbed, since fluctuations with wall normal direction are attenuated and redistributed, but strongly anisotrop. In this layer, viscous forces are dominating the flow structure. With increasing distance from the wall turbulence increases, but still remain anisotrop (Fig. 2.11).

With decreasing distance to the wall, the velocity fluctuations as well as the Reynolds shear stresses become zero. Therefore, integration of the RANS-equation in vertical direction taken into account the boundary condition $z = 0$ results in the wall shear stress equation, which can be written as:

$$\tau_b = \rho\nu_m \frac{\partial \overline{u}}{\partial z} - \rho\overline{u'v'} = \tau_{mol} + \tau_t \tag{2.14}$$

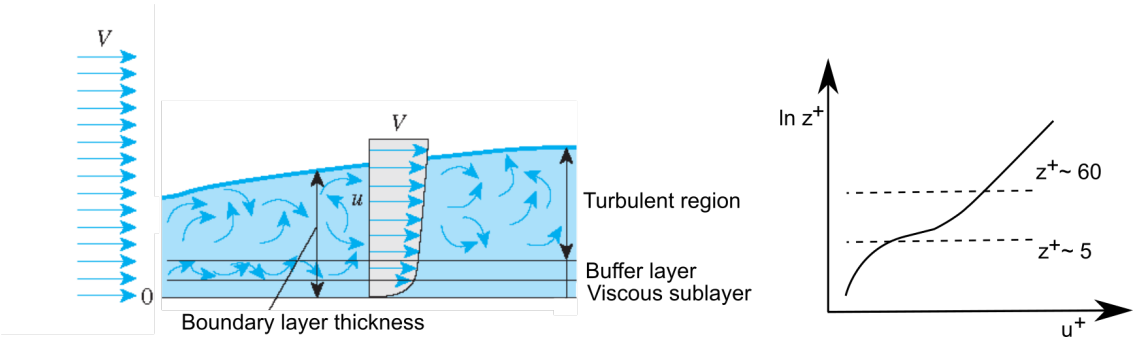

Figure 2.11: Left: Vertical structure of the wall boundary layer, and the different flow regions (left panel). Right: Dimensionless velocity profile of a turbulent boundary layer (modified from Baumann, 2012)

The wall shear stress formulation consist of a molecular (viscous) and a turbulent part. The first term of the right side describes the molecular (viscous) part, while the second term describes the turbulent part based on the fluctuating velocity quantities. In the turbulent region, the molecular part in Eq. 2.14 can be neglected, while within the viscous sublayer the turbulent quantity becomes zero. To identify the interface between molecular and turbulent region two dimensionless parameters are used, the dimensionless distance to the wall, and the dimensionless mean velocity. The mean velocity ($\overline{u}$) becomes dimensionless by achievement of the bed shear velocity (u_*), which is described by the relation of acting shear stress to fluid density. Also, the distance to the wall becomes dimensionless by taken into account the velocity u_*:

$$u^+ = \frac{\overline{u}}{u_*} \qquad z^+ = \frac{z u_*}{\nu_m} \qquad u_* = \sqrt{\frac{\tau_b}{\rho}} \tag{2.15}$$

Thereby, the non-dimensional distance to the wall is additionally dependent on the molecular viscosity. Based on this distance to the wall (z^+), the velocity distribution near the wall can be subdivided into three regions with a continuous transition (Fig. 2.11):

$z^+ < 5$	laminar (viscous) sublayer	$\tau_{mol} << \tau_t$
$5 < z^+ < 60$	transition region	$\tau_{mol} \sim \tau_t$
$z^+ > 60$	turbulent (logarithmic) layer	$\tau_{mol} >> \tau_t$

This classification is confirmed by different studies (e.g. Schlichting and Gersten, 2000). The velocity distribution within the viscous sublayer can be written considering the no-slip boundary condition (u(z=0)=0) as:

$$u^+ = z^+ \tag{2.16}$$

Based on above equation the velocity profile in the viscous sublayer (z^+ <5) is assumed to be linear distributed and increases with distance to the wall. For locations further away from the wall (z^+ >60) the velocity distribution can be assumed as a logarithmic distributed profile (dimensionless) and was developed firstly by Prandtl (1932):

$$u^+(z^+) = \frac{1}{\kappa} \log z^+ + IC \tag{2.17}$$

with $\kappa = 0.41$ the von Karman constant and the integration constant $IC = 5$ for a fully developed flow in hydraulically smooth conditions (e.g. Zanke (1982), Fernholz et al., 1996; Osaka et al., 1998). Also other values for the integration constant can be found in literature, because it is related to a fix high above the wall boundary, where the turbulent region begins. A good overview can be found in the book of Zanke (1982). This is mainly linked to the texture or roughness of the wall, and can be vary between different physical experiments. Therefore, for rough surfaces (e.g. a sediment bed), the integration constant IC has to be modified and depends strongly on the surface roughness. The wall roughness itself can be described by the roughness Reynolds number, which is equivalent to the dimensionless distance to the wall:

$$Re_r = \frac{k_s u_*}{\nu_m} \tag{2.18}$$

with k_s the equivalent sediment roughness, which can be assumed as the 2.5 of the mean sediment grain diameter in case of only considered particle induced roughness effects (k_s = $2.5d_{50}$) (Fredsøe and Deigaard, 1992). A flow is generally classified as hydraulic smooth, if $Re_r < 5$ and where all the rough elements being part of the viscous sublayer. When $Re_r > 60$ the flow is classified as hydraulic rough and the viscous sublayer is very thin. The roughness elements become part of the turbulent layer (Graf and Altinakar, 1998). Therefore, in case of a rough wall the logarithmic velocity profile must be modified including effects of the wall roughness and is written in physical dimensions as:

$$u(z) = \frac{u_*}{\kappa} \log \left(30 \frac{z}{k_s} \right) \tag{2.19}$$

When k_s is replaced by the effective roughness length $z_0 = k_s/30$ (Nikuradse, 1933) for hydraulically rough flow, the logarithmic velocity equation can be finally written as:

$$u(z) = \frac{u_*}{\kappa} \log \left(\frac{z}{z_0} \right) \tag{2.20}$$

Based on the above description, it becomes clear that the bed shear stress is strongly dependent on respective hydraulic conditions (smooth or rough). The roughness length (z_0) for grain induced roughness effects has to be verified by sediment samples from the river bed. To determine the composition of a sediment sample in terms of mean grain size,

a variety of methods in which always an equivalent diameter (e.g. d_{50}) is determined are proposed in the past.

In modeling of estuarine environments, using RANS-equations, always a turbulent flow near the wall is assumed and therefore, calculating the near bed shear velocity is based only on the turbulent part of the bed shear stress equation (Eq. 4.19). The viscous sublayer is not resolved in such kind of models, because it requires a very fine vertical resolution near the wall boundary layer (typical thickness is less than a millimeter), which causes very high computational times. More information about the turbulent boundary layer and logarithmic velocity law as well as turbulent and rough flows can be found in Zanke (1982) or Malcherek (2007)

Modeling Turbulent Interaction A turbulence model is a mathematical model that approximates the physical behavior of turbulent flow. Modeling of turbulence in large scale estuarine models (solved with RANS equations) is mainly performed by the Boussinessq eddy viscosity approximation (Boussinesq, 1877). It is much simpler and less time-consuming than solving the full time dependent Navier-Stokes equations. In costal and large-scale estuarine models, eddy viscosity models are used. Latter model approximation is based on the Newtonian stress approach and is written as:

$$\tau_f(z) = \rho\nu_t \frac{\partial \overline{u}}{\partial z} \tag{2.21}$$

Here, the Reynolds stress tensor in the time-averaged Navier-Stokes equation is replaced by a turbulent seemingly viscosity and is multiplied with the mean velocity gradient. Compared to the molecular viscosity, the turbulent viscosity is not a material specific constant and is dependent on local conditions and time-averaged velocity. This eddy viscosity model needs an expression for the turbulent viscosity ν_t. First, Prandtl (1925) found an expression to describe the turbulent viscosity based on his mixing length theory:

$$\nu_t = l_m^2 \frac{\partial \overline{u}}{\partial z} \tag{2.22}$$

In this model, also called Prandtl Mixing Length (PML) model, the turbulent velocity scale is given by vertical gradients of the horizontal velocity pattern and the physical mixing length is described as the turbulence length scale (largest eddy size). This simplification is reasonable, because these scales are responsible for most of the transport caused by turbulent diffusion. The mixing length is generally unknown and has to be determined. In the turbulent boundary layer with flow parallel to the boundary it can be assumed as:

$$l_m = \kappa z \tag{2.23}$$

This equation suggests a linear increasing mixing length with increasing distance to the wall

(Prandtl and Tietjens, 1934). With the Prandtl's mixing length approach, it is possible to derive turbulent flow structures with a character of the boundary layer, but in case of free turbulence production a more detailed description is necessary. Independent to the work of Kolmogorov (1942), firstly Prandtl (1945) introduced a new variable, the kinetic turbulence for the calculation of the turbulent viscosity:

$$k = \frac{1}{2}\left(\overline{u'u'}\right) \qquad \nu_t = l_m\sqrt{k} \tag{2.24}$$

For the calculation of the kinetic turbulent energy (k), a transport equation is derived from the momentum and Reynolds-equations. Furthermore, the length scale parameter l_m can be derived by an additional parameter, which is described as the specific dissipation (ϵ) of the turbulent energy. For high Reynolds numbers (turbulent region), the dissipation applies to the relation $\epsilon \sim k^{3/2}/l$. The relation between the three parameter (k, ϵ, ν_t) is described by the modified Prandtl-Kolmogorov relation:

$$\nu_t = c_\mu \frac{k^2}{\epsilon} \tag{2.25}$$

This equation is generally used for the calculation of the turbulent viscosity by the well-known k-ϵ turbulence model. In the latter model, the two quantities k and ϵ are implicitly solved by transport equations, including empirical functions and constants, which are obtained from modeling parameter studies of simplified flow structures (Jones and Launder, 1972).

Meanwhile, different eddy viscosity models can be found in literature. All are based on one or more of above aforementioned formulations and they can be classified by the number and kind of equations:

- **Algebraic models** are the simplest form of eddy viscosity models. The Reynolds stress tensor is solved using a simplified algebraic assumption of the relation of the Reynolds stress tensor to the velocity gradient and the turbulent viscosity. Some known models are the Mixing Length, the Cebeci-Smith or the Baldwin-Lomax model
- **One-equation models** are solving a transport equation for a turbulent quantity (usually the turbulent kinetic energy). The second turbulent quantity (usually the turbulent length scale) is obtained form an algebraic expression. (Models: Wolfstein, Baldwin-Barth, Spalart-Allmaras and kL-model)
- **Two-equation models** are part of eddy viscosity models. Two transport equations are derived which describe transport of two scalars, for example the turbulent kinetic energy k and its dissipation ϵ. (Models: $k-\epsilon$ or $k-\omega$)

From algebraic to the two-equation models, the complexity, accuracy of predictions and computational time increases. Nowadays, in modeling of natural environments such as seas, estuaries or coastal zones mostly the k-ϵ model is used, especially to reproduce salinity-

induced stratifications. It consists of five empirical parameters, which are well calibrated for temperature and salinity induced stratification effects (e.g. Goudsmit et al., 2002; Warner et al., 2005). However, not only two-equations models are used, algebraic models are often become interesting in fields of complex geometry or current interactions and strong stratified conditions (e.g. Lehfeldt and Bloss, 1988). One of the most important advantages of algebraic or one-equation models is related to less empirical parameters. Here, only one parameter (l_m) has to be validated. This makes algebraic or one-equation models as a common tool in terms of relatively unknown sediment-induced stratification effects/problems and its impact on large-scale flow dynamics.

Density-Induced Stratification Effects In the case of vertical density gradients, the turbulent exchange is reduced by means of buoyancy force and the turbulence must be reduced; e.g. by an algebraic formulation. Stratified flow conditions resulting in reduced or complete repealed momentum exchange, which has to be considered in numerical models. Stratification stability can be described in the interaction between gravitational force (buoyancy flux) and turbulent shear production. They can be described by the gradient Richardson number (Ri_g). Stable stratification (Ri_g >0) leads to damping of turbulent mixing while unstable stratification (Ri_g <0) leads to higher mixing. For a Ri_g >0.25 the flow is strongly stratified, while at unstable stratification a higher dense water is located above a lighter dense water, which results in a rapid mixing of the water masses. Therefore, the stratification behavior can be described with an analytical damping function that depends on the gradient Richardson number (e.g. Busch, 1972; Smith and McLean, 1977). Existing damping functions have been determined by fitting mathematical functions, which is in accordance with laboratory stratification investigations. Furthermore, algebraic functions by latter named authors were confirmed by field measurements and numerical studies (e.g. Orton and Kineke, 2001; Wurpts, 2006).

2.3.4 Estuarine Cohesive Sediment Dynamics

Sediment Settling Distribution of a vertical sediment profile is dependent on current eddy diffusivity as well as settling of sediment particles. The settling velocity acts as downward flux, while the eddy diffusivity acts as the upward flux. Vertical concentration profiles in stationary flow conditions with an assumed constant settling rate can be analytical solved by the Rouse-Equation (Rouse, 1937). For low concentrated mud suspensions, usually a constant settling velocity can be assumed, which is determined by the Stokes law. For high-concentrated mud suspensions, the settling velocity can no longer be considered as constant. Generally, muddy sediment settling is classified in three regimes, flocculation, hindered settling and consolidation. Latter regimes are mainly described simplified by the suspended sediment concentration (e.g. Raudkivi, 1998). Fig. 2.12 illustrates the relationship of sediment concentration to the settling velocity and shows the variability of settling velocities of cohesive suspensions.

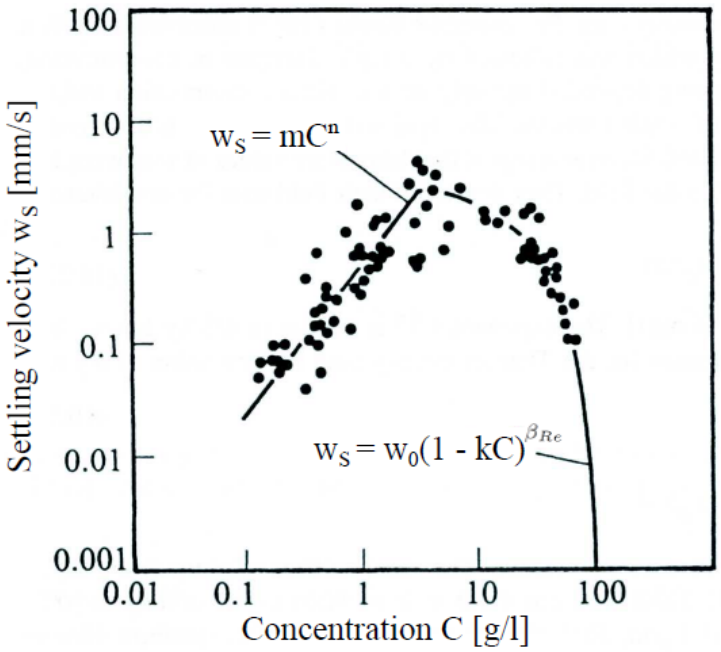

Figure 2.12: Sediment settling velocity w_s as a function of suspended sediment concentration C based on data from the Severn Estuary (UK) for the flocculation and hindered settling regime (Raudkivi, 1998)

A more complex formulation (Eq. 2.26) is used and simplified considers the flocculation process. The formulation is based on a concentration dependent settling approach (Raudkivi, 1998):

$$w_s = kC^m \tag{2.26}$$

where k and m are empirical parameters, which are mostly validated by model calibrations or laboratory data. This empirical formulation of the settling velocity is valid up to a certain sediment concentration. From literature, different values of this threshold can be found and they are usually obtained in a range of ∼8-12 g l^{-1} (Dyer, 1986; Johansen, 1998). Above this threshold the suspension is defined as a high concentrated fluid mud mixture, and the settling velocity of a single particle is reduced due to the presence of surrounding particles (hindering effect). At this hindered settling state, it can be formulated by e.g. following Richardson and Zaki (1954) as:

$$w_s = w_{s,0}\left(1 - \frac{C_s}{C_{gel}}\right)^n \tag{2.27}$$

with the empirical parameter n, which is set to 5 (Richardson and Zaki, 1954). This for-

mulation reduces the settling velocity up to the so-called gelling-concentration C_{gel}, where settling is described as a weak consolidation. In literature, several empirical expressions exists for the hindered settling behavior related to the sediment concentration (e.g. Vesilind, 1968; Takács et al., 1991). However, this settling behavior depends not only on the sediment concentration, but also on floc size and biological effects (e.g. Winterwerp, 2001; Miller et al., 2016). For a simplified approach, aforementioned processes are often neglected in numerical models for estuarine environments, because complexity and unknown quantities arises and are still part of scientific investigations. Above the gel concentration the settling (consolidation) is mainly subjected to the sediment bed. Generally, within the vertical sediment bed discretization a muddy layer is considered. This layer takes into account the consolidation process, by reducing the pore water volume, increasing dry bed density and critical bed shear stress, which additionally results in a reduced thickness of the consolidated layer (e.g. Gibson et al., 1967).

Impact of turbulence Sediment settling is also strongly affected by the turbulence intensity (Argaman and Kaufman, 1970; Dyer, 1989). This behavior is caused by the increased number of collision between particles. Fig. 2.13 illustrates the effect of turbulence intensity by the shear stress on floc size and sediment concentration (Dyer, 1989). It shows, at increasing shear stress the floc diameter increases initially, results in a higher settling velocity at a constant sediment concentration (higher collision frequency). This process is known as the aggregation of flocs. After the initial increase, the break-up of flocs dominates and the settling velocity decreases with further increasing shear stress. Furthermore, at low shear stresses, the floc diameter increases with increasing sediment concentration up to a certain threshold. This threshold is determined by the transition from flocculation settling behavior into hindered settling behavior. Therefore, at lower shear stresses, the aggregation dominates and at higher shear stress the break-up of flocs dominates. Based on this assumption, Van Leussen (1994) developed a heuristic formulation describing this effect:

$$w_s = w_{s,0}\frac{(1 - a_f G)}{(1 - b_f G^2)} \qquad \frac{Aggregation}{Break\ Up} \tag{2.28}$$

where $w_{s,0}$ is the reference settling velocity, G is the dissipation or velocity gradient in turbulent flows and a_f and b_f are empirical coefficients. This simplified formulation of aggregation and break-up of flocs has been successfully applied in numerical simulations of cohesive sediment transport by e.g. Malcherek (1995).

Erosion and Deposition of Cohesive Sediments Deposition and erosion of sediment is computed by sediment flux parametrization from the near bottom computational layer into the bed or vice versa. Both are applied by means of the sediment source and sink term in the advection-diffusion equation. The calculated fluxes are also applied to the morphological bed in order to update local bed level elevations. The bed boundary condition is

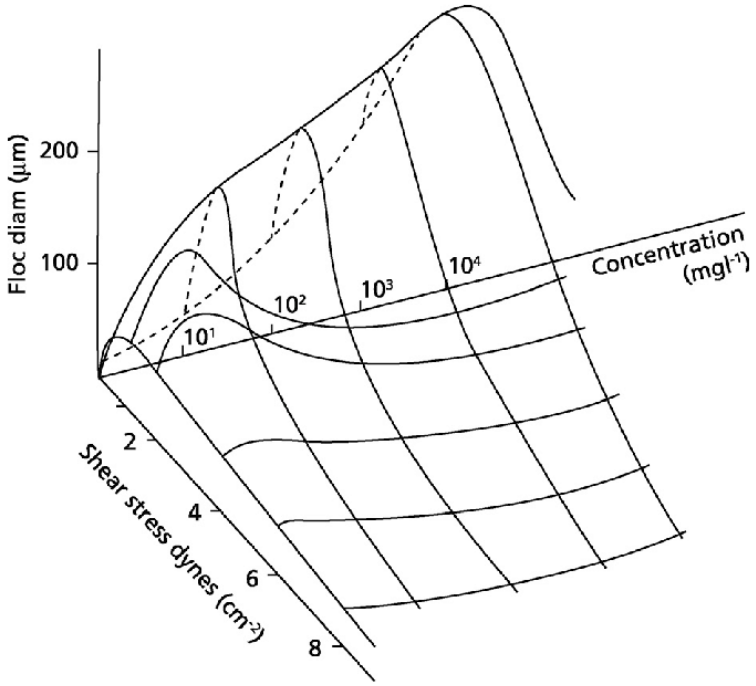

Figure 2.13: Sediment flocculation concept shows the relationship between shear stress, suspended sediment concentration and floc diameter (Dyer, 1989)

given as:

$$-w_s C - \epsilon_z \frac{\partial C}{\partial z} = D - E \tag{2.29}$$

The erosion flux (E) of silty sediments is calculated based on Ariathurai-Partheniades erosion formula (Ariathurai and Arulanandan, 1978) and the deposition flux (D) is a function of the settling velocity and concentration in the near bed layer:

$$\begin{aligned} E &= E_0(\tau/\tau_e - 1) && \Rightarrow \tau \geq \tau_e \\ E &= 0 && \Rightarrow \tau \leq \tau_e \\ D &= w_s C_b \end{aligned} \tag{2.30}$$

with C_b the near bed suspended sediment concentration. Erosion as well as deposition is always a function of available sediment in the water column or sediment bed. In upper formulation, generally E_0 and τ_e are empirical parameters and are calibrated by sediment concentration measurements or knowledge about detailed sediment composition. The formulation is a simplification of the problem itself, but is mostly used in estuarine models. Actually, for silty sediments, the empirical erosion rate E_0 and the critical erosion shear stress τ_e depends strongly on the dry bed density. Increasing of the dry bed density by a consolidation process will result in an increase of sediment bed strength against erosion

and an increase of the erosion rate (e.g. Sanford, 2008). Therefore, the critical bed shear stress and erosion rate is dependent on the degree of consolidation. The process must be actually considered as a time dependent function, but it is mostly determined as a constant parameter in common numerical models (e.g. Hayter et al., 1986; Liu et al., 2002).

Density Calculation The water-density (ρ) is a function of temperature (T), salinity (S) and the suspended sediment concentration (SSC). The water density based on temperature and salinity can be calculated with the UNESCO-equation (UNESCO, 1981):

$$\rho_{T,S} = \rho_0 + AS + BS^{3/2} + CS^2 \tag{2.31}$$

The empirical functions (A, B, C) are temperature as well as salinity dependent and are fitted by previous lab investigations. Taking into account the effect of sediment, the fluid density increases with increasing sediment concentration. The effect of sediment concentration on the water-density can be incorporated and calculated by the following formulation:

$$\rho_f = \rho_{T,S} + C\left(1 - \frac{\rho_{T,S}}{\rho_s}\right) \tag{2.32}$$

with ρ_f the water density and $\rho_s = 2650\ kg\ m^{-3}$ the dry bulk density of sediment.

2.4 Existing Fluid Mud Transport Models

Modeling of fluid mud and resulting flow dynamics are of crucial interest for maintenance measurements or as a required solution for water quality modeling studies. Different previous numerical studies carried out fluid mud layer dynamics with different kind of modeling approaches. Based on literature, three different model concepts for fluid mud dynamics can be found (Isopycnical model concept, multi-phase and single-phase modeling approach). The latter named model approaches are considering the turbulence modeling of stratified flow, non-constant settling velocity approaches and uses a rheological approach for the description of the non-Newtonian flow behavior.

Wehr (2012) developed a three-dimensional fluid mud layer flow model, which is based on the isopycnical modeling concept. This method integrates the non-Newtonian flow behavior in a numerical concept, which is based on the RANS equations. Each vertical grid cell is specified by a constant density and thus by a rheological viscosity. With this classification of vertical grid cells, the model is able to reproduce both fluid behaviors, the non-Newtonian fluid mud and above Newtonian water fluid. But, the isopycnical model concept is limited to only stable stratified flow conditions (Wehr, 2012), because the density of a vertical grid cell has to be defined in advance. Therefore, in highly turbulent flow conditions, this concept cannot be adequately reproduce mixing and associated upward flux of cohesive fines into the upper water column. In particular, the presence of suspended sediment

transport and baroclinic processes may result in unstable stratification and strong mixing processes (Winterwerp, 2001; Hsu et al., 2007).

Achieved by Teisson et al. (1992), the interaction between particles in the fluid mud layer and water needs a multiphase approach. It uses a combination of hydrodynamics and soil mechanics, for which pore-water movement relative to settling particles is considered. However, computations are very time-consuming. Also, unsteady configurations cannot be simulated. Hsu et al. (2007) simplified the multiphase equations to simulate longer timescales (several tidal cycles). This allows consideration of typical processes related to fluid mud transport. Latter authors have shown a multiphase approach provides rigorously derived balance that incorporate fluid-sediment interactions and granular rheology (e.g. Gidaspow, 1994). Furthermore, it allows modeling transport continuously from concentrated aggregate network to dilute suspension. As already mentioned by Guan et al. (2005), all multiphase models are limited to their empirical derived exchange functions between both phases. This strong dependency makes multiphase approaches inconvenient for modeling complex unsteady estuarine environments. Moreover, stability of models is highly dependent on the computational time-step.

LeHir (1997) presented an integrated modeling concept simulating water and fluid mud dynamics by solving the mass conservation and momentum equations over the entire water column. They replaced the integrated formulations with those which allow a continuous transition. Their approach is more representative for the water and mud exchange in the water column compared to a multiphase approach, but it is applied just for a simple test case and not for an estuarine environment. LeHir et al. (2000) itself mentioned, a 3D model is necessary eliminating advection-induced ambiguities. Guan et al. (2005) applied Le Hir's modeling approach to the Jiaojiang estuary in China, using a three dimensional model. Also, Roland et al. (2012) applied the modeling approach of LeHir to the Ems estuary, based on an unstructured modeling grid. They have shown the model is case sensitive to empirical parameters of the turbulence and rheological model formulation and requires process-based studies to improve the parametrization.

In Table 21, previous numerical studies which took into account fluid mud dynamics using the single phase modeling approach are listed with respect to considered physical processes.

Numerical studies of LeHir et al. (2000) Guan et al. (2005) and Roland et al. (2012) dealt with modeling of fluid mud layer dynamics in estuarine environments. In contrast, numerical studies of Hsu, Traykovski, and Kineke (2007) and Kämpf et al. (2018) dealing with fluid mud gravity-driven flow under wave force.

LeHir et al. (2000) pointed out the importance of hindered settling, stratification-induced turbulence damping and the viscoplastic behavior of solid material. The stratification-induced damping is fundamental to determine stability and mixing of lutocline dynamics

Table 21: Previous numerical studies on fluid mud behavior in a single phase modeling approach

•	Le Hir (2000)	Guan (2005)	Hsu (2007)	Roland (2012)	Kaempf (2018)
Dimension	2D/1DV	3D	1DV	3D	1DV
Rheology	Power Law	Power Law	Power Law	Toorman (1997)	Bingham
Thixotropy	-	-	-	Yes	-
Turbulence Model	Mixing Length	Mellor and Yamada	k-ϵ	k-ϵ	k-ϵ
Hindered Settling	Metha (1989)	Winterwerp (2002)	Winterwerp (2002)	Winterwerp (2002)	Camenen (2011)
Rheological Damping	-	-	C/C_{Gel}	-	C/C_{Gel}

(e.g. Wolanski et al., 1989). Another important process is related to the reduction of horizontal velocities and advected transport by the viscous behavior of fluid mud (LeHir et al., 2000; Guan et al., 2005). Although, latter process could not been observed by gravity-driven mud flow under wave force (Lamb et al., 2004), but in the ETM of the Ems estuary, it is responsible for the formation and resuspension characteristic (Becker et al., 2018).

Developed three dimensional model approaches by Guan et al. (2005) and Roland et al. (2012) are specially designed for fluid mud dynamics in estuarine environments. But both studies could not verify a large-scale flow and formation behavior of fluid mud in estuarine turbidity maxima or in detail along the deep channel. Roland et al. (2012) has only shown, that a distinct fluid mud layer is formed in an adjoining harbor. In Guan et al. (2005) the observed fluid mud layer formation during slack times before ebb is missing. The latter existence of the fluid mud layer can be important in case of resuspension and corresponding down-estuary transport of cohesive fines. Furthermore, mentioned strong horizontal flow reduction could not be reproduced in their modeling study, which is important for the large-scale residual sediment transport and formation of sediment trapping zones.

3 Numerical Modeling of Cohesive Sediments in Delft3D

3.1 Modeling System

For mentioned numerical investigations, the well-known three-dimensional hydro- morphodynamic numerical model Delft3D (Deltares, Delft) is used (Lesser et al., 2004). Since 2011, Delft3D is available as open-source version (Deltares, 2011), which offers numerical developments by a larger community. This makes it possible to extend an already existing and established model approach, which has been used in many previous coastal and estuarine research subjects (e.g. Van Kessel et al., 2011; Maren et al., 2015; Hesse et al., 2019).

The hydro-morphodynamic numerical modeling system Delft3D is based on a finite volume discretization with a curvilinear grid model approach. It solves the instationary shallow water equations in three dimensions. The modeling system consists of the horizontal equations for momentum, continuity and transport of tracers (e.g. temperature, salinity or sediment concentration). Horizontal equations are formulated in orthogonal curvilinear co-ordinates and the vertical discretization is realized in $\sigma-$coordinates. Hydrodynamic force at a seaside boundary can be driven by water surface elevation, wind shear stress at sea surface, pressure gradient at sea surface (barotropic) or by means of a horizontal density gradient (baroclinic). Caused by the explicit discretization of the horizontal momentum equations, the maximum numerical time step is restricted to the Courant-Friedrichs-Lewy (CFL) number:

$$CFL = \frac{v\ dt}{dx} \tag{3.1}$$

where v is the numerical characteristic velocity, dt chosen time step and dx the smallest horizontal grid resolution. For a stable solution of explicit integration of the momentum equation, the CFL number must strictly be smaller or equal to one. For higher CFL numbers, the numerical solution becomes instable, and results are maybe not accurate. The explicit solver restricts the use of Delft3D to simplified natural systems. Study areas requiring strong changes in horizontal resolution of the mesh size (e.g. back barrier islands, strong meandering channels) will result in high computational time, because the latter increases with the number of grid cells. For modeling investigations conducted in this study, Delft3D should be suitable enough, because the model domain of the study area is relatively small and grid resolution handles with a sufficient cell size, therefore required time step only become in order of minutes.

3.2 Hydrodynamics

Numerical models for large-scale coastal or estuarine waters are solving all the same equations. The full Navier-Stoke equation is simplified by the Reynolds-Averaging method and

the turbulence interaction is reproduced by a closure scheme based on the Boussinessq approximation. Mostly, only horizontal directions (x, y) are solved by the RANS equations (Eq. 3.2-3.4). The vertical direction is solved by the hydrostatic pressure assumption and considering mass conservation by the continuity equation:

$$\rho(\frac{\partial u}{\partial t} + u\frac{\partial u}{\partial x} + v\frac{\partial u}{\partial y} + w\frac{\partial u}{\partial z}) - f_v = -\frac{\partial p}{\partial x} + \frac{\partial}{\partial x}\nu_h\frac{\partial u}{\partial x} + \frac{\partial}{\partial y}\nu_h\frac{\partial u}{\partial y} + \frac{\partial}{\partial z}\nu_t\frac{\partial u}{\partial z} \tag{3.2}$$

$$\rho(\frac{\partial v}{\partial t} + u\frac{\partial v}{\partial x} + v\frac{\partial v}{\partial y} + w\frac{\partial v}{\partial z}) + f_u = -\frac{\partial p}{\partial y} + \frac{\partial}{\partial x}\nu_h\frac{\partial v}{\partial x} + \frac{\partial}{\partial y}\nu_h\frac{\partial v}{\partial y} + \frac{\partial}{\partial z}\nu_t\frac{\partial v}{\partial z} \tag{3.3}$$

$$\frac{\partial u}{\partial x} + \frac{\partial v}{\partial y} + \frac{\partial w}{\partial z} = 0 \tag{3.4}$$

The RANS equations assume a vertical hydrostatic pressure distribution (hydrostatic pressure approximation). Likewise, vertical momentum is only reduced to this hydrostatic pressure. Therefore, vertical acceleration due to buoyancy effects and variations in the bed geometry are not considered. The hydrostatic pressure is assumed as vertical linear distributed from the surface to the bottom:

$$\frac{\partial}{\partial z}\left(z + \frac{p}{\rho g}\right) = 0 \tag{3.5}$$

The hydrostatic pressure assumption simplifies the model requirements. This application is generally accepted in natural waters without appreciable vertical accelerations, as in ocean, estuaries or rivers. Additionally, this simplified approximation enables significantly reduced computational time efforts.

3.3 Turbulence Modeling

In this study, the one-equation k-L turbulence model is chosen (Prandtl, 1945), where the turbulent viscosity is defined as:

$$\nu_t = c_D l\sqrt{k} \tag{3.6}$$

with $c_D = c_\mu^{3/4} = 0.1925$ a constant parameter. The closure model involves one transport equation for the turbulence production (k) and is a first order turbulence closure scheme. The mixing length (l) will be described analytically. Here, the velocity scale is based on the kinetic energy of turbulent motion.

The turbulent kinetic energy (k) is solved by a transport equation that includes an energy

dissipation term, a buoyancy term (B_k) and a production term (P_k):

$$\frac{\partial k}{\partial t} + u\frac{\partial k}{\partial x} + v\frac{\partial k}{\partial y} + w\frac{\partial k}{\partial z} = \frac{\partial}{\partial z}\left(\nu_t \frac{\partial k}{\partial z}\right) + P_k + B_k - \epsilon \tag{3.7}$$

The production term P_k is given by:

$$P_k = \nu_t \left[\left(\frac{\partial u}{\partial z}\right)^2 + \left(\frac{\partial v}{\partial z}\right)^2\right] \tag{3.8}$$

In stratified flows, turbulent kinetic energy is converted into potential energy. This is represented by the buoyancy flux B_k defined as:

$$B_k = g\frac{\nu_t}{\rho\sigma_p}\frac{\partial \rho}{\partial z} \tag{3.9}$$

with the Prandtl-Schmidt number σ_p. In the k-L model the dissipation term ϵ depends on the mixing length theory (l) and kinetic turbulent energy (k) according to:

$$\epsilon = c_D \frac{k\sqrt{k}}{L} \tag{3.10}$$

where the mixing length (Bakhmeteff, 1932) is described as:

$$l = \kappa(z+d)\sqrt{1 - \frac{z+d}{H}} F_L(Ri_g) \tag{3.11}$$

In the case of stratified flow conditions the mixing length is reduced by a simplified function, which is based on the Richardson-Gradient-Number. Here, the k-L model is extended to stratified flows by the formulation following Busch (1972):

$$F_L(Ri_g) = \begin{cases} e^{-2.3Ri_g} & Ri_g \geq 0 \\ (1 - 14Ri_g)^{0.25} & Ri_g < 0 \end{cases} \tag{3.12}$$

In the case of stable stratified flow conditions ($Ri_g \geq 0$) the mixing length and turbulent viscosity is damped. For unstable stratified conditions ($Ri_g < 0$) with higher dense water masses above lighter masses, the vertical momentum exchange will increase. In proposed studies, a lot of other empirical formulations are available. Generally, all formulations are dependent to the Gradient-Richardson-Number and mostly calibrated by means of local measured sediment or salinity concentration profiles with respect to hydrodynamic behavior (e.g. Smith and McLean, 1977; Orton and Kineke, 2001).

The advantage of Eq. 3.12 is based on existing only one empirical number (-2.3), which can be simply adjusted in case of high-suspended sediment transport. This is required,

because mainly used algebraic turbulence damping functions are only calibrated and validated based on temperature and/or salinity induced density gradients, but not for strong sediment-induced density stratification effects. Furthermore, the vertical diffusivity must also be reduced in terms of density-induced stratification effects. The turbulent diffusivity is calculated by the turbulent Schmidt number (σ_p), which describes the relation of turbulent viscosity to turbulent diffusivity:

$$\epsilon_z = \frac{\nu_t}{\sigma_p} \tag{3.13}$$

with σ_p the Schmidt number, which is usually set to 1.3 for homogeneous and isotropic turbulent environmental flows (Gualtieri et al., 2017).

3.4 Suspended sediment transport

The three dimensional cohesive and non-cohesive sediment transport is solved by the three-dimensional advection-diffusion (mass balance) equation. This transport equation is a combination of advection and diffusion terms, which describes the physical flow behavior of a tracer in a physical system. The general equation is written as:

$$\frac{\partial C}{\partial t} + \frac{\partial uC}{\partial x} + \frac{\partial vC}{\partial y} + \frac{\partial (w - w_s)C}{\partial z} = \frac{\partial}{\partial x}\left(\epsilon_x \frac{\partial C}{\partial x}\right) + \frac{\partial}{\partial y}\left(\epsilon_y \frac{\partial C}{\partial y}\right) + \frac{\partial}{\partial z}\left(\epsilon_z \frac{\partial C}{\partial z}\right) \tag{3.14}$$

with w_s the settling velocity and $\epsilon_{x,y,z}$ are the horizontal (x, y) and vertical (z) diffusivity. The latter is parameterized computed by Eq. 3.13 and the horizontal diffusivity is assumed as a constant grid dependent value. Sediment transport changes in case of baroclinic processes are considered by the turbulence closure scheme and calculation of the momentum equations. Solving Eq. 3.14 a boundary condition has to be defined for the sediment bed and water column exchange rate. This exchange is generally considered by the formulation of Eq. 2.29, which includes erosion and deposition flux of sediment particles (Celik and Rodi, 1988).

Taking into account morphological changes and therefore growing up or deepening of the sediment bed, the bathymetry has to be updated at certain timesteps of the model run. Considering latter process, the Exner equation is an intuitive sediment mass-conservation equation and accounts for the exchange of sediment between the bed and the water column and is written as:

$$\rho_s \left(1 - p_b\right) \frac{\partial z_b}{\partial t} + \nabla \overrightarrow{q_b} + E - D = 0 \tag{3.15}$$

where p_b is the porosity of the bed material and usually assumed to be constant (0.4), z_b describes the bed-surface elevation and $\overrightarrow{q_b}$ is the bed-load flux. Bed load transport is generally not considered in the case of cohesive sediment transport investigation and therefore is neglected in this study. E and D are the erosion and deposition flux from the water column to the sediment bed.

The exchange of material in suspension and the bed is modeled by calculating the sediment fluxes from the bottom computational layer to the bed, and vice versa. These fluxes are then applied to the bottom computational layer by means of a sediment source and sink term in each computational cell. The bed boundary condition of the advection-diffusion equation is given by:

$$-w_s C - \epsilon_z \frac{\partial C}{\partial z} = E - D \tag{3.16}$$

The deposition and erosion rate between the water phase and the sediment bed is calculated in the case of muddy sediment material by e.g. the Partheniades-Krone formulation (Partheniades, 1965):

$$\begin{aligned} E &= E_0(\tfrac{\tau_t}{\tau_e} - 1) \quad \Rightarrow \tau_t \geq \tau_e \\ D &= w_s C_b \end{aligned} \tag{3.17}$$

The empirical erosion rate E_0 and the critical erosion shear rate τ_e depends generally on the consolidation state of muddy sediments or more in detail on the dry bed density. When the dry bed density becomes larger, τ_e and E_0 will increase due to greater strength against the prevailing currents. Increasing empirical erosion rate is further related to an occurring surface erosion (bed failure), then a single-particle erosion, as known from sandy sediment erosion behavior (e.g. Hayter & Mehta 1986; Joensuu et al., 2017).

4 Development of a Numerical Approach for Fluid Mud - Water Interactions

In the present study, the state-of-the-art modeling system Delft3D is significantly extended to allow consideration of fluid mud transport, formation and dynamics in the same three-dimensional numerical grid. The implemented model satisfies a continuous transition from Newtonian to non-Newtonian flow behavior. Using this one grid modeling approach, consideration fulfills the transient dynamics and flow behavior from the stationary mud, mobile fluid mud and overlying free water column. Those, turbulent mixing and stratification of water-fluid mud mixtures within the entire water column is represented.

The Delft3D model was extended by following physical process:

- the complex settling formulation of flocculation, hindered settling and beginning consolidation
- rheology as physical characteristic of non-Newtonian fluids
- turbulence damping approach based on non-Newtonian fluid dynamics

The extended formulations for settling flux and rheology are selected here according to empirical formulations from existing literature. The effect of fluid mud on the turbulence production and damping could not be verified in previous model studies, but it appears as one of the main physical drivers to estimate the fluid mud-water exchange (LeHir et al., 2000). The approach of the non-Newtonian (rheology)-induced turbulence damping is not yet known from previous literature and is presented as a new conceptual physical model.

With those extensions, the model is enabled to reproduce complex stratified situations of Newtonian and non-Newtonian flow dynamics caused by density-stratifications (salinity and/or sediment) and/or rheology. The extended model approach is not only limited to the verification test case (Ems estuary) or areas with fluid mud. It can also be applied to any other estuary or coastal zone, because extended model processes allows only a formation of fluid mud in regions where required conditions present (existing amount of sediment, associated hydrodynamics).

4.1 Review of Relevant Processes

Modeling of large-scale fluid mud dynamics in estuarine environments are of complex matter, which requires a three dimensional model approach, as well as consideration of material specific properties. Following Winterwerp et al. (2004), fluid mud is a type of specific formation of cohesive sediment particles, which requires a numerical model approach. It has to solve the time dependent flow velocities and corresponding sediment transport dynamics. Figure 4.1 shows the numerical flow chart with all the relevant processes for modeling large-scale fluid mud dynamics in estuarine environments (own extensions are highlighted).

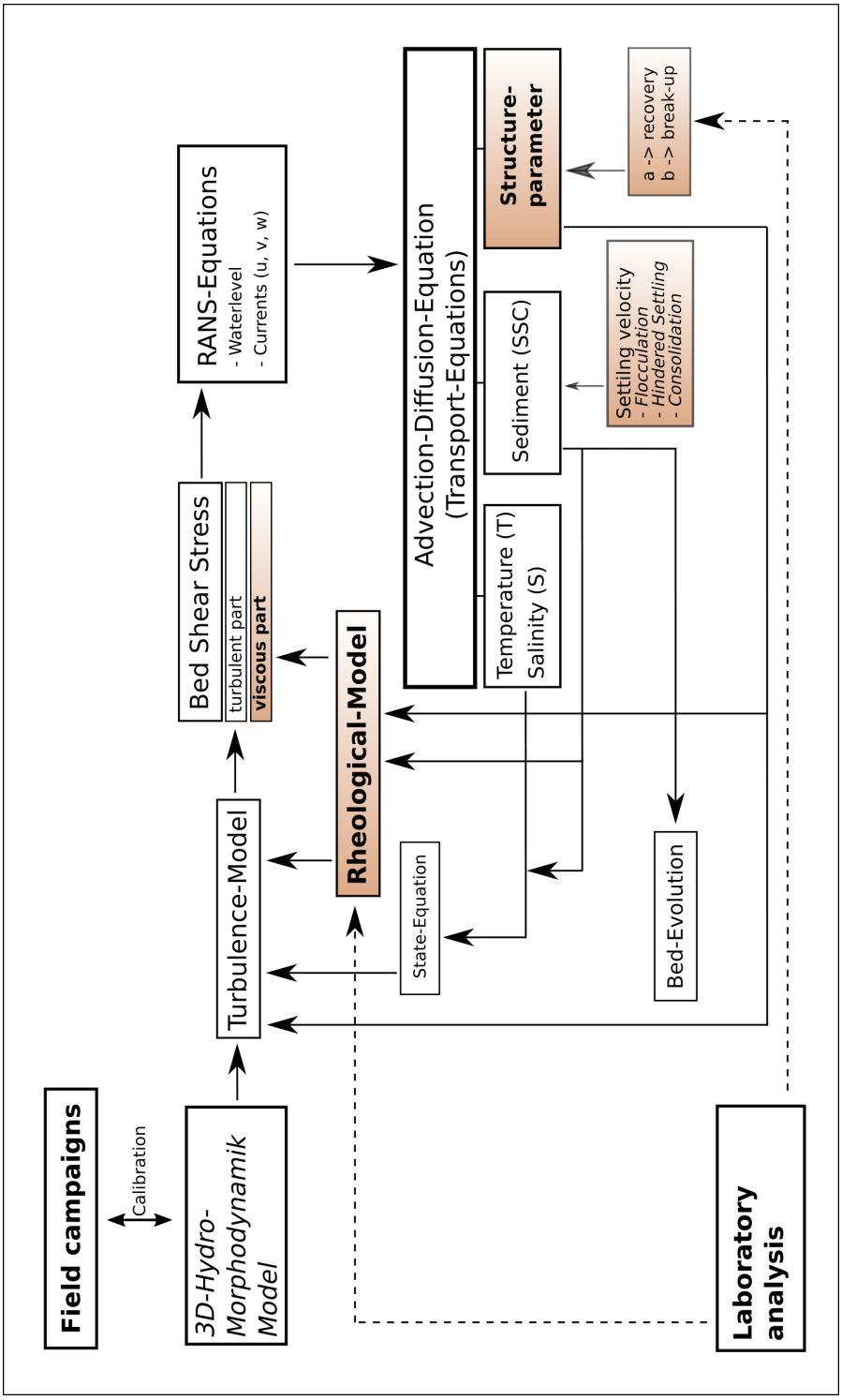

Figure 4.1: Numerical flow chart for modeling three-dimensional hydro- and morphodynamic including developed model extensions (brown areas) considering fluid mud dynamics

The non-linear settling velocity approximation containing flocculation, hindered settling and beginning consolidation is mostly considered in previous modeling studies (e.g. Guan et al., 2005; Wehr et al., 2012). However, it is one of the most important characteristic of modeling high concentrated suspensions, because turbulent mixing and entrainment at lutocline are mainly controlled by this material specific behavior (Wolanski et al., 1989).

Already existing mud transport models have shown that an integration of turbulence damping is strictly necessary based on sediment-induced stratification for the formation and stabilization of a distinct lutocline layer (e.g. Winterwerp, 2001; LeHir et al., 2000, 2001; Hsu et al., 2007). Previous investigations of sediment transport analysis have further shown, turbulence damping is not only an important process for sandy sediments, but also for muddy sediments, to reproduce accurate transport rates and long-term morphological changes (e.g. Lyn, 1988; Van Rijn, 1989).

Sediment-induced stratification effects have been studied by different authors in *unsaturated* conditions. They figured out, it is responsible for e.g. sediment trapping in turbidity maxima (Rijn, 1984; Sheng et al., 1989; Winterwerp, 2001; Toorman et al., 2002; Cantero et al., 2011). Damping and suppression of turbulence by sediment-induced stratification effects may increase sediment trapping by a factor of 20 (Geyer, 1993; Byun and Wang, 2005). However, the rule of turbulence damping in mud induced *saturated* flow conditions with fluid mud formation and its effects on estuarine circulation is not yet well understood. Measurements are very intensive, time and spatial-dependent, and three-dimensional estuarine models are not yet accurate enough to study mentioned effects (Toorman et al., 2002).

The rheology of high concentrated mud suspensions is often neglected in numerical model investigations (Hsu et al., 2007). However, modeling of high concentrated suspension regimes of consolidated or suspended mud requires consideration of the rheology of cohesive fines (LeHir et al., 2000). High suspended sediment suspensions are characterized by means of a non-Newtonian flow behavior, where the rheological viscosity is increased with suspended concentrations. This leads in turn to a strongly reduced horizontal transport rate (Coussot, 1997). Moreover, Becker et al. (2018) have observed and confirmed the latter behavior by means of detailed tidal cycle measurements of current velocity and suspended sediment concentration within a high-concentrated fluid mud layer in the Ems estuary. Guan et al. (2005) mentioned, that the turbulence is significantly damped at high suspended sediment concentrations, which appears due to viscoplastic behavior and is important for the resuspension and entrainment of fluid mud (Wolanski et al., 1989; Kineke et al., 2006). Furthermore, the thixotropic behavior of such dilute suspensions is mainly neglected in previous sediment transport models. However, it is essential for process-based studies of natural environments and is mentioned as a key mechanism for the rheological flow behavior, because of its relation to the current acting rheological viscosity (Toorman, 1997; Wehr, 2012).

4.2 Settling velocity

Settling of cohesive fines shows complex patterns of flocculation, hindered settling and beginning consolidation. In comparison to sandy sediments, a constant settling velocity, depending on the grain diameter cannot be assumed (e.g. Einstein and Krone, 1962; Kranck, 1986; Dankers et al., 2007). Furthermore, Wolanski et al. (1992) have mentioned, settling velocity of cohesive fines is not only a non-linear function related to suspended sediment concentration, but also turbulence intensity becomes important. It is caused by the floc structure stability. The interaction of flocculation and turbulence intensity is complex and still part of scientific investigations, which is beyond the scope of this research. Therefore, in this numerical study, a simplified non-linear method of settling velocity related to suspended sediment concentration was implemented (e.g. Toorman, 1993; McAnally et al., 2007).

The implemented total settling rate formulation covers the entire concentration range of cohesive fines (Fig. 2.8). The settling velocity range is divided into four different groups, covering free particle settling, flocculation, hindered settling and consolidation. Since there is a wide range of formulations for settling rate of cohesive sediments, simplified calculations have been used here and more specific calculations incorporating of e.g. floc size or variable gelling concentration are omitted.

At very low sediment concentrations (C$< C_f$), settling velocity is assumed as constant. Below the critical concentration for hindered settling (C_h), the settling behavior is described as a flocculation process, where the settling velocity increases with increasing sediment concentration (Van Rijn, 1993). If the concentration increases further ($C_h < C < C_{Gel}$), sediment particles begin to hinder each other, because frictional forces become dominant. Here, the settling velocity decreases with increasing concentration. Additionally, the hindered-settling behavior allows the formation of fluid mud. For hindered settling, the formulation presented by Fredsøe and Deigaard (1992) was implemented. The hindered settling formulation is valid up to the gelling concentration (C_{gel}). When the suspension concentration exceeds the gel concentration, the fluid mud layer begins to consolidate. The rate of settling in the consolidation regime is calculated according to a simplified formulation proposed by Toorman (1992). Summarized following formulations were implemented to consider the settling of cohesive sediments (refers also to the corresponding figure 2.8 for following equations 4.1).

$$w_s = \begin{cases} const. & C \leq C_f \\ k_1 C^m & C_f < C \leq C_h \\ w_{s0}(1 - a_h C)^{b_h} & C_h \leq C \leq C_{Gel} \\ w_{sg0}(C/C_{Gel})^{-\beta} & C > C_{Gel} \end{cases} \tag{4.1}$$

Aforementioned conditional equations have been implemented in such a way, that a continuous transition between each settling rate formulation is satisfied. To ensure the continuous

transition, the maximum rate of settling, the suspended matter concentration at the beginning of hindered settling and the suspended concentration and settling velocity at the gel concentration are user specified. The calculation of empirical and user-defined parameters are summarized in following Table 41:

Table 41: List of empirical parameters for the settling velocity formulations used in the numerical model

Parameter	**Description**	**Value**	**Unit**
k_1	empirical flocculation parameter	0.0002	-
m	empirical flocculation parameter	1.1	-
w_{s0}	maximum settling velocity	1.0	mm s^{-1}
a_h	empirical hindered settling parameter	0.024	-
b_h	empirical hindered settling parameter	2.0	-
w_{sG0}	settling velocity at beginning consolidation	0.001	mm s^{-1}
β	empirical consolidation exponent	3.0	-
C_h	start concentration for hindered settling	8.0	g l^{-1}
C_{Gel}	start concentration for consolidation	50.0	g l^{-1}

4.3 Rheology and Thixotropy

For the implementation of the additional material (apparent) viscosity, the modeling concept of LeHir et al. (2000) was followed to integrate the rheological viscosity into the RANS equations (Eq. 4.2). In this model concept, the vertical turbulent viscosity in the viscous term (Reynolds Stress term) of the Reynolds-averaged Navier-Stokes equations (Eq. 4.3 - 4.4) is extended by an additional stress term, which includes the rheological (viscous) stress, which is proportional to the velocity shear. The additional total stress tensor including molecular and rheological stress is then described as:

$$\tau_{ij} = (\mu_m + \mu_r)\left(\frac{\partial \overline{u_i}}{\partial x_j} + \frac{\partial \overline{u_i}}{\partial x_j}\right) \tag{4.2}$$

$$\frac{\partial u}{\partial t} + u\frac{\partial u}{\partial x} + v\frac{\partial u}{\partial y} + w\frac{\partial u}{\partial z}) - f_v = \\ -\frac{1}{\rho}\frac{\partial p}{\partial x} + \frac{\partial}{\partial x}\nu_h\frac{\partial u}{\partial x} + \frac{\partial}{\partial y}\nu_h\frac{\partial u}{\partial y} + \frac{\partial}{\partial z}\nu_t\frac{\partial u}{\partial z} + \frac{\partial}{\partial z}(\nu_r + \nu_m)\frac{\partial u}{\partial z} \tag{4.3}$$

$$\frac{\partial v}{\partial t} + u\frac{\partial v}{\partial x} + v\frac{\partial v}{\partial y} + w\frac{\partial v}{\partial z} + f_u = \\ -\frac{1}{\rho}\frac{\partial p}{\partial y} + \frac{\partial}{\partial x}\nu_h\frac{\partial v}{\partial x} + \frac{\partial}{\partial y}\nu_h\frac{\partial v}{\partial y} + \frac{\partial}{\partial z}\nu_t\frac{\partial v}{\partial z} + \frac{\partial}{\partial z}(\nu_r + \nu_m)\frac{\partial v}{\partial z} \tag{4.4}$$

The vertical turbulent viscosity is calculated by the already implemented one-equation k-L turbulence model, which uses a buoyancy-driven turbulence damping according to Busch and Larsen (1972). The molecular viscosity of clear water is implemented as a constant value of 1 mPa. Actually, the molecular viscosity is temperature dependent, but for short term modeling, along-channel temperature variations can be neglected in relatively small estuaries.

For numerical investigations of the rheology, a multi-parameter rheological model is required, because maximum shear rates in estuaries are relatively small. For example, based on observations, shear rates are in an order of 1.5-2 s^{-1} in the water column of the Ems estuary (Becker et al., 2018), except close to the sediment bed. Figure 4.2 shows a typical result of a rheometer yield stress test. It is apparent that the maximum analyzed shear stress becomes much higher, than a typical one in estuaries. Only the first part of the shear stress curve becomes important in presented modeling approach. It is shown that aforementioned range is located at very low shear within the strong non-Newtonian flow behavior. Above a shear rate of 10 s^{-1} the shear stress can be assumed as linear related to increasing shear rate. Below, the relation is strongly non-linear. This behavior requires a multi-parameter rheology model approach, which is necessary to resolve strong deformation at the low shear rate range.

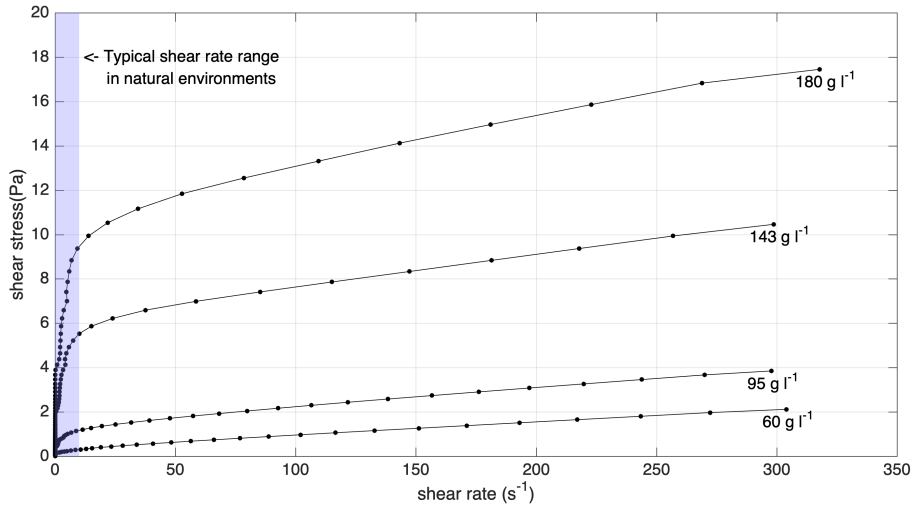

Figure 4.2: Example of a typical result of a yield stress test with shear rate versus shear stress in a linear scale. Results are shown from a 60, 95, 143 and 180 g l^{-1} mud suspension from the Ems estuary (data from Oberrecht and Wurpts, 2014b). It illustrates the strong pre-stressed fluid at already very low shear rates (blue box)

In this study, the model approach is extended by the multi-parameter rheological model formulation following Worrall and Tuliani (1964). Previous studies have shown that this model is suitable to estimate mud-induced rheological viscosities in natural environments

(Malcherek and Cha, 2011; Wehr, 2012). The model approach is based on a statistical fitting of rheological lab investigations. It takes into account the time-dependent (thixotropic) behavior by a parameterized rate-equation. The rheological model approach following Worrall and Tuliani (1964) is written as:

$$\begin{array}{ll} \tau_r = \tau_y + \mu_\infty \dot{\gamma} + (\mu_0 - \mu_\infty)\lambda\dot{\gamma} & \dot{\gamma} \geq 0 \\ \tau < \tau_y & \dot{\gamma} = 0 \end{array} \tag{4.5}$$

with $\dot{\gamma}$ the current shear stress, which is written for the vertical direction as:

$$\dot{\gamma} = \sqrt{\left(\frac{\partial u}{\partial z}^2 + \frac{\partial v}{\partial z}^2\right)} \tag{4.6}$$

When the current shear stress becomes less than the yield stress, the shear rate becomes zero. Therefore, the inner structure of the fluid is recovered and no motion within the floc structure will occur. Here, with increasing shear rate, the shear stress increases proportionally to the yield stress.

The relation of the dynamic viscosity to the shear stress is generally known as $\mu = \tau/\dot{\gamma}$. Eq. 4.5 integrated with the shear rate gives the formulation of the rheological viscosity:

$$\mu_r = \mu_\infty + (\mu_0 - \mu_\infty)\lambda \tag{4.7}$$

The dynamic viscosity is related to the kinematic viscosity by $\mu = \nu\rho$. λ is the non-dimensional structure parameter considering thixotropic effects. This parameter is a measure of the degree of aggregate structure in suspension with a range from 0 at fully broken structure to 1 where the structure is fully recovered (Fig. 4.6). For the calculation of this non-dimensional structure parameter the first-order rate-equation was implemented as source and sink formulation in the advection-diffusion equation following Moore (1959):

$$\frac{\partial \lambda}{\partial t} + \frac{\partial u\lambda}{\partial x} + \frac{\partial v\lambda}{\partial y} + \frac{\partial w\lambda}{\partial z} = \frac{\partial}{\partial x}\left(\epsilon_x \frac{\partial \lambda}{\partial x}\right) + \frac{\partial}{\partial y}\left(\epsilon_y \frac{\partial \lambda}{\partial y}\right) + \frac{\partial}{\partial z}\left(\epsilon_z \frac{\partial \lambda}{\partial z}\right) + Q + S \tag{4.8}$$

$$Q + S = a(\lambda_0 - \lambda) - b\dot{\gamma}\lambda \tag{4.9}$$

where a and b are the empirical recovery and break-down rate, and λ_0 the initial and maximum value of the structured parameter at infinite rest, which is commonly assumed as one at a start of a model run. According to Moore's equation, the breakdown of a floc structure is only dependent on the deformation rate $\dot{\gamma}$. Thus, the rheological viscosity

is strongly dependent on the shear rate. An increasing shear rate leads to a break-down of flocculated aggregates combined with a decrease in viscosity and shear thinning flow behavior. A decrease or constant shear rate leads to a recovery of the floc structure.

4.4 Parametrization of the Rheological Model

The five empirical parameters (τ_y, μ_∞, μ_0, a, b) have to be identified and determined by rheological lab measurement investigations for modeling the rheological flow behavior. In literature a few studies were found, which show rheological results from fluid mud samples. Van Kessel and Blom (1998) analyzed mud samples from the Caland channel (Port of Rotterdam), Wurpts and Torn (2005) from the Port of Emden, Seifert (2011) and Oberrecht and Wurpts (2014b) analyzed samples from the main channel of the Lower Ems estuary. Furthermore, yield stress measurements of various mud samples from Gulport Harbor (US) were found. Seifert (2010) only determined the yield stress and zero shear viscosity, while Oberrecht and Wurpts (2014b) additionally determined the initial viscosity at fully broken structure. They also analyzed the break-up and recovery parameter a and b for the parametrization of the structure parameter λ. Wurpts and Torn (2005) and Van Kessel and Blom (1998) only investigated the yield stress.

The yield stress of a fluid is determined as the point where the fluid begins to flow. This point is associated with a disproportionately large deformation of the fluid structure. The yield stress can be investigated by so-called rheological based yield stress curves program or method (Fig. 4.3). Thereby, the shear stress will be stepwise increased by recording the corresponding shear rate. Latter measurement mode has to be started from a shear stress level well below the yield stress, then being stepwise increased unless plastic motion dominates the process. Given a sufficiently sensitive rheometer, even shear stress levels below the yield point result in (very) small shear, so a decision has to be made which point within the shear curve is the 'real' begin of motion.

For fluid mud good results were obtained by means of a semi graphical procedure, the so called "tangent" method (Mezger, 2006). Applied at log scaled flow curves, it allows reproducible determination of the yield stress. A first tangent slice the linear elastic range below the yield point. A second tangent is appropriated in the pseudo-plastic deformation range above the yield point. The intersection of both tangents determines the yield stress, which can be read from the abscissa. This kind of application of the method is illustrated in Figure 4.3.

Figure 4.3 shows that (extremely low) shear exists already at the lowest stress level applied, which partly result from elastic deformation. The underlying conceptual model for pseudo plastic granular or aggregated suspensions includes an inner structure. This is formed by aggregated grains, flocs and EPS, which contribute to the overall mechanical shear resistance of the suspension. It has to be overcome before relevant plastic motion arises.

Caused by this existing low shear rate and stress below the yield point, a least square fit

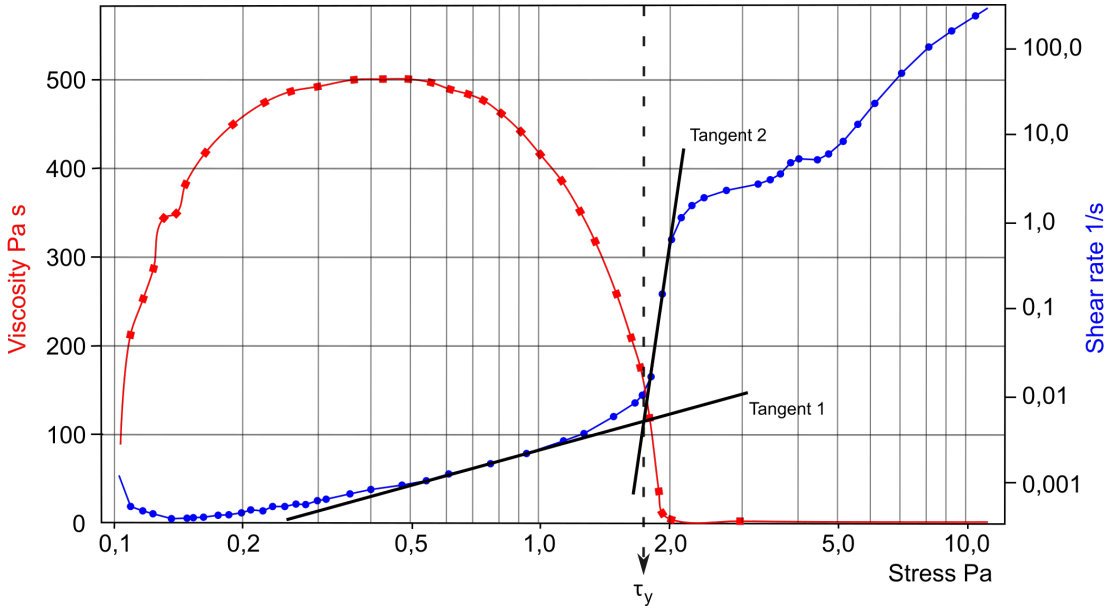

Figure 4.3: Illustration of a yield stress curve and resulting viscosity (according to Oberrecht and Wurpts, 2014b)

of equilibrium flow curves are not suitable enough to determine the real yield stress. The latter method will result in a much lower yield stress value, because zero-crossing of the shear rate will appear at a much lower shear stress level.

The yield stress was determined with respect to suspended sediment concentration from lab analyses found in previous literature (Fig. 4.4). Yield stress investigation from the Ems estuary and the Caland channel are used for an empirical fit. It is shown in Fig. 4.4, that included yield stress lab analysis covers a concentration range from 50 g l^{-1} up to 525 g l^{-1}. This concentration range includes highest concentrations of the mobile fluid mud layer and the full concentration range of a stationary fluid mud layer. Above maximum concentration range, the muddy sediment can be achieved as a strong consolidated bed and becomes part of a natural sediment bed.

The empirical fit of the yield stress to silty sediment concentration is described by an exponential function of all yield stress measures:

$$\tau_y = 4 * 10^{-7} C^{3.07} \tag{4.10}$$

Above empirical fit is able to describe the yield stress for different mud suspensions starting from 50 g l^{-1} up to 525 g l^{-1} based on lab investigations. In case of lower concentrations, the yield stress was extrapolated.

The rheological viscosity is indirectly measured by the yield stress curve measurement

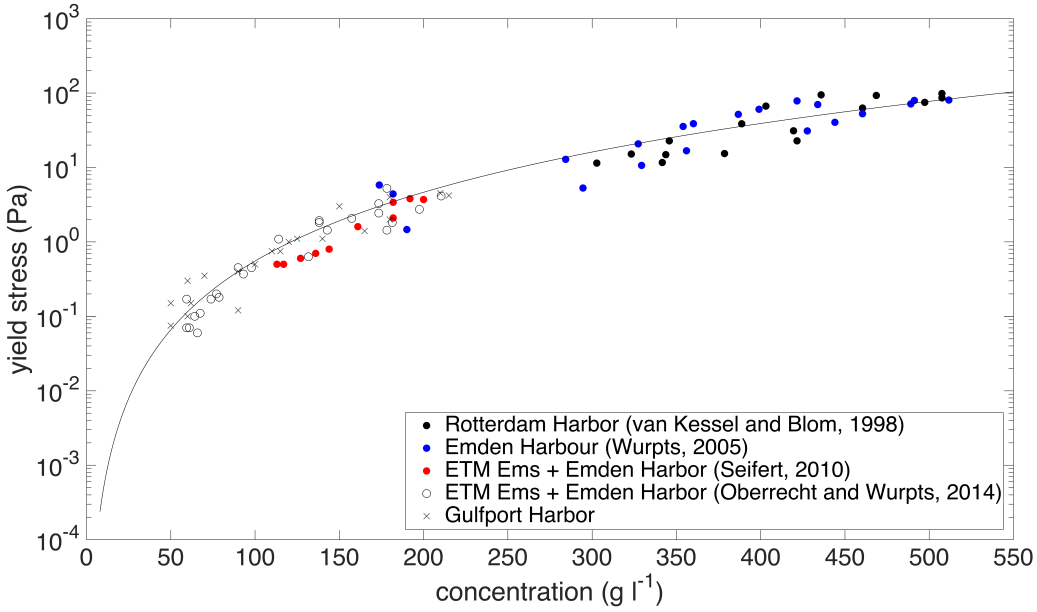

Figure 4.4: Yield stress in dependence to sediment concentration for various fluid mud suspensions. Data-based exponential fitting curve is shown as black line.

method. Based on the relation $\mu = \tau/\dot{\gamma}$, the viscosity of a fluid mud suspension can be calculated based on recorded shear rates by continuously increasing shear stress. The rheological viscosity at the yield stress can be determined by an associated yield point which is found by the tangent method (Fig. 4.3). The infinite viscosity is located by the yield stress curve, when the shear stress increases linearly with the shear rate. At this shear rate, the flow behavior of the mud suspension approaches to a likewise Newtonian fluid flow. Taking into account both previous mentioned studies (Seifert, 2011 and Oberrecht and Wurpts, 2014b), the already existing lab results are covering a wide range of suspended concentrations from 55 to 220 g l^{-1} for the initial and yield viscosity approximation (Fig. 4.5).

Parametrization of the empirical parameters μ_∞ and μ_0 by means of rheological lab results can be best described by an exponential fitting of equilibrium flow curves (Toorman, 1997). Both parameter ranges from the molecular viscosity to increasing magnitudes of the suspended sediment concentration. The rheological viscosity at a fully broken floc structure ($\lambda = 0$) is parameterized as:

$$\mu_\infty = \mu_m + 4.0E - 06 * C^{2.52} \tag{4.11}$$

and the rheological viscosity at the yield stress ($\lambda = 1$) is fitted by following equation:

$$\mu_0 = \mu_m + 6.0E - 08 * C^{4.52} \tag{4.12}$$

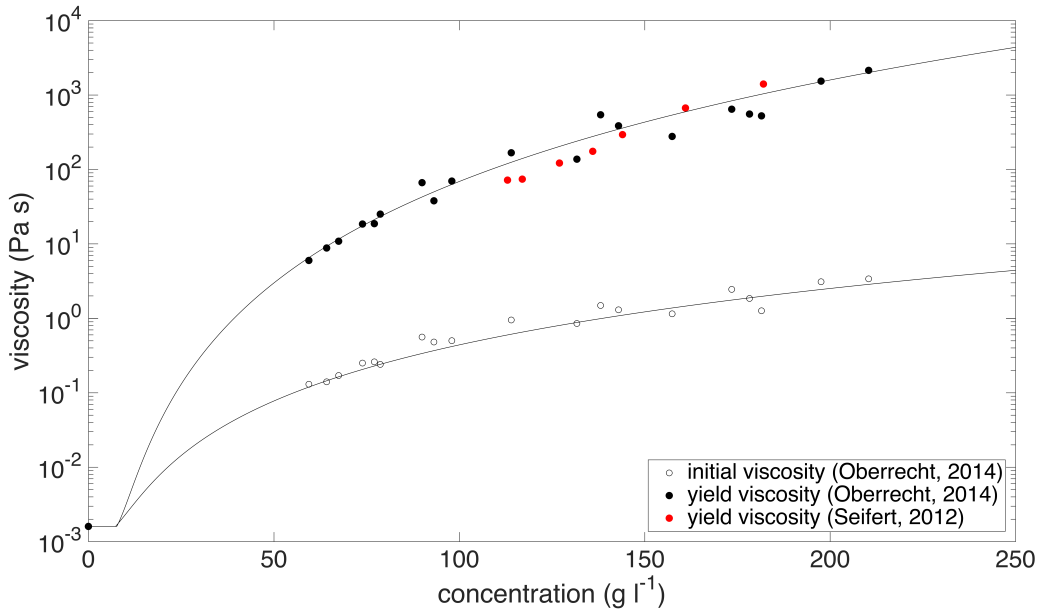

Figure 4.5: Semi-logarithmic plot of the yield (filled circles) and initial (open circles) rheological viscosity against suspended sediment concentrations. Also, empirical fitting curves are shown (black lines) for each parameter

For a time- and shear-dependent pseudo plastic suspension like fluid mud, due to thixotropy there exists a theoretically unlimited number of flow/yield curves depending (among other parameters) on the current shear rate and shear history. Therefore, extended fit of rheological parameters to lower concentrations have to be taken into account carefully. Empirically determined approximations of parameters cover a wide range of concentrations from 8 to 250 g l^{-1}. The lower limit of calculated rheological viscosity is set to the molecular viscosity. For a viscosity which is equal to the molecular viscosity the fluid dynamics are described as Newtonian fluid. This concentration range can also be achieved as change from flocculation to hindered settling regime or a switch from Newtonian to non-Newtonian flow behavior. It shows, that this general simplified approximation fits to overall continuous transition from a Newtonian to non-Newtonian fluid and can be seen as a suitable way of describing properties of fluid mud and its flow behavior. Presented fits of τ_y, μ_∞ and μ_0 can be quantified as a best fit of local mud samples. Rheological parameter fits were also presented by Malcherek and Cha (2011) from the Ems and Weser estuary, but especially determined rheological viscosity are much lower (100x), compared to results used in this study.

The break-down (b) and recovery (a) rate parameter of the rate equation can be determined by equilibrium flow curves equilibrium flow curves (EFC) and constant-rate measuring methods with a rheometer. Based on latter curves, the shear stress becomes time-independent to applied shear rate $d\lambda/dt = 0$, when an equilibrium between breakdown and recovery is reached. With this measuring type a certain shear rate is maintained un-

til a constant (equilibrium) shear stress arises. This equilibrium shear stress is generally illustrated in EFC for different shear rates. The EFC were found by Worrall and Tuliani (1964) and can be mathematically expressed as:

$$\tau_e = \lambda_0 \tau_0 + (\mu_\infty + (\mu_0 - \mu_\infty)\lambda_e)\dot{\gamma} \tag{4.13}$$

The initially shear stress τ_0 is equal to the yield point, when the floc structure is totally recovered ($\lambda = 1$). Therefore, all parameters are given by means of rheological analysis and the equilibrium value of the floc structure (λ_e) can be obtained by equation 4.13. At equilibrium, the rate of break-down is equal to the recovery, so that the relation of both parameter (β) can be obtained by the expression of the equilibrium floc structure equation (e.g. Toorman, 1997):

$$\lambda_e = \frac{\lambda_0}{1 + \beta\dot{\gamma}} \qquad \beta = \frac{b}{a} \tag{4.14}$$

The structure parameter in equilibrium conditions is not a constant coefficient, but dependent on the shear rate. For a specific determination of the recovery parameter, further investigations on equilibrium state have to be investigated. The relaxation of thixotropic fluids describes the transition to the equilibrium state, which occurs at a constant, deformable shear rate. This transition is described by Tiu and Boger (1974) or Nguyen and Boger (1985) for first order quantities according to equation 4.15:

$$ln(\tau_y - \tau_e) = ln(\tau_i - \tau_e) - kt \tag{4.15}$$

with:

$$k = a(1 + \beta\dot{\gamma}) \tag{4.16}$$

From these equations, an analytic solution of a as well as b can be determined. Therefore, the parameters a and b are time-dependent until an equilibrium is reached. Here, the time t must be chosen in such a way that it reflects the required duration to reach the equilibrium state ($d\lambda/dt = 0$). The coefficient of the recovery rate can be obtained from Eq. 4.16. After determining the empirical parameter β, the coefficient of the break-down rate is determined by its ratio ($\beta = b/a$). In this study, for the empirical break-down (b) and recovery (a) formulation, analyzed data of Oberrecht and Wurpts (2014b) leads to constant values, which have been used for the numerical examination. Therefore, the constant recovery parameter is set to $a = 0.05$ and the break-down rate to $b = 0.02$. Fluid mud itself is a thixotropic fluid and recovery rate usually must be higher than break-down rate.

Quality of rheological lab analysis depends strongly on the preprocessing of samples or lab instruments (e.g. rheometer) as well as material composition and therefore examined fitting curves. The resolution of a rheometer can vary in accuracy of applied shear stress

and resulting measured shear rates. In case of this limitation, a higher resolution is required for less concentrated suspensions (Mezger, 2006). For low concentrated suspensions (e.g. < 40 g l^{-1}) only a few investigations can be found in literature (e.g. Mehta et al., 2009). It could explain that rheological viscosity or yield stress investigations can mostly only be estimated in the higher concentration range, because the shear rate resolution of the rheometer is not sufficient enough.

Grain size distribution or mineral composition has an insignificant effect on the rheology (Seifert, 2010), but salinity, temperature, organic matter and the flow strength of samples are more significant. For latter material specifications (e.g. yield stress, viscosity), the resting period before rheometer tests are important (Maciel et al., 2009). Maciel et al. (2009) analyzed mud samples and found out, with an increasing resting period, the flow strength increases, which results in a much higher yield stress. Increase in temperature or salinity results in a decrease of rheological viscosity and yield stress (Makinde et al., 2011; Amani et al., 2015). The latter described effects on rheology were not taken into account in this study and are subject of scientific investigations. As already mentioned above, implemented empirical parameterization can be seen as a best fit of samples available for the study area.

4.5 Non-Newtonian-Induced Turbulence Damping

The effect of high concentrated suspensions on the vertical turbulent structure is unknown and part of scientific investigations (see Chapter 2). It is already known that the existence of high concentrated suspensions with non-Newtonian flow behavior can lead to a laminar flow regime. Occurring laminar flow behavior is not only dependent on vertical density gradients, where turbulence production is damped with a relation to the Richardson Gradient Number, but also by means of the suspension concentration and resulting non-Newtonian flow behavior. In literature, it is proposed an additional turbulence damping function for fluid mud-water mixtures, which includes the relation of the current concentration to the gel concentration (C/C_{Gel}). The latter formulation damps the turbulence linear with increasing suspended sediment concentration. The disadvantage of the mentioned approach is already discussed in Chapter 2.2.3. Therefore, here it will be firstly presented as a turbulence damping function, which is based on the material specific properties of such high concentrated mud suspensions. This additional damping term should be more realistic to reproduce the large-scale flow and transport characteristics of non-Newtonian fluids in estuarine environments.

The conceptual approach for the non-Newtonian (rheology)-induced turbulence damping is related to the floc structure and its aggregation state. Figure 4.6 illustrates the range of introduced approach in relation to the floc structure. The aggregation state of the floc structure in turn strongly depends on the current shear rate. It is expressed as state or degree of the structure with the dimensionless structural parameter. As the shear rate increases, deformation of the floc structure promotes a reduction of the initial viscosity and

maximum aggregation state. Furthermore, shear thinning behavior caused by increasing shear rate reduces the non-Newtonian viscous flow effect. At maximum deformation, flocs are present only as an individual floc in suspension without contact between other particles. In this deformation range, a dilute suspension is present, which consists of a Newtonian flow behavior.

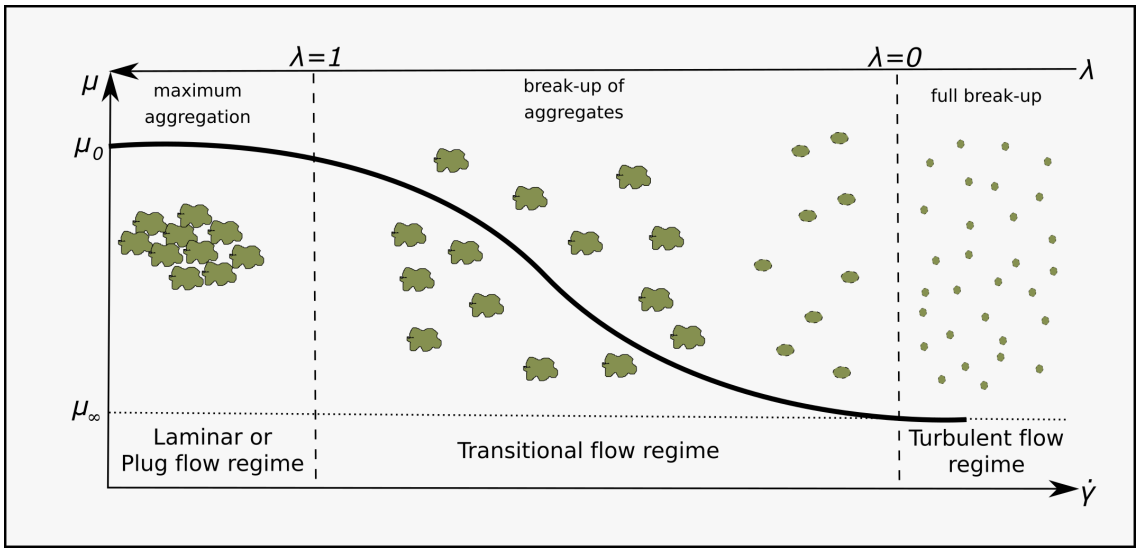

Figure 4.6: Flow regime of fluid mud and its non-Newtonian flow behavior during break-up of flocs with continuous transition from laminar flow regime to fully turbulent flow regime.

For the description of rheology-induced damping of the vertical turbulent momentum flux, the structure parameter is considered. The calculation of the eddy viscosity and diffusivity in terms of a fluid mud-water mixture is modified and the used k-L turbulence model viscosity equation is then finally written as:

$$\nu_t = \epsilon_t/\sigma_p = f_r c_D L\sqrt{k} \tag{4.17}$$

with the new introduced damping term f_r. The latter term is defined as the rheology-induced turbulence damping term, which is dependent on the strength of the floc structure and is expressed as:

$$f_r = (1-\lambda)^{\phi} \tag{4.18}$$

with ϕ an empirical exponent, which is here approximated as a first order term ($\phi = 1$). This rheology-induced damping term is introduced as an assumption, because physical relations are not yet exactly known between rheology and turbulence. Due to the complexity of analyzing rheology flow behavior, in-situ or lab based measurements of velocity, turbulence and floc structure are yet not accurate enough, taking into account a measurement

based validation of the extended damping approach.

This formulation promotes a turbulence damping, which is based on the non-Newtonian flow behavior and is associated with the local rheological flow behavior. In the case of maximum aggregation, turbulence is totally suppressed and the flow is described as a laminar flow regime. In this aggregation state, the structure parameter always assumes the value of $\lambda = 1$. When the floc structure is completely destroyed ($\lambda = 0$), no non-Newtonian induced damping of momentum and mass transfer is considered. Then, only the density stratification and Richardson Gradient Number dependent reduction of vertical exchange is present. Within the transitional regime, which describes the breaking and recovery of the floc structure, both the Richardson Gradient Number and the non-Newtonian induced turbulence damping is considered. Based on presented concept, the non-Newtonian induced turbulence damping is therefore described by the rate-equation according to Moore (1959). It describes additionally (to the rheological viscosity) the damping of momentum and mass exchange dependent to the local shear rate.

The conceptual approach presented here leads to a strong damping of the turbulent eddy viscosity and turbulent mass transfer. The rheology-induced turbulence damping is dependent only on two empirical parameters. The recovery parameter (a) and the breakdown parameter (b). As mentioned above, both empirical parameters are already determined by rheological lab investigations. Furthermore, the damping is directly dependent on the shear rate with respect to the aggregation state of the floc structure. Compared to the concentration dependent approach by Hsu et al. (2007), presented formulation should be reproduce more realistic the current flow structure. This is because it allows laminar flow behavior at already low suspended concentration (mobile fluid mud layer) and not only above the gel concentration. Because estuaries consist of very low shear rates (a few 1 s^{-1}), proposed approach will have a major impact on turbulent flow behavior and promotes a strong formation of fluid mud layers.

4.6 Bed Shear Stress Approximation

The bed shear stress approximation and assumption is important for the bed roughness and bed boundary turbulence production as well as erosion of sediment. The general formulation in Delft3D, which only considers the turbulent shear stress and neglect the viscous term, cannot be used in the case of non-Newtonian flow close to the bed. The Delft3D model was extended to consider not only the turbulent shear stress, but also the viscous shear stress. Therefore, the total fluid shear stress acting on the river bed τ_b is the sum of turbulent and viscous (rheology) contributions:

$$\tau_b = \tau_t + \tau_r = \nu_t \rho \frac{\partial \overrightarrow{u}}{\partial z} + (\nu_r + \nu_m)\rho \frac{\partial \overrightarrow{u}}{\partial z} \tag{4.19}$$

where the first term on the right hand side determines the turbulent induced bed shear stress, while the second term the rheology-induced bed shear stress. In numerical models solving the RANS equations, the viscous term is neglected, because the viscous sublayer is not resolved, where the molecular viscosity becomes important. For modeling of non-Newtonian flow behavior, this term becomes important and has to be considered. As mentioned, the rheological viscosity is not constant and varies significantly with respect to suspended concentration and local shear rate.

The vertical velocity profile is determined by the vertical eddy viscosity and the boundary conditions at the bed by the so-called bed shear velocity. The near bed shear velocity is calculated based on the relation of bed shear stress to local fluid density:

$$u_* = \sqrt{\frac{\tau_b}{\rho}} \tag{4.20}$$

For determination of the turbulent bed shear stress a logarithmic velocity profile in the near bed grid cell is assumed. Following this assumption the bed shear stress formulation is determined for turbulent conditions as:

$$\vec{\tau_t} = f_r g \rho_0 \frac{\vec{u_b}|\vec{u_b}|}{C_D^2} \tag{4.21}$$

with:

$$C_D = \frac{\sqrt{g}}{\kappa} ln\left(\frac{z}{z_0}\right) \tag{4.22}$$

where z_0 is the roughness length, which can be assumed for rough walls as $z_0 = k_s/30$.

As mentioned, in high concentrated suspensions, the above formulation (Eq. 4.21) is no longer only valid for calculating the local bed shear stress. Its calculation by the logarithmic velocity profile (Eq. 4.21) can only be applied in turbulent flows for hydraulically rough conditions, because for laminar flow at the wall z_0 become zero and thus the above equation

system becomes indefinite. This means, in case of fluid mud layer formation and flow behavior (possible laminar flow), classic formulation (turbulent and quadratic wall friction approach) of the bed shear stress must be modified.

The shear stress of fluid mud is described by the rheological model and is used here as the part of the viscous bottom shear stress induced by the viscous (rheological) stress. The rheological part of the bed shear stress is determined following presented rheological model from Worrall and Tuliani (1964) and is already described by Eq. 4.5 and parameterized following Eq. 4.10. Equation 4.5 consists of a yield stress, which has to be overcome before any fluid will flow. Therefore, if the shear stress becomes lower or equal as the yield stress, the turbulent part of the bed shear stress becomes zero, because the shear rate is then assumed as zero. At zero shear rate, the flow can become laminar and the viscous shear stress has to be defined by a minimum value. Otherwise, the rheological viscosity becomes infinite and the equation cannot be solved. This is prevented in the model by setting the minimum viscous shear stress to the yield stress and the maximum rheological viscosity to the zero shear viscosity (Fig. 4.5).

5 Estuarine Test Case - Verification of extended approach

The numerical model approach is verified and validated by process-based field measurements along the high concentrated part of the Ems estuary in Germany for several months of the year. The Ems estuary is known as a very muddy estuary because it shows fluid mud layer along the upper most tidal part. Modeling the fluid mud layer formation and its large-scale distribution requires a process-based approach in order to validate the numerical model. The estuarine situation in combination with fluid mud requires physically correct model reproduction of baroclinic circulation, tidal range and freshwater discharge as well as the availability of sediments that can form fluid mud. Modeling estuarine circulation, a three dimensional model concept is applied due to large-scale density driven buoyancy and stratification effects by salinity and sediment (Pritchard, 1952).

5.1 The Ems estuary

The Ems estuary (Fig. 5.1) is located in the northwest of Germany, partly bordering the Netherlands. At the Ems, four major ports are located (Eemshaven, Delfzijl, Emden and Leer) making the estuary an important sea trading route. The tidally influenced part of the Ems estuary extends a total length of 110 km starting from the east Frisian island Borkum to the tidal weir in Herbrum and consists of a tributary river system in the tidal reach named Leda-Juemme. The total area of river basin is approximately 18.000 km^2. The Ems estuary is divided into four major parts, based on sedimentary and physical behavior:

- (I) from Borkum to Knock the outer part of the estuary, which shows pronounced inter-tidal areas and indicates a funnel-shaped morphology.
- (II) the Emder fairway from Knock to the harbor of Emden, which has significantly altered in depth.
- (III) the Dollard bay south of the Emder fairway. A bay created by a storm surge in the Middle Ages. The spatial extension of the bay is approximately 10 km. The Dollard is separated from the Emder fairway by a dam (Geisedamm).
- (IV) the Lower Ems estuary from Emden to the tidal weir in Herbrum with the tributary river system Leda-Juemme, which take a one third of the tidal volume.

Since the 16^{th} century, the Ems estuary has been altered by human intervention. Until the end of the 19^{th} century, this was primarily about land reclamation in the outer estuarine area. However, in the last 100 years, the focus has been on activities by means of traffic water management measures to adapt to increasing needs of shipping industry and ship-building. Since 1950, the Ems has been deepened several times and the Ems river was straightened between Terborg and Papenburg. Apart from the ports, in Papenburg is located a ship-building yard that builds large passenger ships with an ever increasing draft. These large ships have to be transferred into the adjacent North Sea after completion.

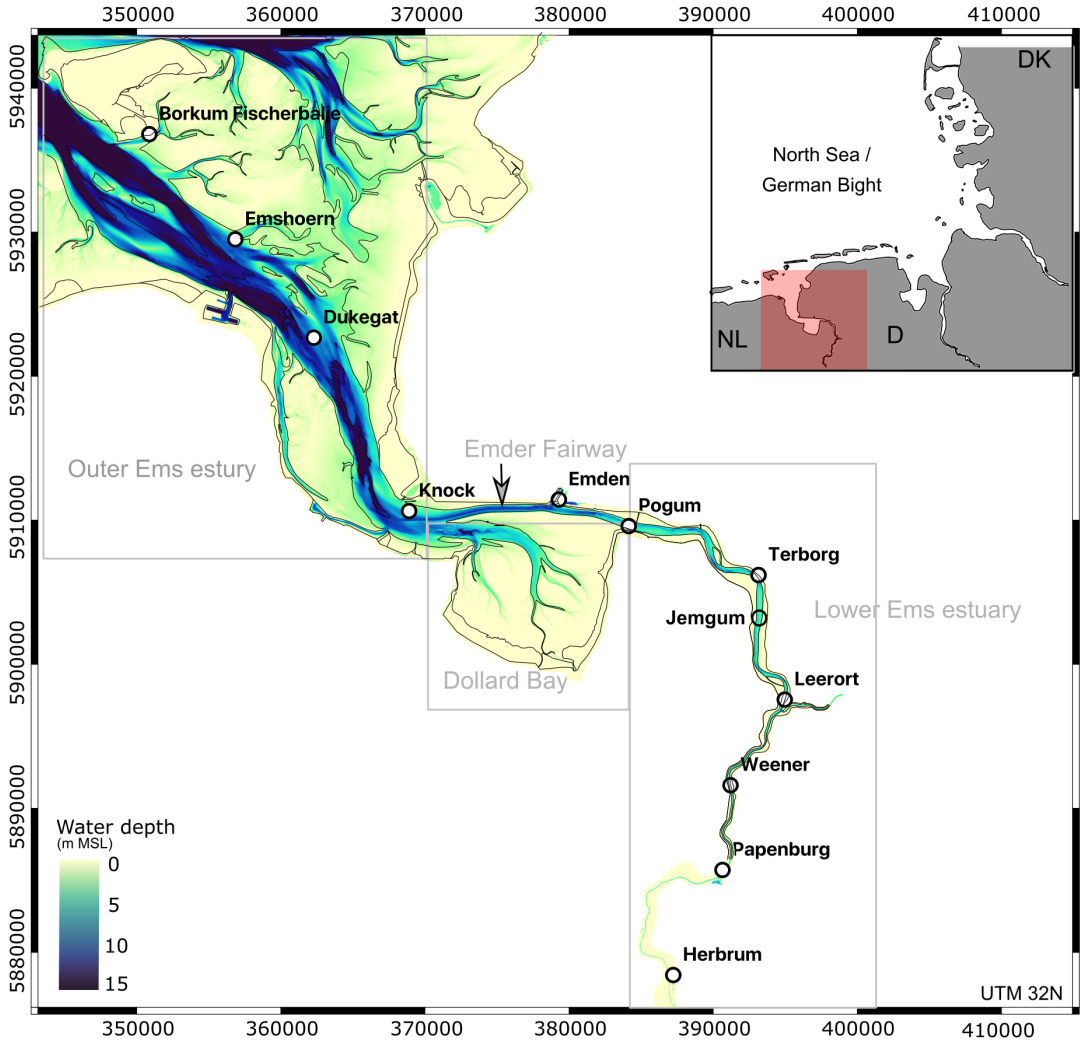

Figure 5.1: Map of the Ems estuary and its location in the southern North Sea. Bathymetric data are shown as colors. Gray boxes illustrate the four major regions.

Especially for the transfer of the passenger ships, the upper part of Lower Ems estuary was deepened after 1984 from 5.0 m to 7.3 m (Tab. 51). Due to the construction of the storm surge barrier near Pogum, the upstream part can be closed and flooded for the transport of ships into the North Sea. Therefore, the maximum dredged depth of 7.30 m was no longer necessary and the current maintenance depth is the former 6.3 m. Deepening and straightening of river bends are main measures, which caused significant changes in tidal dynamics (e.g. significantly increased tidal amplification and volume as well as increasing the sediment transport rates), which is observed in recent decades (Herrling and Niemeyer, 2008; Talke et al., 2006; Maren et al., 2015).

The Ems estuary is a partially mixed and mesoscale estuary. The average fresh water inflow is about 80 $m^3 s^{-1}$, and varies seasonal from 25 $m^3 s^{-1}$ during summer conditions to 300

Table 51: Chronology of channel deepening and other interventions in the lower Ems River (adopted from van Maren et al., 2015)

Year	**Measure**
1984/1985	Emden-Papenburg 5.70 m below NHN
1991	Straightening of bends, reducing the river length by 1 km, Emden-Papenburg 6.30 m below NHN
1993	Emden-Papenburg 6.80 m below NHN
1994/1995	Emden-Papenburg 7.30 m below NHN
2001	Construction of the Ems storm surge barrier near Pogum

$m^3 s^{-1}$ during winter (e.g. Krebs and Weilbeer, 2008). Due to deepening and straightening of the deep channel of the Lower Ems estuary during past decades, the propagation of the tidal wave through the estuary has been altered significantly. The mean tidal range at the seaside boundary amounts 2.20 meters and increases in up-estuary direction to 3.20 meters in Papenburg. From Papenburg to the tidal barrier at Herbrum, the tidal range decreases to 2.70 meters. The tidal range in this upper part of the estuary is mostly dependent on the amount of freshwater inflow. Historical investigations of the year 1937 by Herrling and Niemeyer (2008) have shown that the tidal range at Papenburg (1.25 m) as well as at Herbrum (1.0 m) was much lower. This analysis makes clear that anthropogenic interventions have greatly altered the dynamics in the estuary. Engineering measures have reduced shear and roughness, which implies a less impeded propagation of the tidal wave through the estuary and resulted in higher high water level as well as lower low water levels (Herrling and Niemeyer, 2008; Maren et al., 2015). As a result, the flow behavior shifted to shorter but stronger flood flow and weaker but longer ebb flow. For example, nowadays at Papenburg the mean flood duration is approximately 4.5 hours, while the ebb duration takes about 8 hours.

As the Ems estuary is a partially mixed estuary, sediment transport and salinity intrusion are driven by turbulence intensities, which are modified by vertical salinity stratifications. Model investigations of Oberrecht and Wurpts (2014) have shown, a maximum vertical salinity gradient of 4-5 psu occurs from Knock to Pogum during spring tide. During neap tide conditions, the salinity gradient is slightly higher at Knock (5-6 psu), while near Pogum, the gradient becomes much lower (0-2 psu). Intensity of the vertical salinity gradient is mainly forced by the horizontal salinity gradient along the estuary and local turbulence intensity. Based on these investigations, during neap tide the spatial extension in upstream direction of the baroclinic circulation is smaller compared to spring tide conditions. The existence of this inevitably baroclinic circulation results in a turbidity zone at the landward boundary of salinity intrusion and has a great impact on sediment transport behavior.

The turbidity zone in the Ems estuary is located upstream of the baroclinic circulation and concentrated to the Lower Ems estuary at moderate discharge (Borgsmueller et al.,

2016). The seaside boundary of the turbidity zone varies with horizontal density gradient, wind forcing, seaward water elevation, freshwater inflow and bathymetric impacts. The landward limit is dependent on the discharge situation. Nowadays, the turbidity zone extends over 30 km from Terborg up to the tidal weir in Herbrum. Following Jonge et al. (2014), the large spatial extension is a result of the tenfold increase in sediment concentrations. Following Maren et al. (2015), the reduction of hydraulic drag (from sandy bed to muddy bed) increased the sediment import capacity of the Lower Ems and is therefore responsible for the larger extraction of the turbidity zone. Investigations of Borgsmueller et al. (2016) show yearly mean sediment concentrations from 1979 to 1984 compared to concentration measurements of 2013 at different locations along the Ems estuary. This analysis shows the shift of the turbidity zone with its turbidity maximum as a result of the deepening and straightening measurements. During 1979, the ETM was located near Pogum with a sediment concentration of 1 gl^{-1}. Nowadays, the maximum is located at Weener (25 km upstream of Pogum) with a yearly mean concentration of 19 gl^{-1}. However, partial concentrations of over 40 g$l^{-1}$are measured in the flood phase at low freshwater inflow. Furthermore, the change in flow behavior led to massive accumulation of cohesive sediment in the turbidity zone, which nowadays forms fluid mud layer. This exhibits complex interactions between suspended sediment and tidal currents like dynamic stratification and a non-Newtonian flow behavior in the lower parts of the water column. During slack time and on ebb period, fluid mud layers are formed up to 3 meter thickness with a strong sediment-induced density gradient of 40 gl^{-1} (Habermann and Wurpts, 2008). The formation of fluid mud is most pronounced during summer conditions where the discharge is low. Because of the high amount of cohesive fines, the Lower Ems is defined as a highly concentrated estuary (Talke et al., 2009). The accumulation and formation of fluid mud has further consequences for the ecological state of the Ems estuary. Due to the high amount of fine sediments in the water column, the oxygen level becomes hypoxic during low discharge conditions and high water temperature in summer.

Based on sediment transport behavior and surface bed material content, the Lower Ems estuary can be nowadays divided into three regions:

- **Emden to Terborg (I)**: Following data analysis of Winterwerp et al., (2017), this part is always flood dominant caused by tidal asymmetry and estuarine circulation. The bed material consists mainly of muddy cohesive sediments and local erosion/deposition behavior is controlled by sand-mud interaction dynamics (e.g. Van Kessel et al., 2011).

- **Terborg to Papenburg (II)**: The bed sediment is of mainly cohesive fines with rheological characteristics (Papenmeier et al., 2012). Sediment behavior is strongly dependent on tidal asymmetry and builds a so-called fluid mud pool (Winterwerp et al., 2017). In this area, temporally, a mobile fluid mud layer is developed, which emanates from sediment erosion and can have a thickness of up to 3.0 meters with respect to complex settling processes. It separates the water column into an upper low dense layer and a lower high concentrated fluid mud layer.

- **Papenburg to the tidal weir (III)**: Sandy sediments are mainly found, which are covered temporarily by muddy sediments (at lower discharge periods). Suspended sediment transport from the Ems river into the estuary showing a non-significant influence of sediment capacity of the upper Ems. Measured sediment concentrations are in order of 0.01 g l^{-1} in upstream region of the tidal weir in Herbrum (Tippener and Reinemann, 1979).

The averaged dredging volume of the Lower Ems estuary amounts 2.0 Mio.m^3, which is about 0.36 Mio. tons of dry sediment mass. The dredging sediment mass consists only of muddy sediments (BfG, 2017). A landward sediment transport mass from the North Sea into the estuary is unknown, but marine sediment has been found in the estuarine mixing zone and upstream freshwater zone (BfG, 1998). A long-term fluvial sediment input from the tributary river system Leda-Juemme into the estuary has been measured and amounts of 390 tons per tide, but varies strongly on a seasonal time-scale (Dette et al., 1994).

5.2 Model Set-Up

A three-dimensional structured, finite volume Delft3D model with mentioned extensions was applied to reproduce the hydrodynamics and density-driven flow effects of the Ems estuary. Overall model domain (Fig. 5.2) includes the entire Ems estuary and tributary river system Leda-Juemme, which flows into the Lower Ems estuary at Leerort.

The study area extends from the east Frisian island Borkum up to the tidal barrier 110 km upstream in Herbrum. The lateral model boundaries follow the dyke line and are fixed to nine meters above mean sea level. The horizontal curvilinear grid has in total 33.000 grid points. The horizontal mesh size varies from 50 m in the upper part of the estuary to 700 m at the seaside boundary. Because of large morphological changes in time and space due to fluid mud layer behavior, the most accurate and recent bathymetric data (2010), supplied by NLWKN (Lower Saxony Water Management, Coastal Defense and Nature Conservation Agency) of the Ems estuary has been interpolated to the grid. The vertical direction is discretized by 21 unequally distributed sigma-layers. Guan et al. (2005) show that a higher resolution near the bottom is needed to resolve high concentrated fluid mud layers. Furthermore, van Rijn (1986) found out by numerical investigations, that the maximum error is less than 10 % in vertical sediment distribution using more than 15 vertical layers. Therefore, a higher degree of vertical discretization was applied to keep the error as small as possible.

For the model investigation and validation, a three month simulation period from April to June 2017 was chosen. Complete model time period of three months are later used for analysis of the large-scale fluid mud dynamics and transport behavior. The chosen time period reproduces typical summer conditions where the freshwater inflow was measured at around 40 $m^3 s^{-1}$. This time period consists of strong fluid mud layer formation in the Lower Ems estuary. As this study focuses on large-scale fluid mud layer dynamics,

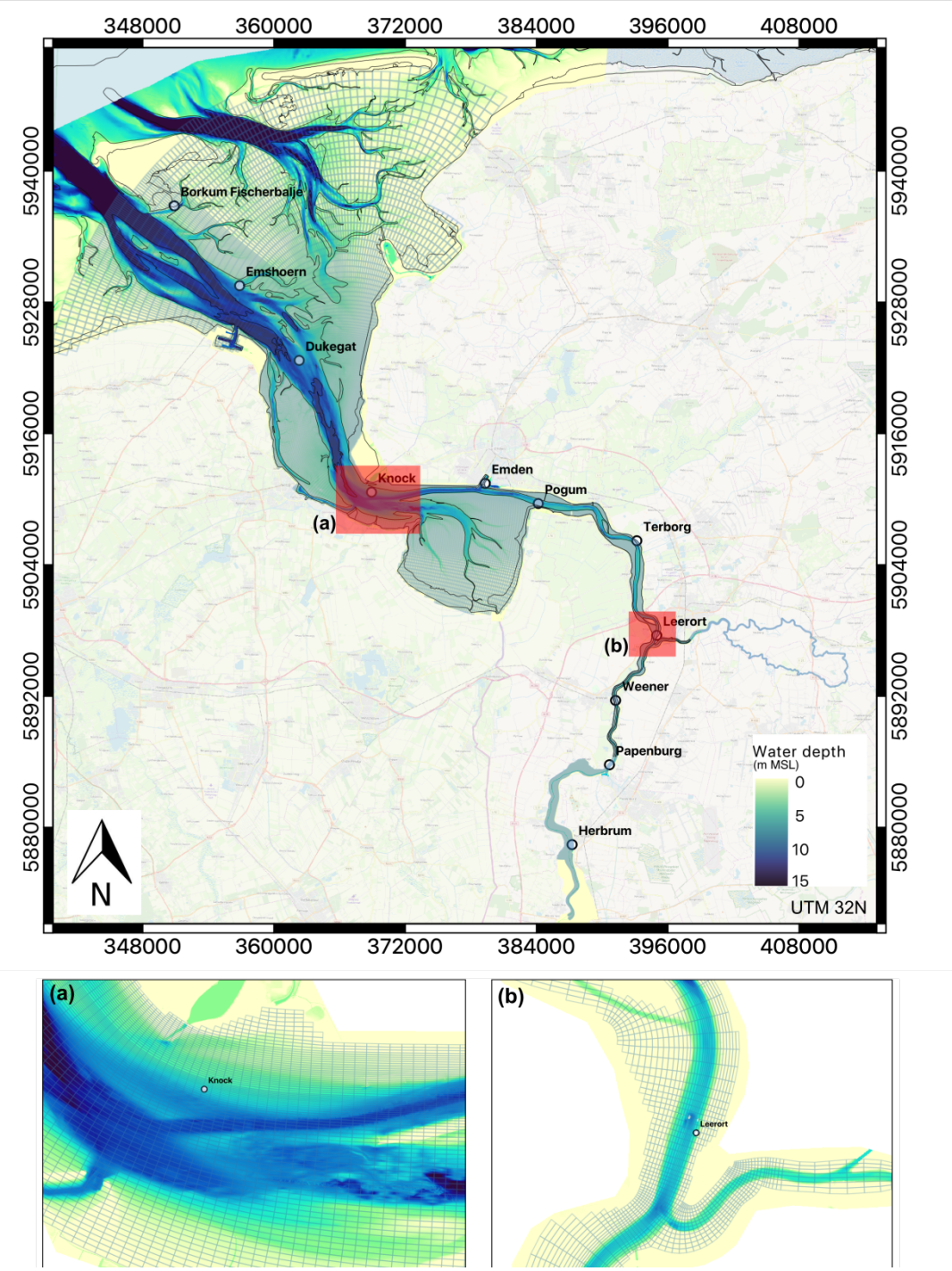

Figure 5.2: Map of available bathymetric data set of the Ems estuary and curvilinear model grid (gray). Lower panels show details of the model grid resolution and bathymetry at location Knock (a) and Leerort (b). Background landside map was generated with OSM (Open Street Maps).

only one muddy sediment fraction is considered. Taken into account entire density-driven dynamics, additionally the salinity is modeled along the estuary.

5.2.1 Boundary conditions

The open boundary condition at the sea-side is implemented by tidal forcing of measured water level time series at station Borkum (Fig. 5.3 a). Both inland boundaries (tidal barrier in Herbrum and Leda-Juemme) have been implemented as a (measured) time-varying discharge time series (Fig. 5.3 b). The freshwater inflow at the tidal weir in Herbrum decreases from 50 $m^3 s^{-1}$ to 35 $m^3 s^{-1}$ within modeling period, while freshwater inflow at landside boundary of the tributary river system Leda-Juemme is assumed to be 30% of the mean discharge at the tidal weir at Herbrum (around 12 $m^3 s^{-1}$).

For the transport of salt a constant value of 28 psu is assumed at sea side boundary, while at both landside boundaries a freshwater salt content of 0.3 psu is assumed. Temperature variations are neglected because of their small effect on density-driven dynamics. Sediment import at the tidal barrier at Herbrum is neglected, because mainly sandy sediments are imported from upstream location (Tippener and Reinemann, 1979). For the sea-side boundary a sediment concentration (0.01 g l^{-1}) is implemented as constant boundary condition. The sediment concentration is based on long-term observations and can be regarded as a mean annual concentration (e.g. Maren et al., 2015).

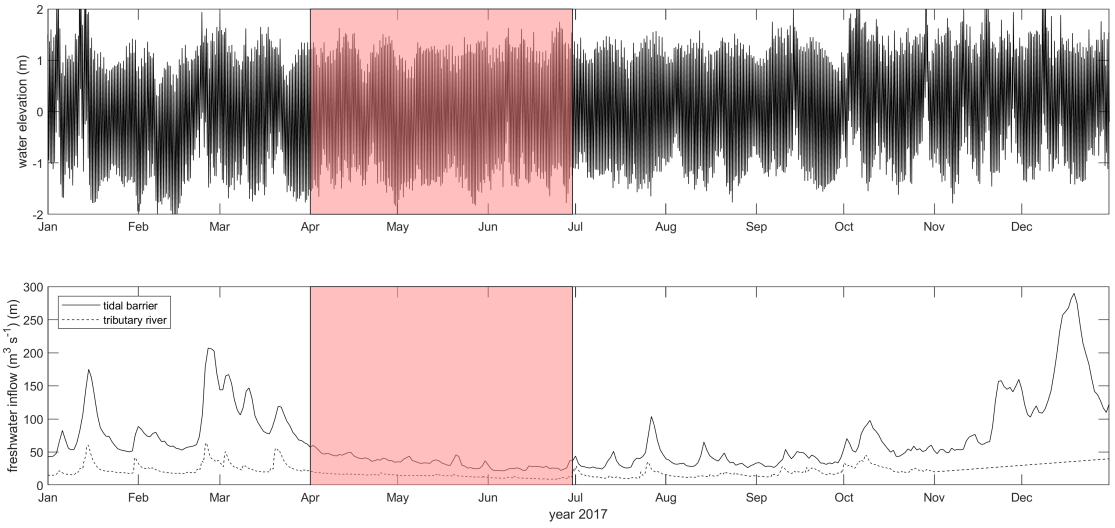

Figure 5.3: Sea and landside boundary conditions of the model run. Upper panel shows the water elevation at the seaside model boundary close to Borkum (Data from WSA Emden). Lower panel shows the discharge time series of the year 2017 at the tidal barrier at Herbrum and for the tributary river system Leda-Juemme (Data from NLWKN Aurich). In red the modeling period for investigations is shown.

5.2.2 Initial conditions

Initial conditions for salinity were calculated based on gauge stations along the estuary. For each station measured salinity of the first five days of modeling period were averaged and then interpolated to the grid nodes along the estuary.

Set-up of the initial sediment concentration follows an analysis of available multi-frequency echo sounder data and vertical suspended sediment concentration profile along the Lower Ems estuary. Based on longitudinal multi-frequency echo sounder profiles and vertical suspended concentration profiles of the Lower Ems estuary the total amount of cohesive fines in suspension can be assumed as approximately 0.3 Mio. tons along the deep channel from Terborg to Papenburg. The calculated total mass is uniformly distributed over the water column in the deep channel of the Lower Ems (Terborg to Papenburg) with a constant sediment concentration of 20 g l^{-1}.

Considering erosion and sedimentation, a one meter thick bed layer of the muddy sediment along the deep channel from Terborg to Papenburg and in the tributary river system Leda-Juemme was initialized. The bed material is characterized as a weak consolidated material with a dry bed density of 500 kg m^{-3}. The critical erosion shear stress (τ_e = 0.2 Pa) and the erosion coefficient of $E_0 = 4 * 10^{-4}$ are derived through model calibration against observed sediment concentrations and fluid mud layer distribution. Vertical momentum and tracer mixing is computed with the standard one equation k-L turbulence model with respect to rheology induced turbulence damping. The bed roughness varies throughout the modeling domain and is calculated for the roughness length z_0 based on mean grain-size sediment diameter, which is based on data sets of McLaren et al. (1998) and Meyer and Ragutzki (1999). The relationship between roughness length and mean sediment diameter is assumed as $z_0 = 2.5 * d_{50}/30$.

5.3 Model Validation

5.3.1 Tidal cycle dynamics

Measurement Campaign As part of the project "*Masterplan Ems 2050*[1]" a stationary measurement campaign was carried out in the Lower Ems at station Jemgum (see Fig. 5.1 for location) from 24.04 to 25.04.2017. The main objective of this campaign was to analyze vertical suspended sediment dynamics and its distribution during a tidal cycle. Therefore, data were collected over a time period of 13 hours covering a whole tidal cycle. This time period represents increasing tidal range of a neap to a spring tide transition. The freshwater inflow during measurement was moderate with Q = 40 $m^3 s^{-1}$ and characterizes the most frequent annual discharge.

Station Jemgum is located between Terborg and Leerort with a fluid mud layer development

[1] `https://www.masterplan-ems.info/`

during low discharge rates (e.g. Winterwerp et al., 2017). Therefore, during measurements a distinct fluid mud layer with a thickness up to 1.5 meters could be observed. This measurement location is located along a straight channel which extends in north-south direction. Thus secondary currents by e.g. river bends do not occur, and therefore resulting effects are not important and can be neglected. Additionally, depth variations are relatively small in along channel direction with an average depth of around six meters, following the bathymetry map (see Fig. 5.1).

For this stationary measurement, the research vessel was moored at the side of the deep channel. An acoustic Doppler current profiler (*ADCP, Teledyne RDI 600 kHz*) and a parametric echo sounder (*TOPAS, Kongsberg*) were deployed at the side next to the deep channel. Vertical high suspended sediment concentrations were collected by a density sounder (*USP, admodus*) and salinity as well as temperature were recorded by a CTD (*Sea & Sun Technology, Trappenkamp*) at 15 min intervals. Measurement results based on acoustic instruments (e.g. ADCP) are sensitive in high concentrated suspensions, because signal-to-noise ratio becomes low. To overcome this problem, velocity measurements were filtered in a 5-min interval. Becker et al. (2018) have shown by a comparison of ADCP and inductive velocity measurement instruments (ECM), that processed ADCP data are valid in mobile fluid mud layers.

Comparison to model results Figure 5.4 shows results of depth resolved measured and modeled suspended sediment concentration with respect to the same location and time period. The time period starts around high water and extracts over a full tidal cycle. It is shown, that high concentrated sediments are only found in the lower part of the water column. At concentrations above 10 g l^{-1}, the suspensions are referred as fluid mud. Therefore, fluid mud is present over the whole tidal cycle at this location. The vertical concentration profile shows a distinct lutocline at 10 g l^{-1}. Below this lutocline, vertical concentration profile is generated mainly by hindered settling and turbulence interaction. A second lutocline builds the interface between mobile and stationary mud at a SSC of 50 g l^{-1}. The water column can be separated based on suspended sediment concentrations in three phases:

- an upper water column with a Newtonian fluid with low SSC (< 8 g l^{-1})
- a weak non-Newtonian fluid with increasing SSC (8 g $l^{-1} <$ SSC < 50 g l^{-1}) and rheological viscosity
- a weak consolidated mud layer, which is also characterized by non-Newtonian flow dynamics (SSC > 50 g l^{-1})

On suspended sediment concentration named classification agrees well with the classification of Papenmeier et al. (2013), which is based on water and sediment samples from the Lower Ems estuary.

Figure 5.5 show associated results of measured ADCP based horizontal flow velocities and

modeled horizontal velocities with respect to the same location and time period as in Fig. 5.4. Horizontal velocities are maximum near the surface, indicated by the model results. During measurements, the down-locking ADCP was mounted 2 meters below surface, therefore, measured velocities in the upper water column are not available. During ebb flow, the maximum velocity is around 1.2 m s^{-1}, while during flood a maximum velocity of 1.5 m s^{-1} is observed.

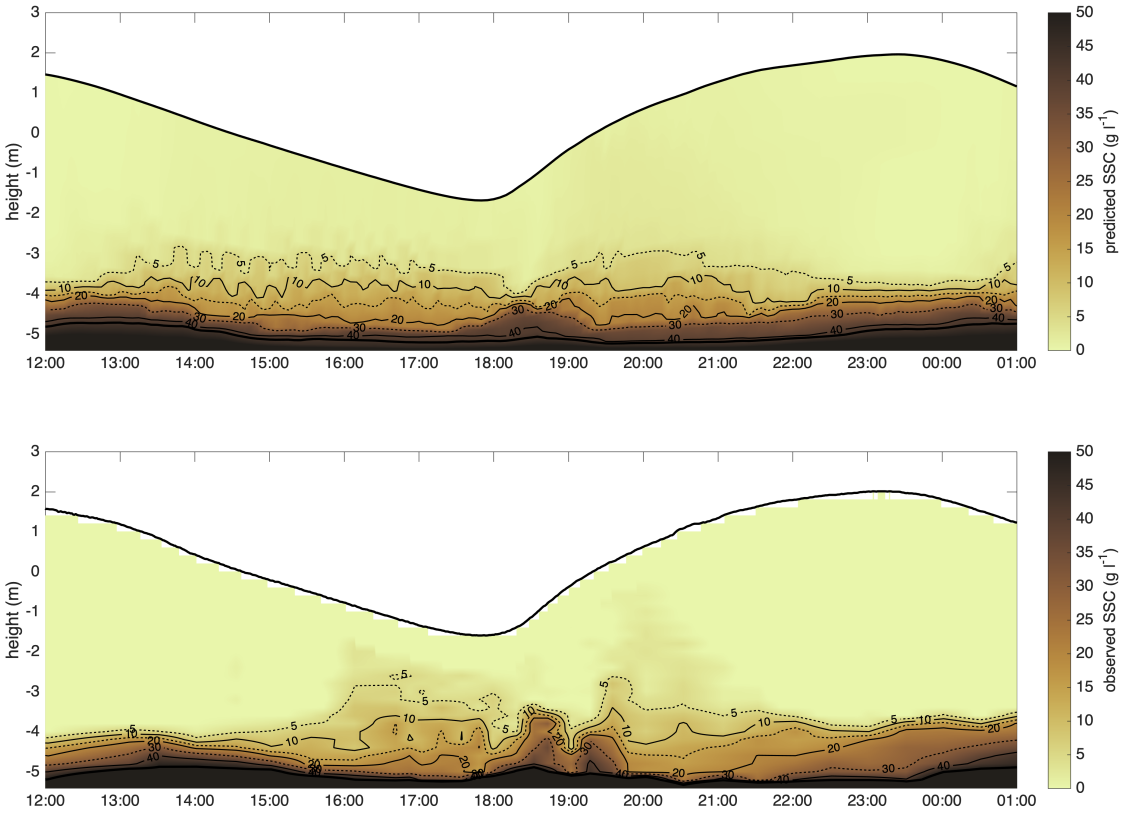

Figure 5.4: Time series of modeled (upper panel) and measured (lower panel) suspended sediment concentration at station Jemgum during a tidal cycle (24.04.2017). Black solid and dashed lines are sediment concentration isocline. Water-level is shown by the black thick line at the top of the figure. The natural bed level is at 5.20 meters below MSL.

The natural bed is found at a depth of 5.20 meters below mean sea level and is determined as a weak consolidated layer of a dry bed concentration greater than 500 g l^{-1}. A weak stationary fluid mud layer (C > 50 g l^{-1}) of a few centimeter thickness covers the natural sediment bed. This was also observed by other authors e.g. in the Gironde estuary (Abril et al., 1999) or Ems estuary (Becker et al., 2018). Above the stationary layer, separated by a strong lutocline, a mobile fluid mud layer is present over the complete tidal range with concentrations of 10 - 50 g l^{-1}. Based on the sub-tidal asymmetry in vertical mixing, the concentration profile differ strongly between flood and ebb phases (Becker et al., 2018). Generally, a rapid increase of sediment concentration in the water column is shown from

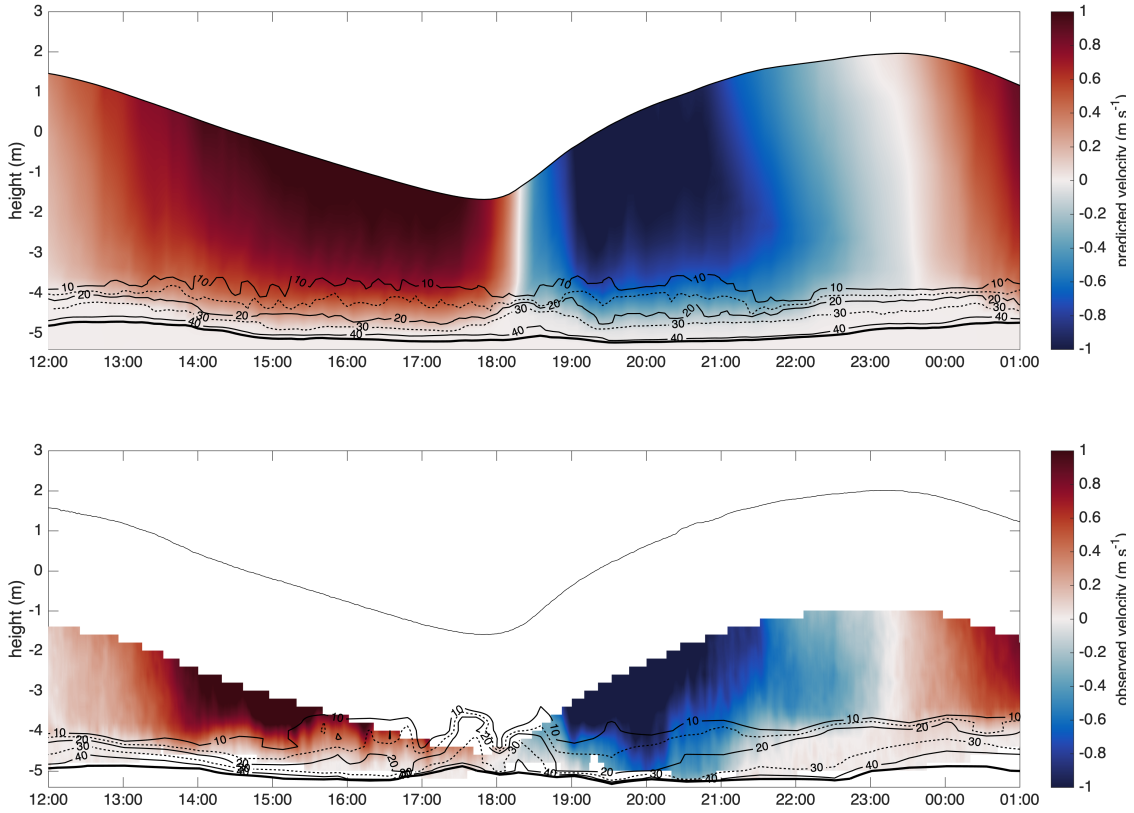

Figure 5.5: Time series of modeled (upper panel) and measured (lower panel) horizontal flow velocity at station Jemgum during a tidal cycle (24.04.2017). Black solid and dashed lines are representing sediment concentration isocline. Water-level is shown by the black thick line at the top of the figure. The natural bed level is at 5.20 meters below MSL.

surface to the bottom. This high concentrated vertical sediment profile is present over the whole tidal cycle.

The velocity profile in the fluid mud layer shows a strong reduction of horizontal flow velocities with increasing sediment concentration. This behavior is generally observed for concentrations above 20 g l^{-1}. It shows, that also the mobile fluid mud layer partly leads to reduced horizontal flow velocities and non-Newtonian flow behavior becomes important. This observation/finding is in contrast to observations of Winterwerp and Van Kesteren (2004), who assume, that non-Newtonian behavior only becomes important at concentrations above 40 g l^{-1}. This cannot be confirmed by presented measurements and modeling results.

Temporally, the mobile fluid mud layer is separated from the upper part of the water column by a strong lutocline, caused by hindered settling of cohesive fines. Furthermore, it is shown, that after formation of the distinct lutocline the horizontal flow velocity directly above the lutocline is higher compared to near surface velocities. This implies a low energy

flow behavior near the lutocline, where turbulence is highly damped. This mechanism leads to further implicit upstream propagation of saltier water masses as proposed by Becker et al. (2018). This flow dynamic is responsible for an inverse salinity profile, which is a specific characteristic of high-concentrated estuaries.

The comparison of observed and simulated tidal driven fluid mud dynamics are well reproduced by the model, including high variations in suspended sediment concentration, horizontal velocities, viscous damping of flow velocities, formation of fluid mud layers, and entrainment from the lutocline and resulting thickness of the fluid mud layer.

5.3.2 Neap-Spring Variation

Modeling estuarine dynamics requires a validation based on long-term measurements e.g. neap-spring tidal cycle variation in suspended sediment transport and hydrodynamic quantities (e.g. water level elevation). Suitable data sets to validate model dynamics with respect to temporal and spatial sediment dynamics are usually limited, which is not the case at the Ems estuary. For model validation over a longer period, gauge station data along the estuary were used. Three gauge stations (*Terborg, Leerort and Papenburg*, see Fig. 5.1 for locations), which are located on the side of the deep channel, which had all the data available within considered time period.

At measuring stations, water level elevation is measured, as well as sediment concentration at a vertical position of about three meters above the bed. Concentrations are measured by turbidity sensors, which are calibrated for high fine sediment concentrations. Following Winterwerp et al. (2017), station *Terborg* is located approximately at the beginning of formed fluid mud layers during low amounts of fresh water. This can be confirmed by the investigation shown here. Station Papenburg is located at the landside end of the highly concentrated suspension layers and Leerort in the middle of the overall large-scale fluid mud layer. Temporal resolution of measured data is a 5 min average interval. This short resolution allows to determine variations in suspension concentration within a tide cycle and over a neap-spring cycle.

Figure 5.6 shows the comparison of modeled and observed time series of water elevation and suspended sediment concentration at mentioned stations along the upper Ems. The validation time period consists of a full spring-neap tidal cycle. The tidal range at station Terborg varies with a minimum value of 2.8 meters during neap tide (day 04/21) to a maximum tidal range of 4.2 meters during spring tide (day 04/28). This strong difference results in different flow and stratification conditions, as well in baroclinic and barotropic estuarine circulation structure. The strong asymmetry in tidal shape shows a longer ebb duration combined by a shorter flood duration. This asymmetry leads to faster increase of the water level after an only short period of low water and consequently a longer duration of high water slack. This further results in a much stronger flood flow and a longer but weaker ebb flow (e.g. Oberrecht and Wurpts, 2014a). Resulting tidal asymmetry has also an effect on sediment concentrations measured at three locations along the upper Ems

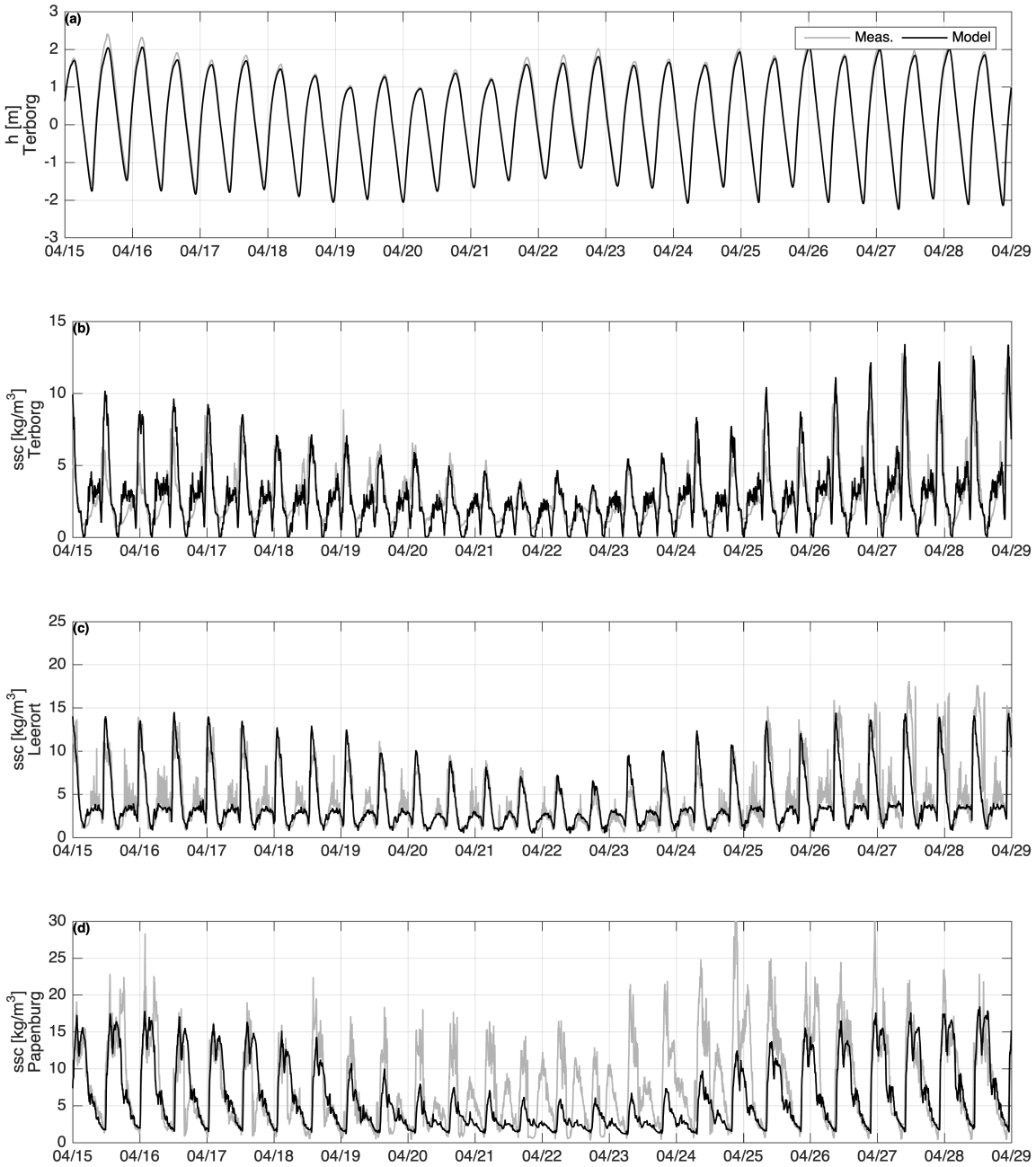

Figure 5.6: Comparison of calculated (black) and observed (gray) a) water elevation at Terborg and suspended sediment concentration at b) Terborg, c) Leerort and d) Papenburg for a spring-neap-spring tidal cycle from 15 to 29 April 2017. Suspended sediment concentrations are measured and extracted 3 meters above the bed.

estuary. A distinct asymmetry has formed between flood and ebb concentration in the high concentrated part.

It is shown that modeled and observed sediment concentrations during flood are much higher than during ebb phase and peak concentrations on flood reach double to threefold values compared to ebb concentrations. Furthermore, peak flood and ebb concentration increase in the upstream direction, but generally ebb concentrations remain constant over entire ebb phase and does not consist of a distinct peak value.

On flood tide only a short peak of suspension concentration is observed and modeled at station Terborg and Leerort during first time of flood. After peak value, sediment concentrations decreases by sediment settling up to high water slack. This behavior can not be observed at station Papenburg, where flood concentrations remain high up to slack water before ebb. During entire ebb phase concentrations are generally decreasing by settling. This dissimilar settling behavior in observed and modeled data can be related to vertical position of instrument sensors with respect to a stable lutocline layer. The lutocline is permanently located below the sensor, while at station Papenburg, the lutocline is located above the sensor. The sensor is located in the high-concentrated fluid mud layer during flood. Therefore, decreasing concentrations can be related to overall sinking of lutocline at Papenburg during ebb phase. Furthermore, fast increase of sediment concentrations arises shortly after slack time before flood with rising water level. This suggests a very short period of slack time around low water and therefore sediments are hindered to accumulate. The lag in sediment settling still keeps particles in suspension, which are entrained from lutocline in the second half of ebb. In contrast, at slack time before ebb, sediment particles settle and build a stable fluid mud layer (lag-phase effect).

Modeled and observed data vary over a neap-spring cycle in both, tidal range and suspended sediment concentrations. The total difference in tidal range is about 1.4 meters. During increasing tidal range (neap to spring tide) an increase of tide-induced velocities leads to stronger vertical mixing. This behavior has an effect on vertical sediment distribution especially during flood. Here, sediment concentrations become much higher during spring tide compared to neap tide conditions. During ebb, concentrations show weaker response to neap and spring tide conditions. Compared to flood concentrations, average ebb sediment concentrations remain similar at values of 3-6 g l^{-1} at all compared stations, except Papenburg. Here, the model under-predicts suspended sediment concentrations, but the overall trends and behaviors are reproduced very well. Mentioned behavior should result in a great effect on residual sediment transport as well as on resuspension and deposition behavior, which can not be directly analyzed with this data. Therefore, three dimensional large-scale investigations based on the numerical model approach is necessary to understand and investigate the detailed large-scale physical behavior of fluid mud in an estuarine environment.

5.3.3 Flow and Resuspension behavior

As known from the tidal cycle model validation and observation, during the first half of flood a massive resuspension of cohesive fines occurs. During this period, sediments are transported vertically into the upper part of the water column. The physical behavior of this mechanism and its reproduction in numerical models is of crucial interest. It is essential for the large-scale up-estuary transport of sediment within the fluid mud forming region. For the reproduction of resuspension in the numerical model, the general flow characteristic of hydrodynamics and sediment has to be understood. To investigate this behavior, in Figure 5.7 model results of the fluid mud-water mixture response on hydrodynamics are shown along the deep channel of the Ems estuary (five minutes after low water slack at station Weener (km 83)). The shown tidal period is only valid at station Weener, but the longitudinal visualization gives an impression of the along channel distribution. In addition, vertical distribution of horizontal velocity, sediment concentration, rheological and turbulent viscosity and the Richardson Gradient Number are shown for station Weener (km 83) in figure 5.7 c-f. This location was chosen for detailed investigation, because it is already described as observed estuarine turbidity maximum during low discharge periods (e.g. Borgsmueller et al., 2016). It should be noted that flood duration is much shorter (∼4h) than ebb duration (∼8.5h), providing strong asymmetry in tidal propagation and instantaneous horizontal pressure gradient in the major up-estuary part from km 65 to km 90 (Oberrecht and Wurpts, 2014a). This is expected to have an effect on subtidal mixing and stratification as well as resuspension and entrainment behavior in the high concentrated region as suggested by Winterwerp et al. (2017).

The longitudinal velocity distribution along the deep channel (Fig. 5.7a) shows a significant reduction within the high concentrated layer (km 65-90). It is, in particular, shown for flood (downstream of km 83) and ebb (upstream of km 83) flow, the horizontal flow velocities are strongly reduced to increasing rheological viscosity in higher concentrated suspension ($SSC > 10$ g l^{-1}). The highly viscous fluid has a higher resistance and flows slower than the low-viscosity overlying water fluid. Furthermore, a nearly linear increasing velocity within the fluid mud layer is shown (e.g. km 68). It indicates a weak turbulent vertical mixing within the mobile fluid mud layer, because velocity profile becomes closer to a laminar flow profile. Above a concentration of 50 g l^{-1}, horizontal velocities are completely suppressed by means of rheological viscosity and yield. Latter is high enough, that momentum cannot overcome the rheology-induced resistance to flow. Local shear velocity is small, and becomes lower than the yield stress, which has to be exceed by the horizontal momentum. This leads to highly structure viscous flow of the higher concentrated mud suspension. It is indicated by a fully built-up floc structure ($\lambda = 1$) and particles interplay as a fully developed network.

Unstable flow stratification is modeled (Ri_g <0.25) in the mobile fluid mud layer as shown by the Richardson Gradient Number at e.g. km 68 in the upper part of the mobile fluid mud layer. Here, the high shear rates lead to higher turbulent induced shear stress and overcomes the yield stress. This behavior produces vertical mixing and an upward flux of

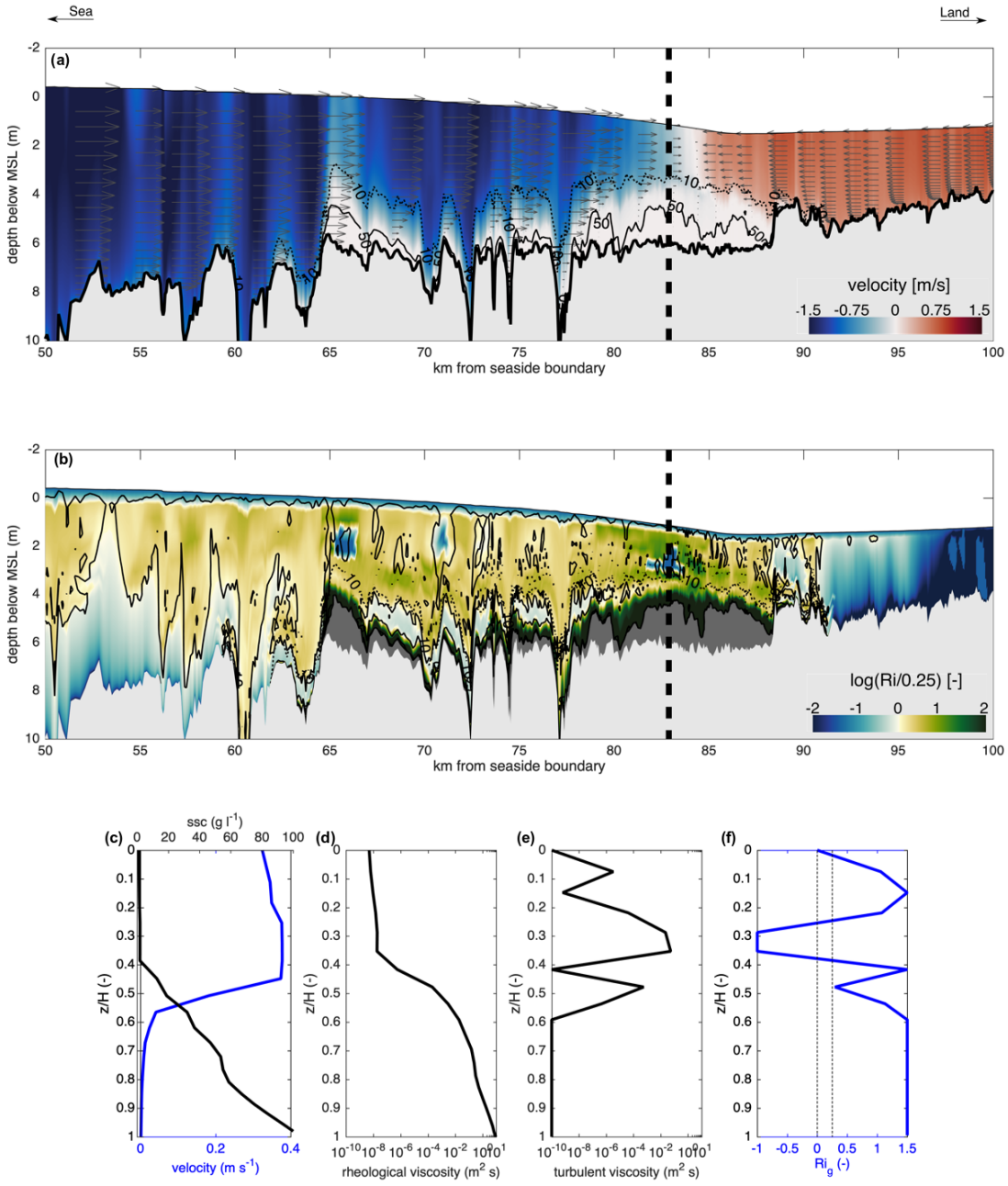

Figure 5.7: Longitudinal velocity (a) and normalized Richardson-Gradient Number (b) distribution along the deep channel five minutes after slack time before flood at station Weener (km 83). The light gray area illustrates the natural sediment bed. Additionally in panel a and b the 10 g l^{-1} (black dashed line) and 50 g l^{-1} (black solid line) are shown. The dark gray area in panel b shows the zone of maximum rheological flow regime indicates by a $\lambda = 1$ value. Black dashed vertical line at km 83 indicates location of extracted vertical profiles shown in lower panels (c-f) of horizontal velocity, sediment concentration (c), rheological (d), turbulent viscosity (e) and the Richardson Gradient Number (f).

momentum within the mobile fluid mud layer. Vertical momentum upward flux is limited to the interface between mobile mud and overlying fluid. Here, a strong sediment induced stratified interface arises and turbulence is completely suppressed. At the interface, the upward suspended flux is in equilibrium with downward settling flux. The vertical position of this equilibrium depends strongly on the settling rate. Therefore, stratification and mixing behavior at the fluid mud-water interface are strongly dependent on the implemented settling velocity approximation and local turbulence distribution.

Turbulence production by bed shear stress and resulting turbulent upward flux (and erosion from natural sediment bed) is totally suppressed, which is caused by the overlying viscous stationary mud layer. This indicates, that turbulence production is mainly related to vertical shear production and less to the bed roughness. At maximum horizontal velocity state (km 68-70), strong vertical shear rates reaches the existing yield stress of current suspensions and λ becomes smaller than one. This indicates the beginning of turbulent production in the mobile fluid mud layer, which is also shown by a peak in turbulent viscosity profile (Fig. 5.7 e) and a weak decrease of the Richardson Gradient Number (Fig. 5.7 f). The water column is still stratified directly above this small layer of turbulence production. This shows that in the non-Newtonian flow layer, turbulence production and vertical mixing are only produced by local acting velocity shear.

The vertical velocity profile at location Weener shows a non-homogeneous distributed profile. An already landward directed flood flow is shown in the upper part of the water column. In the lower part, the flow resistance caused by rheological viscosity and yield induced resistance force. Here, the high rheological viscosity and attributed rheology-induced turbulence damping suppresses the vertical mixing and lead to a laminar flow regime ($\lambda = 1$). The maximum horizontal velocity arises at the lutocline between upper water column (Newtonian) and lower mobile fluid mud layer (laminar, v = 0.38 m s^{-1}). The horizontal velocity decreases strongly to zero flow on the lutocline between mobile and stationary mud layer. The steep decrease of velocities correlates with the increase of rheological viscosity and suppression of turbulent mixing. This confirms that decreasing velocity is directly linked to the resistance force induced by the viscous non-Newtonian flow behavior.

It is known from previous physical lab experiments that during accelerating flow conditions water will be entrained from the upper water column into the higher concentrated layer (Bruens et al., 2011). Consequently, water masses must be downward transported into the fluid mud layer. This flow behavior can be characterized by a negative Richardson Gradient Number, which provides denser water above lighter water. This behavior is also well reproduced by the model as shown in Figure 5.7 f (z/h 0.3-0.4). The development of this vertical density structure is a result of horizontal advected flow at the upper lutocline layer as described earlier in this section. The non-Newtonian flow behavior is characterized by only weak turbulence, based on buoyancy and rheology induced damping. Additionally, the acting rheological viscosity reduces horizontal advection in contrast to the flow situation above the lutocline. As a result, the suspension above the fluid mud layer is propagated faster and promotes this highly unstable stratified flow conditions during accelerating flood

flow. Consequently, it provides vertical mixing during first period of flood, which is assumed as the main mechanism providing rapid observed resuspension. This phenomenon is strongly coupled to the existing fluid mud layer and resulting low energy flow characteristics at its upper lutocline layer. Turbulent mixing and stratification behavior at the beginning of the flood phase have further implications with respect to vertical exchange during the presence of large-scale fluid mud layers. Sediment is vertically mixed into upper water column and is responsible for the strong advective transport in up-estuary direction during flood. Based on modeling results, this sediment-induced mechanism is present only for a short period at the beginning of flood in natural environments and has a large impact on large-scale sediment transport mechanism.

6 Application to Large-Scale Fluid Mud Dynamics

In this chapter, large-scale fluid mud layer dynamics are analyzed with respect to horizontal flow and turbulence interaction in the high-concentrated Ems estuary. The Ems estuary was chosen, because fluid mud layer already exists formatted over a large horizontal area of about 20 km. Additionally, the fluid mud layer thickness is about half water column within the fluid mud layer as shown in the verification chapter. Therefore, in the Ems estuary the formation of fluid mud layers should have a great impact on hydrodynamics and estuarine sediment transport behavior. The extended model approach can also be applied to other estuaries, with or without fluid mud layer dynamics, because the numerical implementation considers both Newtonian and non-Newtonian induced flow dynamics as well as the transition between both.

6.1 Fluid Mud Layer Distribution

6.1.1 Tidal Variation

Fluid mud layers are associated to suspended sediment concentration of higher than 10 g l^{-1}. Therefore, the visualization of longitudinal distribution is based on the mentioned threshold and separated mobile fluid mud layer (<50 g l^{-1}) as well as the stationary fluid mud layer (>50 g l^{-1}). This assumption is in accordance to the definition from Ross and Metha (1989) and the physical behavior, where above 10 g l^{-1} hindered settling and rheology dominate the flow behavior. For specific analysis of tidal periods, the tidal characteristic value was defined at station Terborg. Up-estuary of Terborg, high and low water in up-estuary direction occurs (almost) at the same time (e.g. Winterwerp and Wang, 2013). This effect is mainly related to reduced effective hydraulic drag through sediment-induced stratification (e.g. Winterwerp et al., 2017).

Figure 6.1 shows the longitudinal fluid mud layer distribution along the deep navigational channel of the Ems estuary for high and low tide conditions. The longitudinal sediment distribution represents a mid-tide situation from a neap to a spring tide. The vertical sediment concentration and the fluid mud profile in the water column is characterized by a mobile, weakly concentrated (light gray) and a stationary, high concentrated layer (dark gray). As a result, the stationary layer, where existent, is covered with the mobile layer. The total length of developed fluid mud layer spreads out of about 30 km from Terborg up to a location upstream from Papenburg during modeled low discharge conditions ($Q \sim 40$ $m^3 s^{-1}$). The shown longitudinal distribution represents a typical low discharge situation during spring or early summer. The fluid mud is still formed 60 km up-estuary from the mouth in the upper most tidal part, which confirms the observations from previous studies (e.g. Talke et al., 2009).

The longitudinal distribution of the fluid mud layer varies between high and low water. The fluid mud layer observed during high tide develops during second half of flood (see Chapter

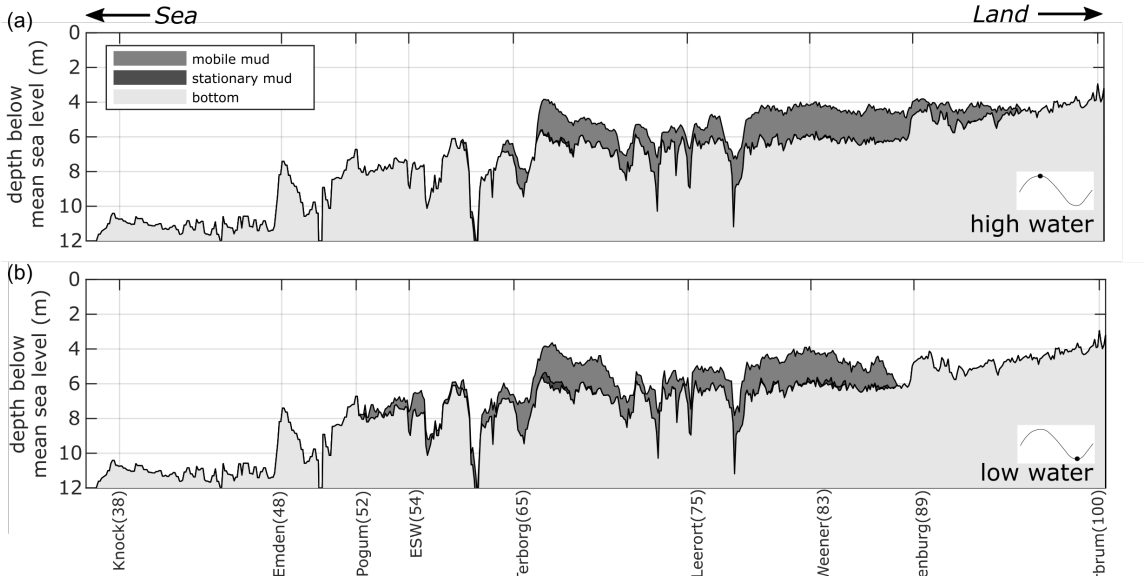

Figure 6.1: Predicted mobile and stationary fluid mud layer distribution during high water (a) and low water (b) along the deep channel of the Lower Ems from entrance of the Emder navigational channel up to the landward tidal limit Herbrum (km from seaside boundary in brackets) at 23.04.2017 (mid tide conditions). Light gray area marks natural sediment bed, mid gray area the mobile fluid mud layer with sediment concentrations higher than 10 g l^{-1} and the dark gray area illustrates the stationary fluid mud layer (SSC>50 g l^{-1}).

4.3). At high tide, the layer spreads out from a few kilometers downstream from Terborg up to 5 km upstream from Papenburg (Fig. 6.1 a). The fluid mud layer consists mainly of the mobile, weakly concentrated suspension. But, a weak stationary layer of a few tens of centimeters shortly up-estuary of Terborg can also be observed. Furthermore, the mobile mud layer with its lutocline reaches a maximum thickness of about 2 meters. This layer thickness is developed shortly upstream from Terborg and up-estuary from Leerort up to Papenburg. A thinner layer (∼1 m) is modeled around station Leerort up to 10 km in down-estuary direction. Here, the weak thickness of the mobile layer is assumed as a result of the inflow of the tributary river system Leda-Juemme.

In contrast to the high water situation, the fluid mud layer is located further down-estuary during low tide (Fig. 6.1 b). The layer spreads out from Pogum (entrance to the Lower Ems) up to 3 km down-estuary of Papenburg. In the region from Pogum to Terborg only a thin mobile layer of < 0.5 m is formed, which is caused by increasing cross-sectional areas with seaward direction. In larger cross-sectional areas the same suspension mass with similar vertical concentration profile forms thinner layers compares to smaller cross-sectional areas. Upstream from Terborg, the fluid mud layer is similarly thick compared to high water situation. Furthermore, a thin layer of a stationary fluid mud layer develops upstream from Terborg and upstream from Leerort. This is related to a weaker entrainment

and stronger settling behavior, caused by less turbulent mixing in these areas during ebb.

The tide-induced dynamics results found in slightly different locations as well as in the intensity of the fluid mud layer between high and low water level. Upstream of Papenburg, the existing fluid mud layer is completely migrated downstream during ebb phase. This behavior can be explained by a) the sediment-induced increase of longitudinal pressure gradient during fluid mud formation as suggested by Talke et al. (2009) combined with b) weak entrainment and mixing at the lutocline at this up-estuary location. A complete mixing into the upper water column with a downstream transport of the entrained material is not modeled during ebb (especially at this location). The weak mixing during ebb is caused by the strong increase of the tidal asymmetry in up-estuary direction, in e.g. flow velocities in the upper water column. The flood currents become stronger and ebb currents become weaker. Thus, in up-estuary direction ebb current velocities decrease, which leads to reduced mixing at the lutocline and consequently entrainment is inhibited. The weak sediment entrainment is limited, because settling flux is in equilibrium with turbulent mixing, which is also observed in salinity induced strong stratified estuaries (e.g. Geyer and MacCready, 2014). Furthermore, during ebb flow, the water column is mostly decoupled caused by strong stratification effects at the upper lutocline of the mobile layer. This combination of interface stratification with rheology induced viscosity prevents generally momentum exchange from upper water column into the fluid mud layer (Geyer et al., 2008). Due to the early reverse of the flow direction in the fluid mud layer during flood flow, the pressure gradient must be relatively increased during fluid mud layer formation, compared to the pressure gradient in the upper part of the water column (Becker et al., 2018). This behavior supports a down-estuary directed sediment-induced pressure gradient during ebb tide, and thus a downward flushing of the fluid mud layer. This mechanism is the strongest at the most up-estuary part of the fluid mud layer, but becomes weaker in seaward direction. The tidal asymmetry decreases in down-estuary direction and therefore mixing during ebb increases. This supports a seaward transport of cohesive fines in the upper water column during ebb. Therefore, down-estuary sediment transport is a combination of both the mixing and stratification behavior and the formation of the sediment-induced longitudinal pressure gradient.

The stationary fluid mud layer increases up-estuary of Terborg during ebb phase. As mentioned above, turbulence is highly damped by buoyancy and rheological flow behavior. This prevents a total upward mixing of the fluid mud layer during ebb. In the fluid mud layer, the settling of muddy sediment particles is favored, which leads to a growing stationary fluid mud layer thickness during ebb flow. From this mechanism it can be assumed that the weak consolidation of the mobile mud layer into stationary layer mainly occurs during this tidal period. Following Abril et al. (2000), the dynamics of the stationary layer are different between neap-spring tidal fluctuations (e.g. tidal amplification, velocities). This weak acting (in mainly resuspension) stationary layer builds the high concentrated fluid mud layer pool above the natural bed in the uppermost tidal part of the Ems estuary as suggested by Winterwerp et al. (2017).

6.1.2 Neap-Spring Variation

Fluid mud layer variations during neap-spring conditions are significant tidal dominated estuaries. Associated variations in tidal amplification, velocities as well as density stratification effects are usually acting on large-scale distribution of the fluid mud layer during a neap-spring cycle. To quantify these large-scale variations, figure 6.2 shows the longitudinal distribution of the fluid mud layer in the Ems River during high water at neap and spring tide.

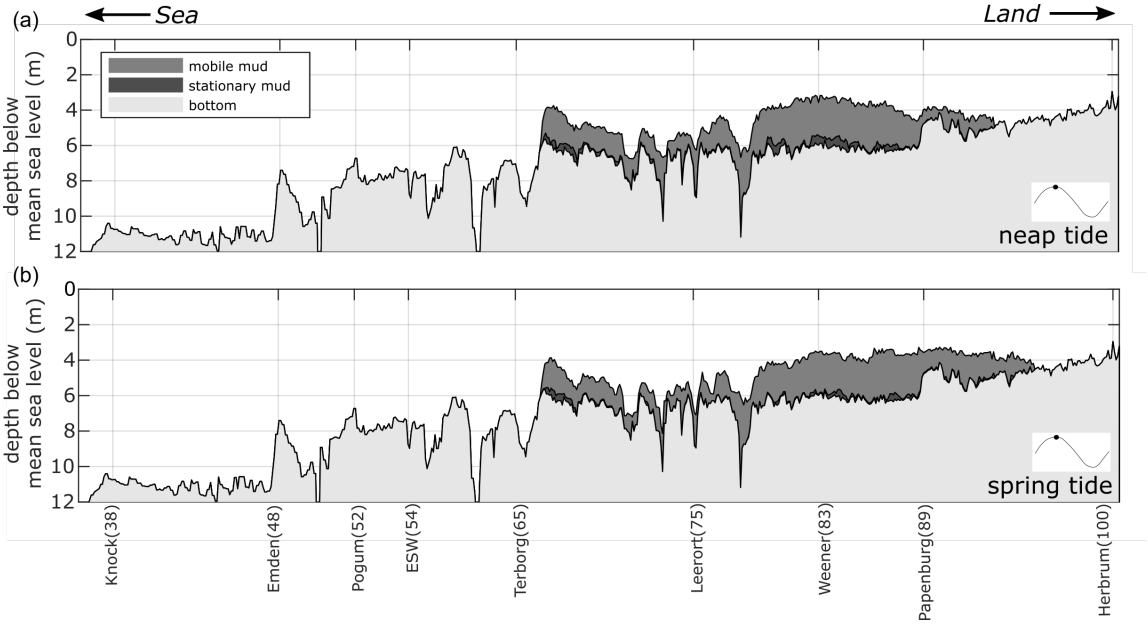

Figure 6.2: Predicted mobile and stationary fluid mud layer distribution during neap (a, 20.04.2017) and spring tide (b, 28.04.2017) condition at high water along the deep channel of the Lower Ems (km from seaside boundary in brackets). Light gray area marks natural sediment bed, mid gray area the mobile fluid mud layer with sediment concentrations higher than 10 g l^{-1} and the dark gray area illustrates the stationary fluid mud layer (SSC>50 g l^{-1}).

It is shown that variations between neap and spring tide are mainly characterized by the total suspended sediment mass forming fluid mud layers and its longitudinal distribution along the estuary. During spring tide, the fluid mud layer is more extended in up-estuary direction compared to neap tide. This is shown by a thicker mobile mud layer upstream of Papenburg along the deep channel. The seaside boundary of the fluid mud layer is similar between neap and spring tide and is located at Terborg. Another significant difference is shown of the location and thickness of the stationary fluid mud layer. The stationary fluid mud layer is thicker during neap (∼0.5 m) than during spring (∼0.2 m) tide, especially in the area upstream from Leerort. Latter confirms with fluid mud layer dynamics observations of Abril et al. (2000) from the Gironde estuary in France. From neap to spring tide

sediment particles are eroded from the stationary layer. This leads to the less pronounced stationary layer. From spring to neap tide, particle settling from the mobile layer into the stationary layer leads to increasing thickness of the stationary layer. It is shown that a less-thick stationary layer during spring tide leads to an increase of the mobile layer thickness. Latter is caused by entrained sediment particles from the stationary layer into the water column with respect to hindered settling approximation building the mobile layer.

Neap-spring variations in the fluid mud layer distribution can be explained by variations in hydrodynamic behavior during neap and spring tide and consequently its impact on suspended sediment transport. The peak sediment concentrations in the upper water column are much higher along the Ems estuary during flood in spring tides (see Fig. 5.6), during the investigated period. This behavior is related to intensified turbulent mixing within the mobile fluid mud layer. Based on increasing tidal range from neap to spring tide, maximum velocity and associated shear become higher, which results in intensified turbulent mixing. Entrained sediment particles from the fluid mud layer are transported more upward into the upper water column. Furthermore, increased velocities lead to an increase of the near bed shear stresses, which promotes stronger erosion during spring tides (e.g. Allen et al., 1980). The combination of intensified turbulent mixing and (higher) entrainment rates from the stationary layer leads to a higher suspension mass. Due to intensified horizontal velocities, a higher up-estuary transport of cohesive fines occurs and, with respect to hindered settling an extended mobile fluid mud layer (e.g. Guézennec et al., 1999). This indicates that the neap-spring cycle controls the longitudinal extension, transport as well as the formation of fluid mud layers in the hyper-concentrated, upper part of the Ems estuary.

6.2 Lateral Distribution in Longitudinal Transport

Sediment trapping zones require convergent sediment transport patterns, thus building a quasi dynamic equilibrium of sediment transport, averaged over several tides. This equilibrium can be analyzed by e.g. lateral distribution of longitudinal sediment transport within a cross-channel. Due to geomorphological structure of natural estuarine environments, many processes are involved in cross-sectional hydrodynamics and resulting sediment dynamics (e.g. Huijts et al., 2006; Chernetsky et al., 2010). To investigate cross-sectional longitudinal transport processes, a specific cross-section in the fluid mud region was decided (Fig. 6.3). The location (Weener) of the cross-section was chosen by the hydrodynamic quantities and existing formation of a fluid mud layer. At station Weener, hydrodynamics are only influenced by tidal dynamics and freshwater discharge from the tidal weir in Herbrum. More downstream locations are additionally influenced by tributary river in-/outflow, especially during ebb tide. The additional inflow makes analyzes much more complex and it is a specific characteristic of the Ems estuary. Therefore, the more upstream located location should make possible a comparison to other fluid mud carrying estuaries. The investigated cross channel is characterized by a deep channel of 40 meters width and site

flanks with a slope of around 12 %. Total width is about 226 meters.

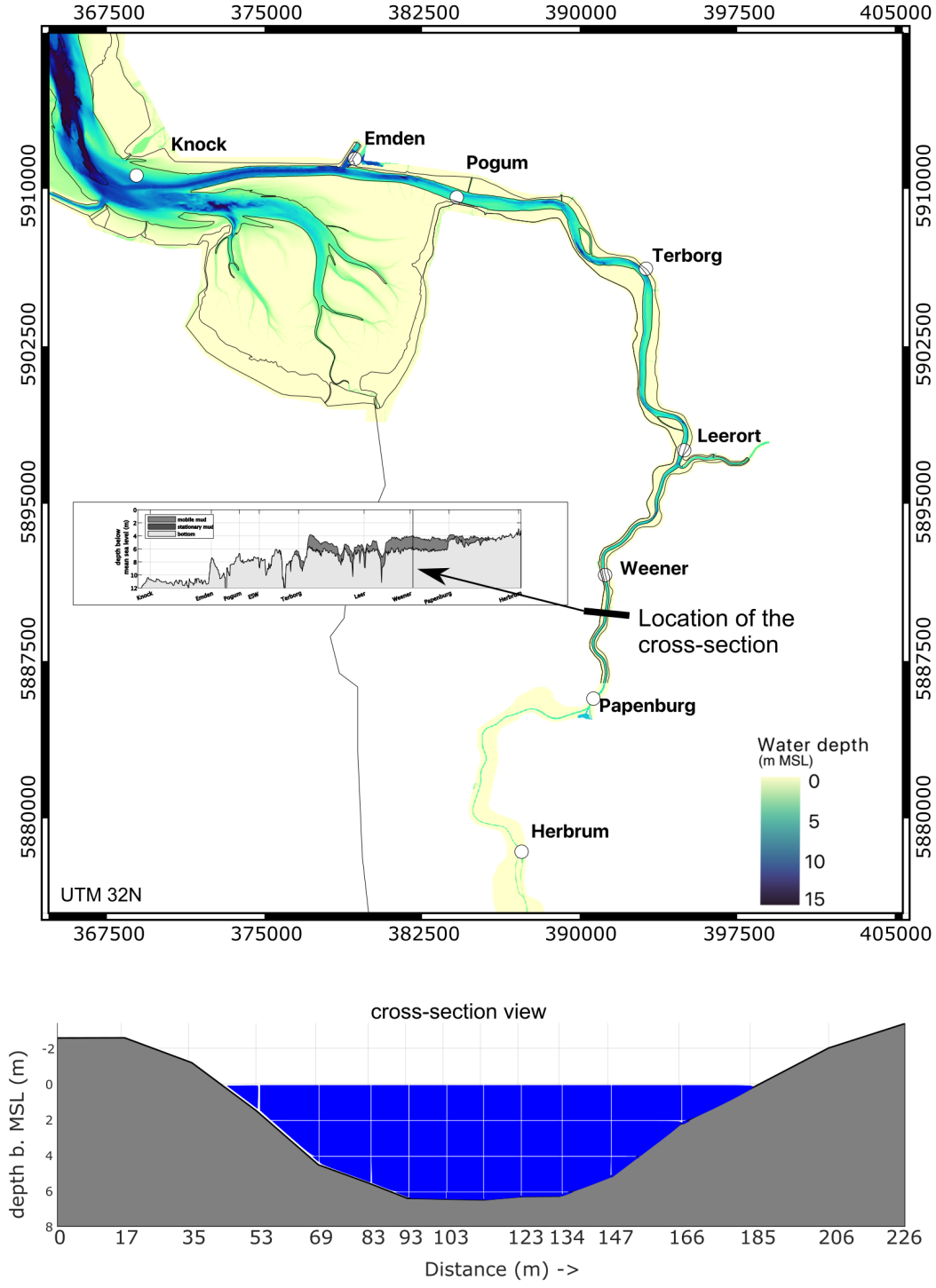

Figure 6.3: Map of the upper Ems estuary and the location of the cross-section (thick black line) for long-term transport investigations (upper panel). Lower panel shows the cross-sectional width and area.

Figure 6.4 shows the cumulative tidal averaged horizontal sediment flux along the cross-section, divided into a transport component on the bank and in the deep channel. It shows a net landward directed sediment transport on the bank and a net seaward directed transport in the deep channel. This behavior can be associated with the net erosion potential of fine material at both locations. In contrast to the bank, the sediment bed in the deep channel is mostly covered with a fluid mud layer. Therefore, a different erosion ratio is present. In the deep channel, the yield stress has to be overcome by current induced shear stress before entrainment. On the bank, sediment is only eroded when the critical shear stress for erosion is exceeded. Furthermore to determine shear stress assumption, the fluid mud layer is additionally driven and transported by the longitudinal acting pressure gradient, mainly during ebb. This additional force can lead to the seaward flux in the deep channel. Generally, the banks are not covered with fluid mud and the additional driver is missing. Therefore, the bed erosion tends to a net landward transport of cohesive fines.

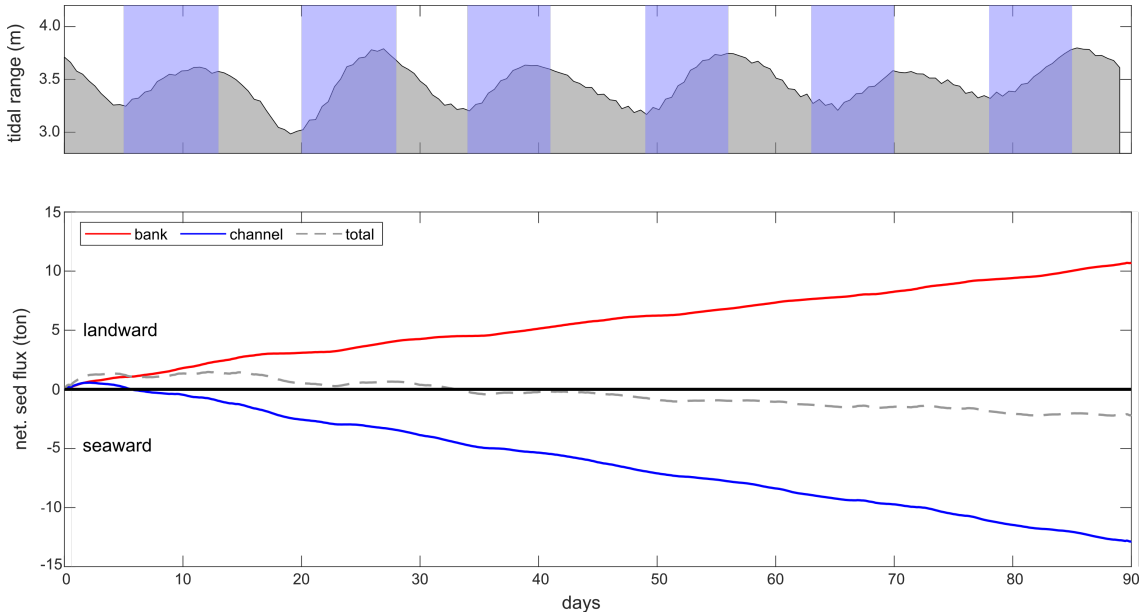

Figure 6.4: Time series of tidal range (upper) and tidal averaged sediment flux (lower) in the channel (blue) and on the bank (red) extracted from model run and selected cross-section at Weener. Positive values means landward directed sediment flow and negative values seaward transport. Shading in upper panel illustrates time periods of neap to spring tide.

The total sediment transport as a residual of both transport locations indicates a total net seaward transport of around 2-3 tons in 90 days. This weak seaward transport characteristic can be related to a) natural fluctuations in tidal-induced hydrodynamics by e.g. further out-estuary heavy wind periods deform tidal shape compared to astronomical tidal cycle or b) general seaward directed transport mechanism as known from up-estuary freshwater zones in estuaries (longitudinal barotropic gradient). Moreover, local variations in bathymetry

can form a local seaward transport. Especially, a weak longitudinal slope can lead to distinct weak downward net transport, supported by viscous flow behavior of the fluid mud layer itself (Traykovski et al., 2000).

Net sediment transport between channel and shoal are not only different by its transport direction, but also in strength of transport. A variability exists along the cross section within a neap-spring cycle (Fig. 6.5). During accelerating tide (neap to spring tidal), the up-estuary transport on the banks is weaker compared to the sediment transport from spring to neap tide conditions. This can be explained by decelerating tides (spring to neap), which indicates reducing tidal velocities. This dynamic leads to reduced erosion ability caused by becoming weaker bed shear stress.

It is shown that an increasing tidal range is combined with increasing up-estuary directed transport on both banks. On the west bank, erosion ability is general weaker compare to the east bank, because the cross section lies in a weak right turn (in flood direction). This promotes higher tidal currents on the outside (right bank) of the channel curve (see Fig. 6.3). In contrast to slightly different transport dynamics on the banks, across the deep channel, a constant sediment transport is modeled.

As shown, the net sediment transport is directed seaward in the channel, but can be directed in the opposite direction or in balance at shorter time scales, when tidal currents become stronger e.g. from neap to spring tide. During these periods, the total net sediment transport along the cross section can become landward. It is shown by a weaker seaward transport during an accelerating tide in the deep channel and stronger up-estuary transport on the banks (Fig. 6.5). This behavior shows that diurnal variability in the tidal range has a great effect on the net sediment transport behavior. The variability in transport strength is caused by tidal velocity fluctuations combined with dependent turbulent mixing (mainly during flood). It is shown in Fig. 6.5, that latter variability is much more pronounced in the deep channel than in shallow areas. This is mainly caused by the fluid mud layer existence and its sediment-induced stratification behavior. During neap to spring tide conditions, sediment-induced stratification is reduced by stronger horizontal velocity shear and thus higher entrainment rates. This leads to a stronger sediment transport during flood and it weakens modeled long term seaward transport on a short timescale. At decreasing tidal ranges, stratification intensifies and reduces upward turbulent mixing. Here, the longitudinal pressure gradient becomes dominant during ebb and it mainly controls the net sediment transport. Additionally, settling is intensified from the mobile fluid mud layer into the stationary layer, which actually requires higher shear rates for a stronger landward transport during flood. Therefore, the stronger acting horizontal pressure gradient (caused by the fluid mud layer existence) has to be overcome in order to shift the seaward into a landward directed net sediment transport or at least to dampen the seaward transport.

At the beginning of the investigated time period, a net landward directed transport occurs in the deep channel, as can be seen in Fig. 6.4 and 6.5 (days 0-5). This transport behavior is in contrast to further net seaward transport direction of the channel. It is reasoned to

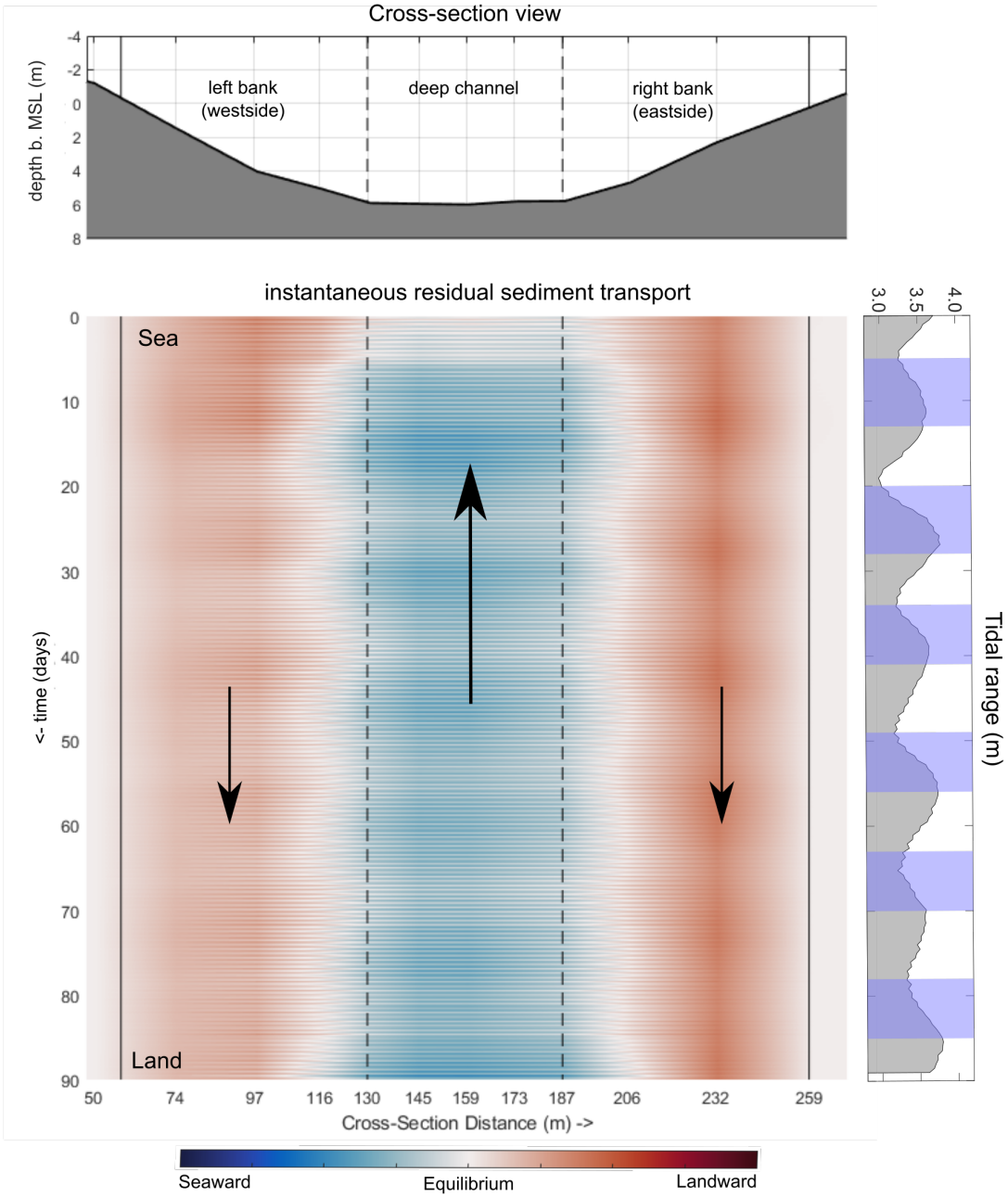

Figure 6.5: Depth integrated time series of instantaneous total advective along channel sediment transport (g m^{-1} s^{-1}) at cross sectional locations close to Weener (see Fig. 6.3). Positive fluxes marked as blue (sediment import) and negative values are red (sediment export). In the right panel the tidal range is shown. Here, blue shaded areas indicating neap to spring tide conditions and white areas spring to neap tide conditions. The upper panel shows the cross-channel area and location of the deep channel and the banks.

the warm-up and initial period of the model, where local sediment transport and fluid mud layer formation are still dependent on the initial conditions.

The net landward directed transport on the banks and seaward directed transport in the deep channel requires an equilibrium in erosion and deposition of the bed material. Otherwise, deepening of both, channel and banks will occur. This does not happen along the fluid mud layer formation zone. The large-scale fluid mud layer forms a dynamic equilibrium, and consequently prevents a large-scale deepening. Based on this transport analysis, it can be concluded that a fluid mud is able to build this equilibrium in longitudinal suspended sediment transport with respect to its own physical dynamics (settling, rheology, turbulence) and hydrodynamic boundary conditions.

6.3 Residual Flow Circulation

In the previous section a dynamic equilibrium in the sediment transport could be identified within the fluid mud layer distribution. This equilibrium should also have an effect on the residual velocity profile over a tidal cycle within this high concentrated area. In a turbidity zone, which is mainly driven by a baroclinic (estuarine) circulation, the residual velocity profile should be directed seaward. In the longitudinal estuarine direction, a residual velocity profile with different flow directions is e.g. known from the salinity driven baroclinic circulation. In the turbidity zone, the accumulation and trapping of sediment is mainly caused by settling and existing threshold against erosion of the sediment particle with respect to hydrodynamic conditions. The interaction between estuarine circulation and downstream flushing originate the zone of sediment trapping by existing convergent transport pattern. Knowledge about residual circulation pattern driven by sediment-induced density effects are mainly unknown and their impact on overall estuarine dynamics (e.g. Burchard et al., 2018). This behavior is of great interest in case of sediment management strategies or maintenance actions.

The modeled residual flow patterns along the deep channel of the Ems estuary are shown in Figure 6.6 for a neap tide (21.04.2017) and a spring tide (28.04.2017). The residual flow was calculated over two tides for each tidal period. The longitudinal residual flow distribution includes the high concentrated fluid mud-forming region in the upper Ems estuary. The horizontal and vertical salinity structure is also shown, as well as the averaged fluid mud layer distribution (SSC $>$ 10 g l^{-1}). Additionally, three vertical profiles at different locations within the fluid mud-forming region are shown for neap and spring tide (km 68, 74 and 83). The first vertical profile is located between the first half of the fluid mud area between Terborg and Leerort. The second is near the inflow of the tributary river system Leda-Juemme and the third is between Leerort and Papenburg at the estuarine turbidity maximum.

In the modeling period, it is shown that a seaward transport in the upper water column and a landward directed flow in the lower water column arises seaside from the high-concentrated region during neap tide. In this area, the residual velocity profile is mainly driven by salinity-induced stratification effects ($>$ 5 psu). Here, during spring tide, the residual velocity flow is directed seaward over the entire water column. Therefore, during

neap-tide, the outer estuary is partially mixed, while during neap tides well-mixed flow behavior is present. The difference in residual flow behavior results from the large scale estuarine circulation and the strength is generally dependent on freshwater inflow and seaside tidal range. Here, the freshwater inflow is equal during both times ($Q = 40\ m^3 s{-}1$). The main difference is subject to the seaside boundary variations. During spring-tide, modeled well-mixed conditions are a result of higher flood and ebb velocities (compare to neap) leading to a higher turbulence production which overcomes the stratifying intensity. During neap tide, the stratifying intensity tendency is dominant to turbulent mixing and a weakly stratified flow behavior arises. As mentioned, the residual flow is strongly dependent on hydrodynamic quantities (tidal range and discharge). For example, Pein et al. (2014) modeled a weak stratified residual flow at the same location (Emder fairway) during spring tide (June 2012), using an astronomical water elevation boundary condition. The existing seasonal variability in tidal range can lead to variations in the residual flow pattern and residual sediment transport pattern (e.g. Gräwe et al., 2014). The variability in both numerical studies clarifies that investigations of the salinity-induced stratification is only limited to the investigated time period with respect to seasonal fluctuations in turbulent mixing based on freshwater and seaside tide-induced inflow.

In the high concentrated region (Terborg (km 65) to Papenburg (km 90)), a seaward directed residual flow exists in the upper water column. In the lower water column a landward directed residual flow arises. This residual flow behavior develops during both, neap and spring tide. The effect of salinity-induced stratification effects can be neglected, because salinity is quite low (< 2 psu) and homogeneous distributed. Therefore, the residual flow pattern is dominated by sediment-induced density effects in this region. This behavior is confirmed by observations of high concentrated mud suspensions of Becker et al. (2018).

The residual landward directed flow exists when the flood tide becomes stronger than the ebb tide (Fig. 6.6 c-e). Thus it is highly dependent on asymmetry of horizontal velocities and associated vertical mixing potential. During the flood tide, the lower part of the water column is characterized by strong vertical mixing and entrainment of cohesive fines from the mobile and stationary mud layer. Additionally, tidal asymmetry in the slack water duration leads to increased settling and results in a full recovered floc structure, building a fully viscous fluid during high water slack. During much shorter low water slack the settling of sediment particles are limited and particles still keep in suspension. During ebb flow, rheology and buoyancy-driven turbulence damping prevents vertical mixing in the lower water column. Furthermore, the horizontal transport is weakened caused by the non-Newtonian rheology induced viscosity. Consequently, in the lower water column, most of the horizontal advection arises only during the flood phase. This effect results in the clear visible residual landward directed flow within the high concentrated region. The vertical limit of this landward directed flow is dependent on the vertical position of the lutocline between upper water column and the fluid mud layer. The vertical position of the lutocline depends on both, thickness of the mobile fluid mud layer and the upward

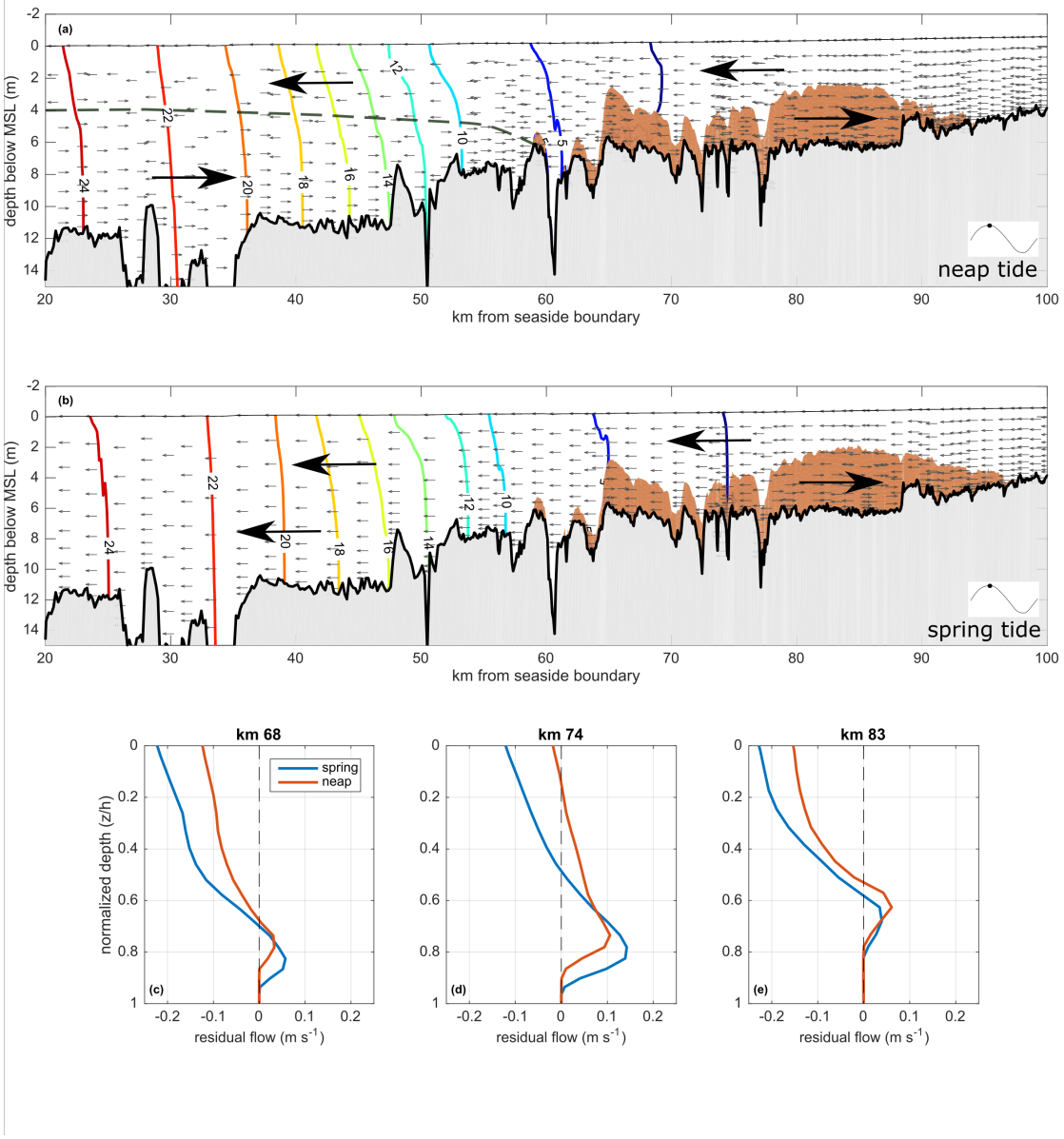

Figure 6.6: Subtidal averaged and normalized residual flow velocities (gray arrows) along the deep channel of the Ems estuary from Dukegat to tidal weir in Herbrum during neap (a) and spring (b) tide conditions. Vertical isocline illustrates salinity distribution along the estuary. Suspended sediment concentration higher than 10 g/l marked light brown. The light gray area represents the natural bottom. Lower panels (c-e) are showing vertical profiles of residual flow at neap (red line) and spring (blue line) tide at different horizontal locations along the fluid mud distribution. The dashed black line in the upper panel shows the vertical position of salinity-induced change in net flow direction.

directed flux during flood (sediment forming fluid mud layer). Both latter effects are strongly dependent on locally available suspended sediment mass. Therefore, the landward residual flow is also dependent on the locally available sediment mass and the fluid mud

layer formation intensity.

The seaward directed residual flow is concentrated to the upper water column (in the fluid mud layer region). This layer is characterized by a low suspended sediment concentration ($C < 8$ g l^{-1}) and the Newtonian flow behavior is dominant. The seaward directed flow behavior within this region follows a typical pattern within upper estuary locations (landward from salinity intrusion limit). Here, residual flow dynamics are dominated by the freshwater inflow, and therefore seaward directed. Also here, the effective vertical thickness of the seaward directed flow layer depends mainly on the vertical position of the lutocline and therefore on the fluid mud layer thickness, as well as available suspended sediment mass.

Differences between neap and spring tide illustrate a generally stronger residual landward flow during spring tide. They are combined with stronger velocities, which are able to significantly reduce the vertical stratification. In the mobile fluid mud layer, this leads to less dominant viscous behavior, which results in both, higher entrainment rate from the stationary layer and stronger horizontal advective transport within the mobile layer. Furthermore, a higher entrainment from the mobile layer into upper water column is shown by a lower vertical position of the interface, where the landward flux shifts to the seaward flux (Fig. 6.6 c-e) during spring tide. Higher shear stress and vertical shear rate reduce the floc structure and pronounce further break up of flocs, leading to an increase of turbulence intensity. As noted, bed shear stress induced turbulence production is mainly prevented by the coverage of the bed with the stationary mud layer. Thus, increased vertical shear of horizontal velocities and increase of turbulence production is a result of the horizontal barotropic pressure gradient.

This is much stronger during spring tide compared to neap tide conditions. Additionally, the seaward directed flux is increased closer to the tidal barrier (Fig. 6.6 c and e), because of freshwater inflow impact increasing in up-estuary direction. Except at km 74, where the tributary river system impacts on residual flow profile (Fig. 6.6 d).

The residual flow pattern in terms of equal strength within the fluid mud layer region is similar and comparable to a salinity-induced baroclinic circulation. As mentioned above, latter circulation is mainly associated to salinity-induced estuarine circulation, but here it is based on a strong sediment-induced circulation within the turbidity zone. In addition to a salinity induced baroclinic circulation (e.g. estuarine circulation), the sediment-induced circulation has to develop an equilibrium not only by flow and stratification effects, but also by the sediment settling and rheological behavior over longer time periods (neap-spring cycle). Here, fluid mud with its non-Newtonian flow and buoyancy driven stratification behavior acts as the driving mechanism to develop such a circulation.

The interface between landward and seaward directed flows is located at the vertical position, where rheology induced effects become dominant. This location is attributed to the vertical position of the lutocline (tidal cycle average). The shift in residual flow directions is attributed to the strong sediment-induced stratification at lutocline, where vertical turbulent flux is completely dampened. Therefore, shown residual flow structure is dependent

on the buoyancy and rheology turbulence damping mechanism, with respect to current seaside and landside hydrodynamic boundary conditions. Without fluid mud layer formation and its sediment-induced stratification behavior, an only seaward directed residual flow profile can be assumed because of homogeneous salinity profiles. Therefore, modeling the Ems estuary without the sediment-induced turbulence damping effects (buoyancy and rheology) will lead to non-realistic flow and sediment transport rates.

Following Becker et al. (2018), the landward directed residual flow with strong vertical mixing must be in balance with longitudinal acting shear dissipation. The shear dissipation results mainly from stratification effects, which are caused by density gradients. Based on this modeling study, it is shown, that the non-Newtonian flow behavior has also a great impact on existing shear dissipation. The yield stress, which has to be overcome and the rheology dependent turbulence damping, allow strong vertical shear rates by laminar flow without any turbulence production.

The model shows that a dynamic equilibrium of cohesive sediment transport over large distances can arise and consequently leads to a convergent sediment transport pattern. Based on residual flow dynamics, large scale fluid mud layer stabilizes itself by interaction of Newtonian and non-Newtonian flow dynamics, which is able to build a sediment trapping zone by its own circulation behavior with respect to local density-induced hydrodynamics.

6.4 Total Sediment Transport

From literature, it is suggested that the massive import (tidal pumping mechanism) and accumulation of cohesive fines are a result of reduced bed roughness, with respect to anthropogenic interventions. The import of the cohesive material is suggested from seaside location and was investigated by simplified modeling studies without considering fluid mud flow dynamics (e.g. Maren et al., 2015; Dijkstra et al., 2019).

Here, investigations of the sediment transport behavior within the turbidity and fluid mud layer forming zone of the Ems estuary are undertaken by calculation of the sediment amounts. The total sediment quantification provides information about the origin of the cohesive fines, which are responsible for the large-scale fluid mud layer formation. In the complete area from Pogum to the tidal barrier (see map of Fig. 6.7) the instantaneous suspended sediment mass, the total erosion mass and the total sediment mass was calculated (Fig. 6.7). The calculation of suspended sediment mass is limited to this area, because distribution of the fluid mud layer is present only upstream of Pogum (see Section 5.1). Therefore, a net sediment transport direction into or out of the control volume can be analyzed.

Figure 6.7 shows an average suspended sediment mass of around 0.335 Mio. tons in the Lower Ems estuary. A distinct variation of the suspended mass in the neap-spring cycle is clearly visible. This behavior is explained in a previous section and is caused by the entrainment and deposition behavior during a neap-spring cycle. During the spring tides,

increase of the suspended mass is related to the dominant erosion behavior, while during the neap tides mainly deposition occurs and reduces the mass in suspension. But, with advancing time, the fluctuation between neap and spring tide becomes weaker. This behavior confirms with observed suspended sediment concentration measurements along the estuary. The peak concentrations only change slightly after a certain period (>2 months) within a neap spring cycle (see Fig. 3 in Winterwerp et al., 2017). This shows and emphasizes, that a dynamic equilibrium of erosion, deposition and fluid mud layer dynamics will be reached by consideration of a constant freshwater inflow over longer time periods.

Furthermore, a slightly increase of the mean suspended sediment mass (0.32 - 0.35 Mio. tons) during modeling period is shown. The amount of total suspended mass should be dependent on the freshwater inflow, building the large-scale fluid mud layer. Here, a weak decrease of the freshwater inflow caused by using the measured time-series during the modeling period (weak decreasing discharge) is implemented. This makes clear that in the case of lower discharges, a higher suspended sediment mass exists, while during higher discharges, the amount becomes smaller.

The total amount of suspended material from erosion of the sediment bed (eroded mud) increases within the investigated area and modeling period. During accelerating tides (neap to spring) net erosion of fine sediment occurs, while during decelerating tides (spring to neap) a net deposition in the Lower Ems estuary is present. The deposition rate of cohesive fines is much weaker compared to the erosion rate, which leads to the increasing sediment mass originated from the sediment bed. Here it is shown, that the eroded sediment mass is larger than required for the formation of the equilibrium conditions of the fluid mud layer. The total eroded mass can also be larger or smaller as modeled by varying the critical bed shear stress, but the effect of residual transport direction remains unchanged.

The total sediment mass (bed + suspension) decreases during the modeling period. From this behavior it can be derived that the net cohesive sediment transport direction is seaward (down-estuary of Pogum). This means that cohesive fines are transported from the Lower Ems estuary (fluid mud layer region) and tributary river system Leda-Juemme into the Emder fairway or more seaward into the Outer Ems estuary. Previous (modeling) studies have shown that the import of muddy sediments form the Outer Ems into the Lower Ems estuary was amplified due to deepening and leads to the formation of the pronounced ETM, formation of fluid mud and massive mud depositions (e.g. Jonge et al., 2014; Maren et al., 2015). The predicted total sediment mass shows a seaward transport of cohesive fines, when the fluid mud layer is formed under the low discharge conditions. This behavior suggests that the net sediment transport direction can change, even when a fluid mud layer is formed. Therefore, the net sediment transport can be partly landward directed up to a specific threshold of a fluid mud layer thickness or until a dynamic equilibrium of the fluid mud layer with local hydrodynamics is reached.

Modeled total sediment decrease suggests a mean deepening of the Lower Ems estuary, which is not observed, but rather a net deposition of material, because the Lower Ems is

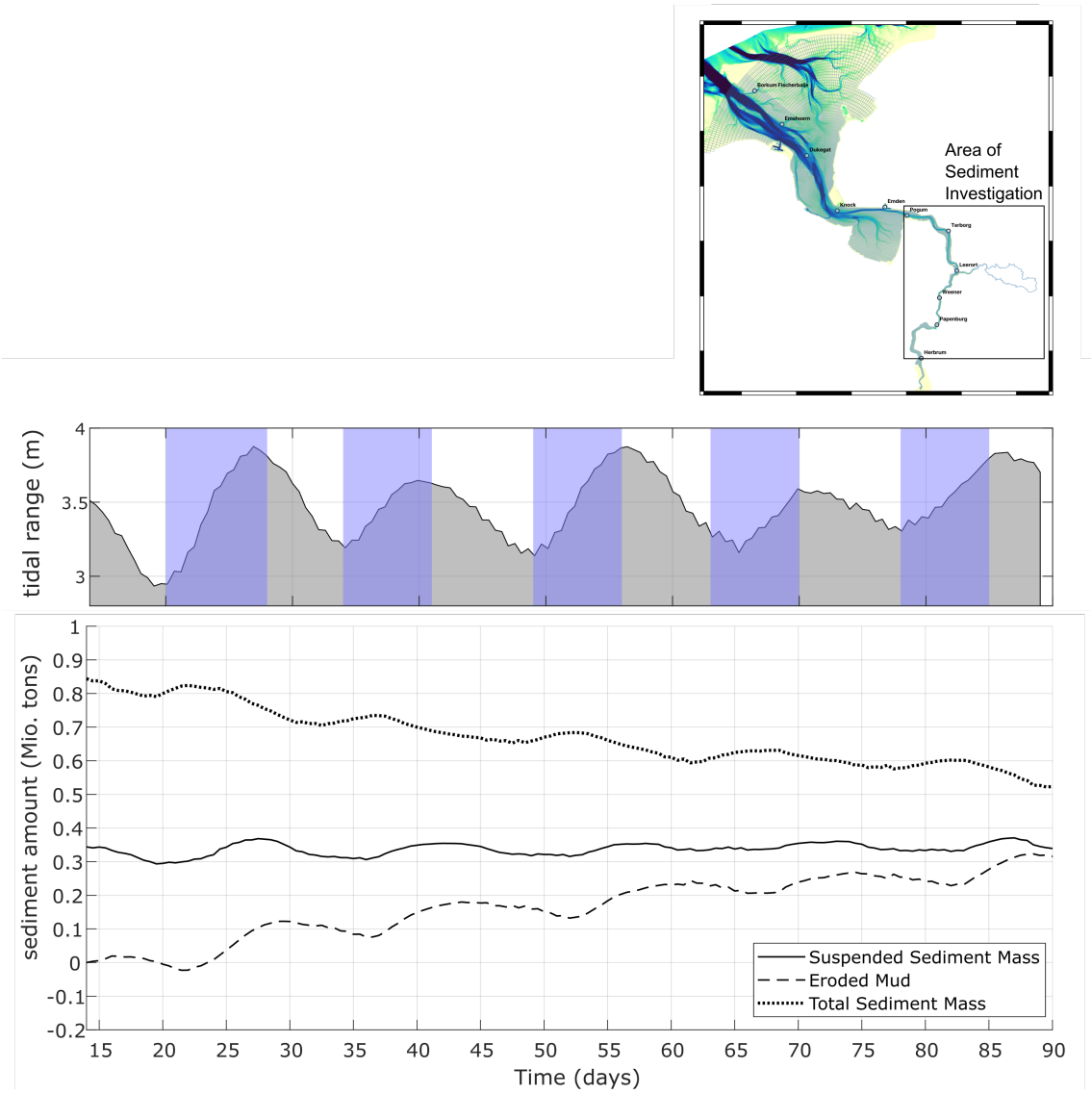

Figure 6.7: Time series of total suspended sediment mass, eroded sediment mass and total sediment mass of fine material from Pogum to the tidal weir in Herbrum. Mid panel shows the tidal range and blue areas marks the transition from neap to spring tide. Upper panel shows the map of the Ems estuary and the area of sediment transport investigation (black square).

subject of maintenance dredging efforts (BfG, 2017). The latter can only arise when a net sediment import into the Lower Ems estuary exists. Generally, this required net sediment import can be present, when a) sediment is transported up-estuary from a seaward location or b) by discharge from the landside limits of the estuary (tidal barrier, tributary river system). A principal sediment import from a seaside location can be excluded. Sediment is already transported seaward and therefore, cohesive fines are available in down-estuary

regions, but they are not transported back. Furthermore, a seaward boundary condition of a sediment mass is conducted. This import of cohesive sediment from seaside is not imported into the Lower Ems estuary during the modeled time period. Additionally, for a net landward directed transport the total sediment mass in the Lower Ems estuary must rise, which is not modeled.

Both other remaining available sediment sources are the Ems river (upstream from the tidal barrier) and the tributary river system Leda-Juemme. A sediment inflow from both locations are not considered in this study. A net fluvial sediment import from the tidal barrier at Herbrum is observed, but it consists mainly of sandy sediments (Tippener and Reinemann, 1979), which are not subject for the fluid mud layer formation. The tributary river system Leda-Juemme is known as a *Marschland*, which is characterized by massive accumulation of silt and clay (formation of peat) over the last centuries and millennia, therefore fine sediments are available. Based on model results, the main erosion of material arises in the tributary river and is then imported in the Lower Ems estuary. Furthermore, the model shows, that the inflow of fine sediment is required to keep the high concentrated layer in suspension, mainly between Terborg and Leerort. Following Dette et al. (1994), an average sediment import from this river system into the Lower Ems estuary exists with an amount of 390 tons per tide of cohesive fines (silt and clay). The instantaneous import is dependent on hydrological boundary conditions, such as rainfall and mean air temperature as well as the size of the river basin. This simple quantification was confirmed by a long-term measurement campaign from 1990 to 1992. On an annual basis, the imported mass becomes similar to the total suspended mass in the water column. Due to increasing tidal asymmetry in the Lower Ems and adjacent river system compared to 1990, the current sediment import can be much higher, as in the nineties but detailed analysis or data are not available for further investigations. Therefore, nowadays the sediment source forming the large-scale equilibrium of the fluid mud layer and hydrodynamics can be (partly) originated from the tributary river system Leda-Juemme, which must be further studied. When the net seaward transport of cohesive fines can be compensated by the import of sediment from the tributary river system, the Ems estuary becomes balanced or shifts to a primary depositing system (when more sediment is imported as needed).

7 Summary & Outlook

Formation and existence of fluid mud layers in natural environments are of major interest in sediment transport processes. The lowest energy state of such estuaries is strong stratification over longer stretches, where this is possible with respect to the equilibrium of acting hydrodynamic forces. Fluid mud lutoclines strongly influence sediment transport and morphological processes. Further aspects of practical relevance are low oxygen levels due to massive oxygen depletion in the high concentrated regions and are all related to management of fairways and harbors at such estuaries. Fluid mud properties are already well described in several studies covering a broad range of field observations and their interpretation. On the modeling side, several approaches basically covering single aspects of fluid mud dynamics on a local scale can be found. Fundamental model based research on the large scale dynamics and formation of fluid mud is attributed to the lack of a suitable modeling tool which combines estuarine hydro and sediment dynamics with the ability to handle turbulent and non-Newtonian laminar flow and steady transitions between them. The major objective of this work contributes to the missing knowledge of large-scale fluid mud dynamics and improves the understanding of the fluid mud specific related impact. Investigations of the large-scale dynamics have been carried out by using the three-dimensional numerical modeling system Delft3D. For the consideration of fluid mud, the Delft3D code was extended by several fluid mud related processes. The major issue in modeling fluid mud dynamics within a single-phase modeling approach is related to the transition from turbulent to laminar flow behavior, where the laminar part is characterized by complex thixotropic rheology with a yield point.

7.1 Extended model approach considering fluid mud behavior

Numerical modeling of large-scale fluid mud layer dynamics requires a three-dimensional modeling approach with sufficiently high vertical resolution due to sediment-induced stratification effects. Le Hir (2000) extended the classical single-phase estuarine modeling concept towards combined Newtonian and non-Newtonian rheological flow and named it continuous modeling approach. This concept was adopted for the investigations shown here, since it can easily be implemented in existing RANS-solvers for estuarine models. This also significantly reduces the efforts for empirical closures, such as in multiphase or isopycnical models and substantially broadens the applicability to virtually all estuaries. The continuous modeling concept benefits from the similitude of how kinematic, rheological and (apparent) turbulent viscosity are considered in the Reynolds-Averaged momentum equations. In order to deal with rheology, it basically introduces an additional stress term, which feeds the results of a rheological model into the viscous term of the momentum equation. To solve this stress term a rheological model is needed, which is able to resolve the stress term at already low shear rates. Good results were obtained with the rheological model of Worrall & Tuliani (1964), which also considers thixotropy based on a rate

equation. The empirical parameters of the model were determined by lab investigations of fluid mud samples from different locations and estuaries, which makes the model approach applicable for a much wider range of applications.

The characteristic stratification pattern is also a result of the complex settling behavior of suspended fines, which is still part of ongoing research. Good results were obtained with a simplified concentration dependent formulation that considers flocculation, hindered settling and beginning consolidation settling behavior.

The interaction of turbulent mixing and laminar flow behavior was considered by introducing a new additional turbulence damping approach based on the local, instantaneous aggregation state of the fluid mud. This approach considers the break-up and recover processes of the floc network within the fluid mud layer. The turbulence production is damped in case of non-Newtonian flow by the degree of instantaneously aggregated floc structure, which in turn strongly depends on the instantaneously shear rate. The introduced turbulence damping approach allows a smooth transition between Newtonian and non-Newtonian flow states.

The model formulation is validated by means of a three-dimensional Ems-model. The Ems estuary is a high-concentrated estuary which frequently builds thick fluid mud layers in the upper tidal reaches. Furthermore, much data is available and also own measurements were carried out to verify the model approach. All measured data are very well reproduced by the numerical model approach and known limitations and so far non-resolved flow behavior addressed in other studies could be solved. The massive reduction of the horizontal flow velocities within the high-concentrated fluid mud layer, as well as associated entrainment and stratification behavior are very well reproduced by the model. Due to the transitional flow behavior from laminar to fully turbulent flow conditions, measured sediment concentrations along the upper reach of the estuary over a longer period are well reproduced by the model.

7.2 Large-scale fluid mud dynamics in the Ems estuary

The aim of this study beyond the model development is its application to an estuarine environment. The model was applied for the Ems estuary in order to contribute to the (missing) system knowledge of large scale fluid mud layer dynamics on an estuary scale.

The model reproduces the observed fluid mud distribution, which spreads over a total distance of 30 km in the uppermost part of the estuary. It allows a detailed reproduction of observed variations on different time scales. Since it fully resolves the three-dimensional domain, gaps between measurement gauges can be filled and sediment budgets calculated. Model results have shown a semi-diurnal and neap-spring variation in the longitudinal distribution as a result of the hydrodynamic variations. Consequently, the impact on residual suspended sediment transport varies strongly at different time-scales. During neap tides consolidation is more dominant, while at spring tide previous consolidated sediment

will be entrained again into the upper water column. This erosion and settling process is in balance when looking at time scales of several weeks. This dynamic equilibrium of cohesive sediment transport over large distances arises and consequently leads to a residual sediment transport pattern forming a sediment trapping zone. The calculated residual flow patterns show that the large scale fluid mud layer stabilizes itself by interaction of Newtonian and non-Newtonian flow dynamics. The stabilization effect is suggested to the decoupling of the fluid mud layer from the free flowing upper water column and an additional sheltering of the lower lutocline parts by yield point and a much higher rheological viscosity.

Total sediment transport investigations were conducted in the overall fluid mud forming region (Lower Ems) for modeled low discharge condition. A weak seaward transport of cohesive fines is observed, when the large-scale fluid mud layer is present. Previous (modeling) studies have shown that the import of muddy sediments from the Outer Ems into the Lower Ems estuary was amplified due to deepening and leads to the formation of the pronounced ETM, formation of fluid mud and massive deposits of cohesive fines. Therefore, the net transport direction can even change when a fluid mud layer is formed compared to situations without such layers. The aforementioned processes emphasize that fluid mud has to be taken into account for modeling of large-scale suspended sediment transport behavior and estuarine circulation, especially, when fully developed layers exist.

7.3 Future work

The developed numerical approach was validated based on measurements from the Ems estuary. For general validity of the model it has to be further proved to other estuaries which also contain fluid mud to develop stratified conditions. Further rheometrical measurements for the sediment side (rheological input) and hydrodynamic measurements are required as validation data. After this, the applicability of the model should be checked and improved. The process parametrization is sensitive to the rheological parameters in the low suspended sediment concentration range (SSC$<$50 $gl{-}1$). To improve adopted parametrization in this low SSC range, new (rheological) measurements have to be performed of low-concentrated fluid mud samples. Furthermore, the settling velocity is not only dependent on the sediment concentration as assumed here within a simplified empirical approach, but also on floc size and the break-up and aggregation due to turbulence. A flocculation model is expected to further improve the applicability of the model to estuaries with stronger differences in fine sediment composition without empirical tweaking of settling velocity formulations.

The impact of suspended cohesive fines on turbulent mixing is relatively unknown. This includes especially the interaction of rheology and turbulent mixing in the transition between both regimes. The non-Newtonian (rheological) turbulence damping formulation introduced here could not been validated due to the lack of lab measurements. This is considered a challenging task, which requires simultaneous measurements of hydrodynamic process variables and the instantaneous rheological viscosity.

Bibliography

Abril, G. et al. (1999). "Oxic/anoxic oscillations and organic carbon mineralization in an estuarine maximum turbidity zone (The Gironde, France)". In: *Limnology and Oceanography* 44.5, pp. 1304–1315.

Abril, G. et al. (2000). "Transient, Tidal Time-scale, Nitrogen Transformations in an Estuarine Turbidity Maximum — Fluid Mud System (The Gironde, South-west France)". en. In: *Estuarine, Coastal and Shelf Science* 50.5, pp. 703–715. ISSN: 02727714.

Allen, GP et al. (1980). "Effects of tides on mixing and suspended sediment transport in macrotidal estuaries". In: *Sedimentary Geology* 26.1-3, pp. 69–90.

Amani, M. et al. (2015). "Effect of salinity on the viscosity of water based drilling fluids at elevated pressures and temperatures". In: *International Journal of Engineering* 7.04, p. 8269.

Argaman, Yerachmiel and Warren J Kaufman (1970). "Turbulence and flocculation". In: *Journal of the Sanitary Engineering Division* 96.2, pp. 223–241.

Ariathurai, Ranjan and Kandiah Arulanandan (1978). "Erosion rates of cohesive soils". In: *Journal of the hydraulics division* 104.2, pp. 279–283.

Bai, YC et al. (2002). "Rheological properties and incipient motion of cohesive sediment in the Haihe Estuary of China". In: *China Ocean Engineering*.

Bakhmeteff, Boris Aleksandrovich (1932). *Hydraulics of open channels*. Tech. rep.

Bartosik, Artur (Mar. 2010). "Application of Rheological Models in Prediction of Turbulent Slurry Flow". en. In: *Flow, Turbulence and Combustion* 84.2, pp. 277–293. ISSN: 1386-6184, 1573-1987.

Baugh, John V and Andrew J Manning (2007). "An assessment of a new settling velocity parameterisation for cohesive sediment transport modeling". In: *Continental Shelf Research* 27.13, pp. 1835–1855.

Baumann, Thomas (2012). "Turbulenzmodellierung von Stromungen niedriger molekularer Prandtlzahl". PhD thesis. University of Karlsruhe, Germany.

Becker, M., C. Maushake, and C. Winter (2018). "Observations of Mud-Induced Periodic Stratification in a Hyperturbid Estuary". In: *Geophysical Research Letters* 45.11, pp. 5461–5469.

Berlamont, Jean et al. (1993). "The characterisation of cohesive sediment properties". In: *Coastal Engineering* 21.1-3, pp. 105–128.

BfG (1998). “Dynamik der Schwermetallbelastung in feinkoernigen Sedimenten und Schwebstoffen im Tidebereich von Ems, Weser und Elbe”. de. In: *Bundesanstalt fuer Gewaesserkunde (BfG), Koblenz* BfG-Bericht 1188.

– (2017). “Sedimentmanagementkonzept Tideems”. de. In: *Bundesanstalt fuer Gewaesserkunde (BfG), Koblenz* BfG-Bericht 1944.

Bianchi, TS (2013). “Estuaries: Where the river meets the sea”. In: *Nature Education Knowledge* 4.4, pp. 1–6.

Bingham, Eugene Cook (1922). *Fluidity and plasticity*. Vol. 2. McGraw-Hill.

Black, KS et al. (2002). “Working with natural cohesive sediments”. In: *Journal of Hydraulic Engineering* 128.1, pp. 2–8.

Bolle, Annelies et al. (2010). “The influence of changes in tidal asymmetry on residual sediment transport in the Western Scheldt”. In: *Continental Shelf Research* 30.8, pp. 871–882.

Borgsmueller, C., I. Quick, and Y. Baulig (2016). “Application of the hydromorphological assessment framework Valmorph to evaluate the changes in suspended sediment distribution in the Ems estuary”. In:

Boussinesq, Joseph (1877). *Essai sur la théorie des eaux courantes*. Impr. nationale.

Bowden, KF and RM Gilligan (1971). “Characteristic features of estuarine circulaiton as represented in the Mersey estuary”. In: *Limnology and Oceanography* 16.3, pp. 490–502.

Brenon, I and P Le Hir (1999). “Modelling the turbidity maximum in the Seine estuary (France): identification of formation processes”. In: *Estuarine, coastal and shelf science* 49.4, pp. 525–544.

Bruens, Ankie (2003). *Entraining mud suspensions*. Delft University of Technology, Faculty of Civil Engineering and Geosciences.

Bruens, AW, JC Winterwerp, and C Kranenburg (2011). “Physical and numerical modeling of the entrainment by a high-concentration mud suspension”. In: *Journal of Hydraulic Engineering* 138.6, pp. 479–490.

Burchard, H., H. M. Schuttelaars, and D. K. Ralston (Jan. 2018). “Sediment Trapping in Estuaries”. en. In: *Annual Review of Marine Science* 10.1, pp. 371–395. ISSN: 1941-1405, 1941-0611.

Busch, N E (1972). “On the mechanics of atmospheric turbulence”. In: *American Meterological Society*, pp. 1–65.

Busch, Niels E and Søren E Larsen (1972). “Spectra of turbulence in the atmospheric surface layer”. In: *Aspects of Research at Risø*, p. 187.

Byun, Do-Seong and Xiao Hua Wang (Mar. 2005). "The effect of sediment stratification on tidal dynamics and sediment transport patterns: Sediment induced stratification effects". en. In: *Journal of Geophysical Research: Oceans* 110.C3. ISSN: 01480227.

Cameron, WM and DW Pritchard (1963). "Estuaries, The Sea". In: *John Wiley & Sons* 2, pp. 306–324.

Cantero, Mariano I. et al. (Jan. 2012). "Emplacement of massive turbidites linked to extinction of turbulence in turbidity currents". en. In: *Nature Geoscience* 5.1, pp. 42–45. ISSN: 1752-0894, 1752-0908.

Celik, Ismail and Wolfgang Rodi (1988). "Modeling suspended sediment transport in nonequilibrium situations". In: *Journal of Hydraulic Engineering* 114.10, pp. 1157–1191.

Chernetsky, Alexander S, Henk M Schuttelaars, and Stefan A Talke (2010). "The effect of tidal asymmetry and temporal settling lag on sediment trapping in tidal estuaries". In: *Ocean Dynamics* 60.5, pp. 1219–1241.

Chesher, TJ and MC Ockenden (1997). "Numerical modelling of mud and sand mixtures". In: *Cohesive Sediments*, pp. 395–406.

Chorin, Alexandre J (1994). *Vorticity and Turbulence*. Vol. 103. Springer Science & Business Media.

Cook, Aaron and Venkatesh Merwade (2009). "Effect of topographic data, geometric configuration and modeling approach on flood inundation mapping". In: *Journal of Hydrology* 377.1-2, pp. 131–142.

Coussot, P. (1997). "Mudflow Rheology and Dynamics". In: *International Association for Hydraulic Research: Rotterdam, The Netherlands*, 255p.

Coussot, Philippe (1994). "Steady, laminar, flow of concentrated mud suspensions in open channel". In: *Journal of Hydraulic Research* 32.4, pp. 535–559.

Coussot, Philippe and Jean Michel Piau (1994). "On the behavior of fine mud suspensions". In: *Rheologica acta* 33.3, pp. 175–184.

Cox, TJS et al. (2009). "A macro-tidal freshwater ecosystem recovering from hypereutrophication: the Schelde case study". In: *Biogeosciences* 6.12, pp. 2935–2948.

Dade, WB, ARM Nowell, and PA Jumars (1992). "Predicting erosion resistance of muds". In: *Marine geology* 105.1-4, pp. 285–297.

Dankers, PJT and JC Winterwerp (2007). "Hindered settling of mud flocs: theory and validation". In: *Continental shelf research* 27.14, pp. 1893–1907.

Dette, H.H. et al. (1994). "Anpassung des Emsfahrwassers an ein 7.30m tiefgehendes Schiff - Beurteilung der Auswirkungen aus Sicht der Hydrologie". de. In: *Leichtweiss Institut fuer Wasserbau, Technnische Universitaet Braunschweig* 770, p. 149.

Dijkstra, Yoeri M, Henk M Schuttelaars, and George P Schramkowski (2019). "A regime shift from low to high sediment concentrations in a tide-dominated estuary". In: *Geophysical Research Letters*.

Dimitriadis, Panayiotis et al. (2016). "Comparative evaluation of 1D and quasi-2D hydraulic models based on benchmark and real-world applications for uncertainty assessment in flood mapping". In: *Journal of Hydrology* 534, pp. 478–492.

Dupont, Jean-Paul et al. (1994). "Continental/marine ratio changes in suspended and settled matter across a macrotidal estuary (the Seine estuary, northwestern France)". In: *Marine Geology* 120.1-2, pp. 27–40.

Dyer, K (1986). "Coastal and estuarine sediment dynamics". In: *John Wiley and Sons, Chichester, Susses (UK), 1986, 358*.

Dyer, Keith R (1997). *Estuaries: a physical introduction*.

Dyer, KR (1989). "Sediment processes in estuaries: future research requirements". In: *Journal of Geophysical Research: Oceans* 94.C10, pp. 14327–14339.

Edwards, RW and HLJ Rolley (1965). "Oxygen consumption of river muds". In: *The Journal of Ecology*, pp. 1–19.

Einstein, Hans Albert and Ray B Krone (1962). "Experiments to determine modes of cohesive sediment transport in salt water". In: *Journal of Geophysical Research* 67.4, pp. 1451–1461.

Faas, Richard W (1984). "Time and density-dependent properties of fluid mud suspensions, NE Brazilian continental shelf". In: *Geo-Marine Letters* 4.3-4, pp. 147–152.

Faas, Richard W and Stanislas I Wartel (2006). "Rheological properties of sediment suspensions from Eckernforde and Kieler Forde bays, western Baltic Sea". In: *International Journal of Sediment Research* 21.1, p. 24.

Fernholz, HH and PJ Finleyt (1996). "The incompressible zero-pressure-gradient turbulent boundary layer: an assessment of the data". In: *Progress in Aerospace Sciences* 32.4, pp. 245–311.

Festa, John F and Donald V Hansen (1978). "Turbidity maxima in partially mixed estuaries: A two-dimensional numerical model". In: *Estuarine and Coastal Marine Science* 7.4, pp. 347–359.

Fischer, Hugo B (1976). "Mixing and dispersion in estuaries". In: *Annual review of fluid mechanics* 8.1, pp. 107–133.

Fredsøe, J and R Deigaard (1992). "Mechanics of coastal sediment transport, Adv. Ser". In: *Ocean Eng* 3, p. 369.

Gabioux, Mariela, Susana B Vinzon, and Afonso M Paiva (2005). "Tidal propagation over fluid mud layers on the Amazon shelf". In: *Continental Shelf Research* 25.1, pp. 113–125.

Garnier, Josette et al. (2001). "Lower Seine river and estuary (France) carbon and oxygen budgets during low flow". In: *Estuaries* 24.6, pp. 964–976.

Geyer, W. Rockwell (Mar. 1993). "The Importance of Suppression of Turbulence by Stratification on the Estuarine Turbidity Maximum". en. In: *Estuaries* 16.1, p. 113. ISSN: 01608347.

Geyer, W Rockwell, R Chant, and R Houghton (2008). "Tidal and spring-neap variations in horizontal dispersion in a partially mixed estuary". In: *Journal of Geophysical Research: Oceans* 113.C7.

Geyer, W. Rockwell and Parker MacCready (Jan. 2014). "The Estuarine Circulation". en. In: *Annual Review of Fluid Mechanics* 46.1, pp. 175–197. ISSN: 0066-4189, 1545-4479.

Geyer, W Rockwell and DK Ralston (2018). "A mobile pool of contaminated sediment in the Penobscot Estuary, Maine, USA". In: *Science of the Total Environment* 612, pp. 694–707.

Geyer, W Rockwell and Richard P Signell (1992). "A reassessment of the role of tidal dispersion in estuaries and bays". In: *Estuaries* 15.2, pp. 97–108.

Geyer, W Rockwell, Jonathan D Woodruff, and Peter Traykovski (2001). "Sediment transport and trapping in the Hudson River estuary". In: *Estuaries* 24.5, pp. 670–679.

Gibson, RE, GL England, and MJL Hussey (1967). "The Theory of one-dimensional consolidation of saturated clays: 1. finite non-Linear consildation of thin homogeneous layers". In: *Geotechnique* 17.3, pp. 261–273.

Gidaspow, Dimitri (1994). *Multiphase flow and fluidization: continuum and kinetic theory descriptions*.

Goosen, Nico K et al. (1999). "Bacterial and phytoplankton production in the maximum turbidity zone of three European estuaries: the Elbe, Westerschelde and Gironde". In: *Journal of Marine Systems* 22.2-3, pp. 151–171.

Goudsmit, G-H et al. (2002). "Application of k-ε turbulence models to enclosed basins: The role of internal seiches". In: *Journal of Geophysical Research: Oceans* 107.C12.

Graf, Walter Hans and MS Altinakar (1998). *Fluvial hydraulics: Flow and transport processes in channels of simple geometry*. 551.483 G7. Wiley New York.

Granboulan, J et al. (1989). "Study of the sedimentological and rheological properties of fluid mud in the fluvio-estuarine system of the Gironde estuary". In: *Ocean and Shoreline Management* 12.1, pp. 23–46.

Gräwe, Ulf et al. (2014). "Seasonal variability in M2 and M4 tidal constituents and its implications for the coastal residual sediment transport". In: *Geophysical Research Letters* 41.15, pp. 5563–5570.

Gualtieri, C. et al. (2017). "On the values for the turbulent Schmidt number in environmental flows". In: *Fluids* 2.2, p. 17.

Guan, W.B., S.C. Kot, and E. Wolanski (Dec. 2005). "3-D fluid-mud dynamics in the Jiaojiang Estuary, China". en. In: *Estuarine, Coastal and Shelf Science* 65.4, pp. 747–762. ISSN: 02727714.

Guan, Wei-Bing, Eric Wolanski, and Li-Xian Dong (1998). "Cohesive sediment transport in the Jiaojiang River estuary, China". In: *Estuarine, Coastal and Shelf Science* 46.6, pp. 861–871.

Guézennec, Loïc et al. (1999). "Hydrodynamics of suspended particulate matter in the tidal freshwater zone of a macrotidal estuary (the Seine estuary, France)". In: *Estuaries* 22.3, pp. 717–727.

Guo, Yakun et al. (2011). "Numerical simulation of the tidal flow and suspended sediment transport in the Qiantang Estuary". In: *Journal of waterway, port, coastal, and ocean engineering* 138.3, pp. 192–202.

Habermann, Christine and Andreas Wurpts (2008). "Occurence, behavior and physical properties of fluid mud". en. In: p. 6.

Hansen, Donald V and Maurice Rattray (1966). "New dimensions in estuary classification1". In: *Limnology and Oceanography* 11.3, pp. 319–326.

Hayter, EJ and AJ Mehta (1986). "Modelling cohesive sediment transport in estuarial waters". In: *Applied Mathematical Modelling* 10.4, pp. 294–303.

Herrling, G and HD Niemeyer (2008). "Comparison of the hydrodynamic regime of 1937 and 2005 in the Ems-Dollard estuary by applying mathematical modeling". In: *NLWKN Coastal Research Station*.

Herschel, Winslow H and Ronald Bulkley (1926). "Konsistenzmessungen von gummibenzollösungen". In: *Colloid & Polymer Science* 39.4, pp. 291–300.

Hesse, Roland F, Anna Zorndt, and Peter Fröhle (2019). "Modelling dynamics of the estuarine turbidity maximum and local net deposition". In: *Ocean Dynamics* 69.4, pp. 489–507.

Hjulstrom, Filip (1935). "Studies of the morphological activity of rivers as illustrated by the River Fyris, Bulletin". In: *Geological Institute Upsalsa* 25, pp. 221–527.

HongbinZhou, Lin Bingnan Han Zengcui Sun and Zhide He Shading Wang Lianxiang (1988). "Two-D Simulation of Sediment Transport and Bed Deformation by Tides [J]". In: *Journal of Sediment Research* 2.

Hsu, T.-J., P. A. Traykovski, and G. C. Kineke (Apr. 2007a). "On modeling boundary layer and gravity-driven fluid mud transport". en. In: *Journal of Geophysical Research* 112.C4. ISSN: 0148-0227.

Hsu, T-J, PA Traykovski, and GC Kineke (2007b). "On modeling boundary layer and gravity-driven fluid mud transport". In: *Journal of Geophysical Research: Oceans* 112.C4.

Hsu, Tian-Jian and Peter A Traykovski (2007). "A Fluid Mud Transport Model in Multi-dimensions". en. In: p. 17.

Huang, Zhenhua and Huhe Aode (2009). "A laboratory study of rheological properties of mudflows in Hangzhou Bay, China". In: *International Journal of Sediment Research* 24.4, pp. 410–424.

Huijts, KMH et al. (2006). "Lateral entrapment of sediment in tidal estuaries: An idealized model study". In: *Journal of Geophysical Research: Oceans* 111.C12.

Jay, David A. and Jeffery D. Musiak (1994). "Particle trapping in estuarine tidal flows". en. In: *Journal of Geophysical Research* 99.C10, p. 20445. ISSN: 0148-0227.

Jiang, Chenjuan, Jiufa Li, and Huib E de Swart (2012). "Effects of navigational works on morphological changes in the bar area of the Yangtze Estuary". In: *Geomorphology* 139, pp. 205–219.

Jinghui, Liu et al. (2005). "Monitoring and analysis of changes of wetlands and tidal flat environment in the Yangtze River estuary". In: *Proceedings. 2005 IEEE International Geoscience and Remote Sensing Symposium, 2005. IGARSS'05.* Vol. 4. Ieee, pp. 2307–2310.

Johansen, Claus (1998). "Dynamics of cohesive sediments". PhD thesis. Hydraulics & Coastal Engineering Lab., Department of Civil Engineering ...

Jones, WP and Brian Edward Launder (1972). "The prediction of laminarization with a two-equation model of turbulence". In: *International journal of heat and mass transfer* 15.2, pp. 301–314.

Jonge, Victor N. de et al. (Feb. 2014). "The influence of channel deepening on estuarine turbidity levels and dynamics, as exemplified by the Ems estuary". en. In: *Estuarine, Coastal and Shelf Science* 139, pp. 46–59. ISSN: 02727714.

Kämpf, Jochen and Paul Myrow (Mar. 2018). "Wave-Created Mud Suspensions: A Theoretical Study". en. In: *Journal of Marine Science and Engineering* 6.2, p. 29. ISSN: 2077-1312.

Kappenberg, Jens and Iris Grabemann (2001). "Variability of the mixing zones and estuarine turbidity maxima in the Elbe and Weser estuaries". In: *Estuaries* 24.5, pp. 699–706.

Kärnä, Tuomas et al. (Apr. 2015). "Numerical modeling of circulation in high-energy estuaries: A Columbia River estuary benchmark". en. In: *Ocean Modelling* 88, pp. 54–71. ISSN: 14635003.

Kent, R and D Pritchard (1959). "A test of mixing-length theories in a coastal plain estuary." In:

Kerner, Martin (2007). "Effects of deepening the Elbe Estuary on sediment regime and water quality". In: *Estuarine, coastal and shelf science* 75.4, pp. 492–500.

Kessel, Thijs van and C Kranenburg (1996). "Gravity current of fluid mud on sloping bed". In: *Journal of Hydraulic Engineering* 122.12, pp. 710–717.

Kineke, G. C. et al. (2006). "Fine-sediment transport associated with cold-front passages on the shallow shelf, Gulf of Mexico". In: *Continental Shelf Research* 26.17-18, pp. 2073–2091.

Kineke, GC et al. (1996). "Fluid-mud processes on the Amazon continental shelf". In: *Continental shelf research* 16.5-6, pp. 667–696.

Kirby, R (1988). "High concentration suspension (fluid mud) layers in estuaries". In: *Physical processes in estuaries*. Springer, pp. 463–487.

Kirby, R and WR Parker (1983). "Distribution and behavior of fine sediment in the Severn Estuary and Inner Bristol Channel, UK". In: *Canadian Journal of Fisheries and Aquatic Sciences* 40.S1, s83–s95.

Kolmogorov, A (1942). "Equations of motion of an incompressible turbulent fluid". In: *Izv Akad Nauk SSSR Ser Phys* 6.6, pp. 56–58.

Kranck, Kate (1986). "Settling behavior of cohesive sediment". In: *Estuarine cohesive sediment dynamics*. Springer, pp. 151–169.

Kranenburg, C (1994). "The fractal structure of cohesive sediment aggregates". In: *Estuarine, Coastal and Shelf Science* 39.5, pp. 451–460.

– (1998). "Saturation concentrations of suspended fine sediment: computations with the Prandtl Mixing-Length model". In: *Report no. 5-98*.

Kranenburg, C and JC Winterwerp (1997). "Erosion of fluid mud layers. I: Entrainment model". In: *Journal of Hydraulic Engineering* 123.6, pp. 504–511.

Krebs, Martin and Holger Weilbeer (2008). "Ems-dollart estuary". In: *Die Küste, 74 ICCE* 74, pp. 252–262.

Lamb, M.P., E.D. Asaro, and J.D. Parson (2004). "Turbulent structure of high-density suspensions formed under waves". en. In: *Journal of Geophysical Research* 109.C12. ISSN: 0148-0227.

Lehfeldt, R and S Bloss (1988). "Algebraic turbulence model for stratified tidal flows". In: *Physical processes in estuaries*. Springer, pp. 278–291.

LeHir, P. (1997). "Fluid and sediment integrated modeling aplication to fluid mud flows in estuaries". In: *Cohesive Sediments*, pp. 417–428.

LeHir, P., P. Bassoullet, and H. Jestin (2000). "Application of the continuous modeling concept to simulate high-concentration suspended sediment in a macrotidal estuary". In: *Proceedings in Marine Science* 3, pp. 229–247.

Lesourd, S et al. (2003). "Seasonal variations in the characteristics of superficial sediments in a macrotidal estuary (the Seine inlet, France)". In: *Estuarine, Coastal and Shelf Science* 58.1, pp. 3–16.

Lesser, Giles R et al. (2004). "Development and validation of a three-dimensional morphological model". In: *Coastal engineering* 51.8-9, pp. 883–915.

Lin, Jing and Albert Y Kuo (2003). "A model study of turbidity maxima in the York River Estuary, Virginia". In: *Estuaries* 26.5, pp. 1269–1280.

Liu, Wen-Cheng, Ming-Hsi Hsu, and Albert Y Kuo (2002). "Modelling of hydrodynamics and cohesive sediment transport in Tanshui River estuarine system, Taiwan". In: *Marine Pollution Bulletin* 44.10, pp. 1076–1088.

Lyn, DA (1988). "A similarity approach to turbulent sediment-laden flows in open channels". In: *Journal of Fluid Mechanics* 193, pp. 1–26.

Maciel, Geraldo de F, Hamilton Kiryu dos Santos, and Fabiana de O Ferreira (2009). "Rheological analysis of water clay compositions in order to investigate mudflows developing in canals". In: *Journal of the Brazilian Society of Mechanical Sciences and Engineering* 31.1, pp. 64–74.

Makinde, FA et al. (2011). "Modelling the effects of temperature and aging time on the rheological properties of drilling fluids". In: *Petroleum & Coal* 53.3, pp. 167–182.

Malcherek, A (1995). "Mathematische Modellierung von Strömungen und Stofftransportprozessen in Ästuaren". In: *Dissertation*. University of Hannover.

Malcherek, A (2007). "Sedimenttransport und Morphodynamik". In: *Scriptum Institut für Wasserwesen, Universität München.*

Malcherek, A. and H. Cha (2011). *Zur Rheologie von Fluessigschlicken: experimentelle Untersuchungen und theoretische Ansaetze.*

Marchand, Jocelyne (1993). "The influence of seasonal salinity and turbidity maximum variations on the nursery function of the Loire estuary (France)". In: *Netherland Journal of Aquatic Ecology* 27.2-4, pp. 427–436.

Maren, Dirk S. van, Johan C. Winterwerp, and Julia Vroom (2015). "Fine sediment transport into the hyper-turbid lower Ems River: the role of channel deepening and sediment-induced drag reduction". en. In: *Ocean Dynamics* 65.4, pp. 589–605. ISSN: 1616-7341, 1616-7228.

Maren, D.S. van et al. (Mar. 2015). "The impact of channel deepening and dredging on estuarine sediment concentration". en. In: *Continental Shelf Research* 95, pp. 1–14. ISSN: 02784343.

Martin, DP et al. (2008). "Tidal and seasonal dynamics of a muddy inner shelf environment, Gulf of Papua". In: *Journal of Geophysical Research: Earth Surface* 113.F1.

McAnally, William H. et al. (Jan. 2007). "Management of Fluid Mud in Estuaries, Bays, and Lakes. I: Present State of Understanding on Character and Behavior". en. In: *Journal of Hydraulic Engineering* 133.1, pp. 9–22. ISSN: 0733-9429, 1943-7900.

McLaren, Patrick, Frank Steyaert, and Richard Powys (1998). "Sediment transport studies in the tidal basins of the Dutch Waddenzee". In: *Senckenbergiana maritima* 29.1-6, pp. 53–61.

McLusky, DS and M Elliot (2004). *The estuarine ecology: ecology, threats and management.*

Mehta, AJ et al. (2009). *Resuspension Dynamics in Lake Apopka, Florida. Final Synopsis Report, submitted to St. Johns River Water Management District, Palatka, Florida, June 2009.* Tech. rep. Report No. UFL/COEL-2009/00, 158p.

Mehta, Ashish J et al. (1989). "Cohesive sediment transport. I: Process description". In: *Journal of Hydraulic Engineering* 115.8, pp. 1076–1093.

Merckelbach, Lucas Maria (2000). "Consolidation and strength evolution of soft mud layers". In:

Meyer, C and G Ragutzki (1999). "KFKI Forschungsvorhaben Sedimentverteilung als Indikator für morphodynamische Prozesse, MTK 0591". In: *Dienstbericht Forschungsstelle Küste 21/1999. Niedersächsisches Landesamt für Ökologie (in german).*

Mezger, TG (2006). "The rheology handbook: For users of rotational and oscillatory rheometers". In: *Aufl. Hannover: Vincentz Network*, p. 148.

Miller, M et al. (2016). "Settling and dewatering characteristics of an A-stage activated sludge process proceeded by shortcut biological nitrogen removal". In: *Int J Water Wastewater Treat* 2.5, pp. 1–8.

Mittal, Neha et al. (2014). "Flow regime alteration due to anthropogenic and climatic changes in the Kangsabati River, India". In: *Ecohydrology & Hydrobiology* 14.3, pp. 182–191.

Mittal, Neha et al. (2016). "Impact of human intervention and climate change on natural flow regime". In: *Water resources management* 30.2, pp. 685–699.

Moore, George Richard (1959). "Vaporization of superheated drops in liquids". In: *AIChE Journal* 5.4, pp. 458–466.

Nakagawa, Yasuyuki et al. (2012). "Field measurement and modeling of near-bed sediment transport processes with fluid mud layer in Tokyo Bay". In: *Ocean Dynamics* 62.10-12, pp. 1535–1544.

Nguyen, QD and DV Boger (1985). "Thixotropic behaviour of concentrated bauxite residue suspensions". In: *Rheologica Acta* 24.4, pp. 427–437.

Nikuradse, Johann (1933). "Gesetzmäßigkeiten der turbulenten Strömung in glatten Rohren (Nachtrag)". In: *Forschung im Ingenieurwesen* 4.1, pp. 44–44.

North, Elizabeth W and Edward D Houde (2001). "Retention of white perch and striped bass larvae: biological-physical interactions in Chesapeake Bay estuarine turbidity maximum". In: *Estuaries* 24.5, pp. 756–769.

Oberrecht, D. and A. Wurpts (2014a). "Impact of controlled tidal barrier operation on tidal dynamics in the Ems estuary". In: *Die Keuste, 81 Modelling* 81, pp. 427–433.

– (2014b). "Investigations of rheological flow properties based on lab data of fluid mud samples and an extended model approach". In: *Die Kueste, 81 Modelling* 81, pp. 455–462.

Orton, PM and GC Kineke (2001). "Comparing calculated and observed vertical suspended-sediment distributions from a Hudson River estuary turbidity maximum". In: *Estuarine, Coastal and Shelf Science* 52.3, pp. 401–410.

Osaka, Hideo, Takatsugu Kameda, and Shinsuke Mochizuki (1998). "Re-examination of the Reynolds-number-effect on the mean flow quantities in a smooth wall turbulent boundary layer". In: *JSME International Journal Series B Fluids and Thermal Engineering* 41.1, pp. 123–129.

Papenmeier, Svenja et al. (July 2012). "Sedimentological and Rheological Properties of the Water–Solid Bed Interface in the Weser and Ems Estuaries, North Sea, Germany: Implications for Fluid Mud Classification". en. In: *Journal of Coastal Research* 289, pp. 797–808. ISSN: 0749-0208, 1551-5036.

Parsons, Jeffrey D, Kelin X Whipple, and Alessandro Simoni (2001). "Experimental study of the grain-flow, fluid-mud transition in debris flows". In: *The Journal of Geology* 109.4, pp. 427–447.

Pein, Johannes Ulrich, Emil Vassilev Stanev, and Yinglong Joseph Zhang (Dec. 2014). "The tidal asymmetries and residual flows in Ems Estuary". en. In: *Ocean Dynamics* 64.12, pp. 1719–1741. ISSN: 1616-7341, 1616-7228.

Piirto, Mika and Pentti Saarenrinne (1999). "Interaction between Flocculation and Turbulence-A Method Using the Combination of Image Processing and PIV". In: *Symposium on Optical Methods and Image Processing in Fluid Flow Measurements, ASME/JSME Fluids Engineering Conference,(San Francisco, California, USA)*.

Postma, H and K Kalle (1955). "Die Entstehung von Trübungszonen im Unterlauf der Flüsse, speziell im Hinblick auf die Verhältnisse in der Unterelbe". In: *Deutsche Hydrografische Zeitschrift* 8.4, pp. 137–144.

Prandtl, L (1925). "The Magnus effect and windpowered ships". In: *Naturwissenschaften* 13.6, pp. 93–108.

– (1945). "Über ein neues Formelsystem fur die ausgebildete Turbulenz. Nach. Ges. Wiss. Göttingen, Math". In: *Phys. Kl*, pp. 6–18.

Prandtl, Ludwig (1932). "Zur turbulenten Strömung in Rohren und längs Platten". In: *Ergebnisse der aerodynamischen versuchsanstalt zu göttingen* 4, pp. 18–29.

Prandtl, Ludwig and OG Tietjens (1934). *Applied hydro-and aerodynamics*.

Pritchard, Donald W (1967). "What is an estuary: physical viewpoint". In: American Association for the Advancement of Science.

Pritchard, D.W. (1952). "Estuarine hydrography". In: *Adv. Geophys.* Pp. 243–280.

Ralston, David K, W Rockwell Geyer, and James A Lerczak (2010). "Structure, variability, and salt flux in a strongly forced salt wedge estuary". In: *Journal of Geophysical Research: Oceans* 115.C6.

Raudkivi, Arved J (1998). *Loose boundary hydraulics*. CRC Press.

Revil-Baudard, Thibaud et al. (2015). "Investigation of sheet-flow processes based on novel acoustic high-resolution velocity and concentration measurements". In: *Journal of Fluid Mechanics* 767, pp. 1–30.

Reynolds, Osborne (1883a). "III. An experimental investigation of the circumstances which determine whether the motion of water shall be direct or sinuous, and of the law of resistance in parallel channels". In: *Proceedings of the royal society of London* 35.224-226, pp. 84–99.

– (1883b). “XXIX. An experimental investigation of the circumstances which determine whether the motion of water shall be direct or sinuous, and of the law of resistance in parallel channels”. In: *Philosophical Transactions of the Royal society of London* 174, pp. 935–982.

Richardson, JF and WN Zaki (1954). “The sedimentation of a suspension of uniform spheres under conditions of viscous flow”. In: *Chemical Engineering Science* 3.2, pp. 65–73.

Richardson, Lewis Fry (1922). *Weather prediction by numerical process*. Cambridge University Press.

Rijn, Leo C van (1984). “Sediment transport, part II: suspended load transport”. In: *Journal of hydraulic engineering* 110.11, pp. 1613–1641.

Roland, Aron et al. (2012). “Über Strömungsmodelle auf unstrukturierten Gitternetzen zur Simulation der Dynamik von Flüssigschlick”. In: *Die Küste, 79* 79, pp. 53–81.

Ross, M.R. and A.J. Metha (1989). “On the mechanics of lutocline and fluid mud”. In: *Journal of Coastal Research* 5, pp. 51–61.

Rouse, Hunter (1937). “Modern conceptions of the mechanics of fluid turbulence”. In: *Trans ASCE* 102, pp. 463–505.

Sanford, Lawrence P (2008). “Modeling a dynamically varying mixed sediment bed with erosion, deposition, bioturbation, consolidation, and armoring”. In: *Computers & Geosciences* 34.10, pp. 1263–1283.

Schlichting, Hermann and Klaus Gersten (2016). *Boundary-layer theory*. Springer.

Schrottke, Kerstin et al. (Sept. 2006). “Fluid mud dynamics in the Weser estuary turbidity zone tracked by high-resolution side-scan sonar and parametric sub-bottom profiler”. en. In: *Geo-Marine Letters* 26.3, pp. 185–198. ISSN: 0276-0460, 1432-1157.

Seifert, Annedore (2011). *In situ detection and characterisation of fluid mud and soft cohesive sediments by dynamic piezocone penetrometer testing*.

Sheng, Y Peter and Catherine Villaret (1989). “Modeling the effect of suspended sediment stratification on bottom exchange processes”. In: *Journal of Geophysical Research: Oceans* 94.C10, pp. 14429–14444.

Shields, Albert (1936). “Anwendung der Aehnlichkeitsmechanik und der Turbulenzforschung auf die Geschiebebewegung”. In: *PhD Thesis Technical University Berlin*.

Sills, Gilliane C and Don McG Elder (1986). “The transition from sediment suspension to settling bed”. In: *Estuarine cohesive sediment dynamics*. Springer, pp. 192–205.

Smith, J Dungan and SR McLean (1977). "Spatially averaged flow over a wavy surface". In: *Journal of Geophysical research* 82.12, pp. 1735–1746.

Sommerfield, Christopher K and Kuo-Chuin Wong (2011). "Mechanisms of sediment flux and turbidity maintenance in the Delaware Estuary". In: *Journal of Geophysical Research: Oceans* 116.C1.

Sottolichio, Aldo and Patrice Castaing (1999). "A synthesis on seasonal dynamics of highly-concentrated structures in the Gironde estuary". In: *Comptes Rendus de l'Académie des Sciences-Series IIA-Earth and Planetary Science* 329.11, pp. 795–800.

Soulsby, RL et al. (2013). "Settling velocity and mass settling flux of flocculated estuarine sediments". In: *Marine Geology* 339, pp. 1–12.

Takács, Imre, Gilles G Patry, and Daniel Nolasco (1991). "A dynamic model of the clarification-thickening process". In: *Water research* 25.10, pp. 1263–1271.

Talke, Stefan A and Huib E De Swart (2006). *Hydrodynamics and morphology in the Ems/Dollard estuary: review of models, measurements, scientific literature and the effects of changing conditions.*

Talke, Stefan A, Huib E de Swart, and VN De Jonge (2009). "An idealized model and systematic process study of oxygen depletion in highly turbid estuaries". In: *Estuaries and coasts* 32.4, pp. 602–620.

Talke, Stefan A, Huib E de Swart, and HM Schuttelaars (2009). "Feedback between residual circulations and sediment distribution in highly turbid estuaries: an analytical model". In: *Continental Shelf Research* 29.1, pp. 119–135.

Teisson, Ch. et al. (1992). "Turbulence and mud sedimentation: A Reynolds stress model and a two-phase flow model". In: *Coastal Engineering Proceedings* 1.23.

Terzaghi, K and R Peck. "B. 1948". In: *Soil mechanics in engineering practice* 1 ().

Tippener, M. and L. Reinemann (1979). "Schwebstoffmessungen in der Ems an der Durchflussmessstelle Nuettermoor am 06.09.1979". de. In: *Bundesanstalt fuer Gewaesserkunde (BfG), Koblenz* M2/126/4874.

Tiu, C and DV Boger (1974). "Complete rheological characterization of time-dependent food products". In: *Journal of texture studies* 5.3, pp. 329–338.

Toorman, E.A. (1992). "Modeling of fluid mud flow and consolidation". In: *PhD Thesis, Katholieke Universiteit Leuven.*

– (1996). "Sedimentation and self-weight consolidation: general unifying theory". In: *Géotechnique* 46.1, pp. 103–113.

– (1997). “Modelling the thixotropic behaviour of dense cohesive sediment suspensions”. en. In: *Rheologica Acta* 36.1, pp. 56–65. ISSN: 0035-4511, 1435-1528.

Toorman, E.A. et al. (2002). “Interaction of suspended cohesive sediment and turbulence”. en. In: *Proceedings in Marine Science*. Vol. 5. Elsevier, pp. 7–23. ISBN: 978-0-444-51136-2.

Toorman E.A.and Berlamont, Jean E (1993). “Mathematical modeling of cohesive sediment settling and consolidation”. In: *Coastal and Estuarine Studies*, pp. 167–167.

Traykovski, P et al. (2000). “The role of wave-induced density-driven fluid mud flows for cross-shelf transport on the Eel River continental shelf”. In: *Continental Shelf Research* 20.16, pp. 2113–2140.

Uncles, R.J. (Dec. 2002). “Estuarine Physical Processes Research: Some Recent Studies and Progress”. en. In: *Estuarine, Coastal and Shelf Science* 55.6, pp. 829–856. ISSN: 02727714.

Uncles, RJ and JA Stephens (1993). “The freshwater-saltwater interface and its relationship to the turbidity maximum in the Tamar estuary, United Kingdom”. In: *Estuaries* 16.1, pp. 126–141.

Uncles, RJ, JA Stephens, and DJ Law (2006). “Turbidity maximum in the macrotidal, highly turbid Humber Estuary, UK: Flocs, fluid mud, stationary suspensions and tidal bores”. In: *Estuarine, Coastal and Shelf Science* 67.1-2, pp. 30–52.

Unesco, Ices (1981). *Background papers and supporting data on the international equation of state of seawater 1980*.

Valle-Levinson, Arnoldo (2010). *Contemporary issues in estuarine physics*. Cambridge University Press.

Van Kessel, Thijs and C Blom (1998). “Rheology of cohesive sediments: comparison between a natural and an artificial mud”. In: *Journal of Hydraulic Research* 36.4, pp. 591–612.

Van Kessel, Thijs, Joris Vanlede, and Johan de Kok (2011). “Development of a mud transport model for the Scheldt estuary”. In: *Continental Shelf Research* 31.10, S165–S181.

Van Ledden, M (2002). “A process-based sand-mud model”. In: *Proceedings in Marine Science*. Vol. 5. Elsevier, pp. 577–594.

Van Leussen, W (1988). “Aggregation of particles, settling velocity of mud flocs a review”. In: *Physical processes in estuaries*. Springer, pp. 347–403.

– (1994). “Estuarine macroflocs and their role in fine-grained sediment transport”. In: *Phd*. University of Utrecht.

Van Rijn, Leo C (1989). "Mathematical modelling of morphological processes in the case of suspended sediment transport." In:

Van Rijn, Leo C et al. (1993). *Principles of sediment transport in rivers, estuaries and coastal seas*. Vol. 1006. Aqua publications Amsterdam.

Vesilind, P Aarne (1968). "Design of prototype thickeners from batch settling tests". In: *Water Sewage Works* 115.7, pp. 302–307.

Waeles, Benoît, Pierre Le Hir, and Patrick Lesueur (2008). "A 3D morphodynamic process-based modelling of a mixed sand/mud coastal environment: the Seine estuary, France". In: *Proceedings in Marine Science*. Vol. 9. Elsevier, pp. 477–498.

Walther, Regis et al. (2012). "Coupled 3D modeling of turbidity maximum dynamics in the Loire estuary, France". In: *Coastal Engineering Proceedings* 1.33, p. 22.

Warner, John C et al. (2005). "Performance of four turbulence closure models implemented using a generic length scale method". In: *Ocean Modelling* 8.1-2, pp. 81–113.

Wehr, Denise (2012). "An isopycnal numerical model for the simulation of fluid mud dynamics". In:

Wehr, Denise and Andreas Malcherek (2012). "Numerical simulation of fluid mud dynamics–The isopycnal model MudSim". In: *Die Küste, 79* 79, pp. 1–52.

Widdows, John and Mary Brinsley (2002). "Impact of biotic and abiotic processes on sediment dynamics and the consequences to the structure and functioning of the intertidal zone". In: *Journal of sea Research* 48.2, pp. 143–156.

Winterwerp, J. C. (Oct. 2001). "Stratification effects by cohesive and noncohesive sediment". en. In: *Journal of Geophysical Research: Oceans* 106.C10, pp. 22559–22574. ISSN: 01480227.

Winterwerp, Johan C and Walther GM Van Kesteren (2004). *Introduction to the physics of cohesive sediment dynamics in the marine environment*. Vol. 56. Elsevier.

Winterwerp, Johan C and Zheng Bing Wang (2013). "Man-induced regime shifts in small estuaries—I: theory". In: *Ocean Dynamics* 63.11-12, pp. 1279–1292.

Winterwerp, Johan C. et al. (May 2017). "SPM response to tide and river flow in the hyper-turbid Ems River". en. In: *Ocean Dynamics* 67.5, pp. 559–583. ISSN: 1616-7341, 1616-7228.

Winterwerp, Johan Christian (1999). "On the dynamics of high-concentrated mud suspensions". In:

Wolanski, Eric, Takashi Asaeda, and Jorg Imberger (July 1989). "Mixing across a lutocline". en. In: *Limnology and Oceanography* 34.5, pp. 931–938. ISSN: 00243590.

Wolanski, Eric et al. (1992). “The role of turbulence in the settling of mud flocs”. In: *Journal of Coastal Research*, pp. 35–46.

Worrall, WE and S Tuliani (1964). “Viscosity changes during the ageing of clay-water suspensions”. In: *Trans Brit Ceramic Soc* 63, pp. 167–185.

Wotton, Roger S (2004). “The utiquity and many roles of exopolymers (EPS) in aquatic systems”. In: *Scientia marina* 68.S1, pp. 13–21.

Wurpts, Andreas (2006). “Numerische Suimulation von Dichteeffekten am Beispiel der Umlagerung von Baggergut im Aestuarbereich”. PhD thesis. University of Darmstadt.

Wurpts, Rewert and Patrick Torn (2005). “15 years experience with fluid mud: Definition of the nautical bottom with rheological parameters”. In: *Terra et Aqua* 99, pp. 22–32.

Xu, Jingyu and Aode Huhe (2016). “Rheological study of mudflows at Lianyungang in China”. In: *International Journal of Sediment Research* 31.1, pp. 71–78.

Yang, Wenyu et al. (2013). “Rheological properties of bed sediments subjected to shear and vibration loads”. In: *Journal of Waterway, Port, Coastal, and Ocean Engineering* 140.1, pp. 109–113.

Zanke, U (1982). “Grundlagen der Sedimentbewegung”. In: *Springer-Verlag, Berlin Heidelberg*.

Curriculum Vitae

Personal Details

Name	Dennis Oberrecht
Date & place of birth	December 28, 1984 in Neuenkirchen
Personal status	unmarried

Work experience

Mar. 2008 - Apr. 2011	Student assistant at Franzius-Institute for Hydraulic, Waterways and Coastal Engineering, Leibniz University Hannover
May 2011 - current	Research Assistant in Coastal Engineering at the Coastal Research Station in the Lower Saxony Water Management, Coastal Defense and Nature Conservation Agency, Norderney

Education

Oct. 2005 - Sept. 2009	University education in civil engineering at the Leibniz University of Hannover Degree: Bachelor of Science (B.Sc)
Oct. 2009 - Mar. 2011	University education in civil engineering at the Leibniz University of Hannover Degree: Master of Science (M.Sc)

Visits Abroad

Nov. 2010 - Mar. 2011	Master thesis at Oceans Institute of the University of Western Australia, Perth, Australia

School Education

Aug. 1995 - Jun. 2004	Missionsgymnasium Arnold-Jansen, Neuenkirchen Graduated with German Abitur (equivalent to A-levels)

Memberships

since Mar 2008	Gesellschaft der Förderer des Ludwig-Franzius Instiuts e.V.
since May 2008	Hafentechnische Gesellschaft e.V.